UNIVERSITY OF GRANADA

Faculty of Pharmacy

Physical Chemistry Department

PhD Thesis

NEW FLUORESCENT DYES FOR BIOLOGICALLY RELEVANT ANALYTES DETECTION. DESIGN, SYNTHESIS AND PHOTOPHYSICAL CHARACTERIZATION. APPLICATION IN BIOLOGICAL MEDIA

Virginia Puente Muñoz

Granada, 2017

Editor: Universidad de Granada. Tesis Doctorales
Autor: Virginia Puente Muñoz
ISBN: 978-84-9163-302-0
URI: http://hdl.handle.net/10481/47430

New fluorescent Dyes for Biologically Relevant Analytes Detection. Design, Synthesis and Photophysical Characterization. Application in Biological Media

Los directores,

Fdo. Dr. Luis Crovetto González
(Profesor titular Univ. Granada)

Fdo. Dr. J. M. Paredes Martínez
(Profesor Ayte. Doctor Univ. Granada)

Tesis doctoral para aspirar al grado de Doctor con Mención Internacional por la Universidad de Granada

Fdo. Virginia Puente Muñoz

Granada, 2017

La directora del Departamento certifica que el Departamento de Fisicoquímica de la Universidad de Granada ha dado su conformidad para la presentación de la presente Tesis Doctoral.

Directora Dpto. Fisicoquímica

Universidad de Granada

Fdo. Dra. Eva María Talavera Rodríguez

A mis padres.

A Javi, por hacerlo posible.

Contents

Figure index

GENERAL INTRODUCTION

INSTRUMENTATION

RESULTS

Chapter 1. New Dual Fluorescent Probe for Simultaneous Biothiol and Phosphate Bioimaging

Chapter 2. A New Fluorescent Dye for Oxidative Detection through Thiol Detection in vivo in Cell Culture

Chapter 3. Efficient Acetate Sensor in Biological Media based on a Selective Excited State Proton Transfer (ESPT) Reaction

Scheme index

RESULTS

Chapter 1. New Dual Fluorescent Probe for Simultaneous Biothiol and Phosphate Bioimaging

Chapter 2. A new Fluorescent Dye for Oxidative Stress through Thiol Detection in vivo in Cell Cultures.

Chapter 3. Efficient Acetate Sensor in Biological Media based on a Selective Excited State Proton Transfer (ESPT) Reaction

Table index

Chapter 3. Efficient Acetate Sensor in Biological Media based on a Selective Excited State Proton Transfer (ESPT) Reaction

List of abbreviations

ATP	Potassium Adenosine Triphosphate
BCECF	2`,7`-bis-(2-carboxyethyl)-5-(and-6)-carboxyfluorescein
CHO	Chinese Hamster Ovary Cell line
Cys	Cysteine
DMEM	Dulbecco Modified Eagle Medium
DNBS	2,4-dinitrobenzenesulfinate
FCS	Fluorescence Correlation Spectroscopy
FLIM	Fluorescence Lifetime Imaging Microscopy
GG	Granada Green
GGDNPS	Granada Green Dinitrophenyl sulfonate
GSH	Glutathione
Hcy	Homocysteine
HeLa	Human epithelioid cervix carcinoma cells
HepG	Human Hepatocellular carcinoma cell line
LDH	Laser Diode Head
MOU	Main Optical Unit
NMM	N-methylmaleimide
NMR	Nuclear Magnetic Resonance Spectroscopy
NR	Non Radiative process
ROS	Reactive Oxygen Species
SPAD	Single Photon Avalanche Diodes
TCSPC	Time-correlated Single Photon Counting
TG	Tokyo Green
TLC	Thin Layer Cromatography

TTTR	Time Tagged Time-Resolved
UDPGT	Uridine Diphosphate Glucuronosyltransferase
UIS	Infinity-corrected optical System

SUMMARY

The main research topic of this Thesis is the development of new probes for specifically analytes detection. For this aim, Fluorescence has been the technique of choice because it achieves high level of sensitivity, specificity, simplicity and wide concentration range. Furthermore, it is also a non-invasive method and it is characterized by its low toxicity.

There are some biologically relevant analytes that are interesting to detect due to the fact that their deregulation is related to metabolic changes that promote damage in living organism. In this work it has been selected three analytes with clinical potential application, these are: **phosphate**, **biothiols** and **acetate** ions.

Phoshate anions participate in signal transduction and energy storage in cells and extracellular media. Apart from phosphate anions, biothiols are also widely present in living organisms and are relevant because changes in their normal levels cause cellular disorders and consequently, oxidative stress. The assay of phosphate intracellular measurement as a marker of bone cell differentiation and bone deposition combined with biothiol levels as a marker of cell stress would be a very helpful tool to detect pathological processes that combine both pathologies. In this work, it is described the design of a new molecule with the ability to measure these two parameters that has not been described to date.

For this goal, it has been synthesized a new xanthene-derived molecule that specifically detects phosphate and biothiols simultaneously. This dual probe reacts with biothiols by a thiolysis reaction at near neutral pH that makes changes in fluorescence intensity. The resulting released fluorescent moiety by the thiolysis, reacts simultaneously with phosphate anions in the excited state that elicits changes in fluorescence decay times. This new fluorescent probe has been tested in solution by using steady-state and time-resolved fluorescence and intracellularly by using

Fluorescence Imaging Microscopy (FLIM) in HeLa (Human epithelioid cervix carcinoma cells).

With the aim of studying in more depth cellular stress, this work reports also the design of a new molecule designed to optimize the intracellular biothiols detection for biomedical application and its use in bioimaging. Many cellular stresses are associated with oxidative stress and the response against these disorders cover a wide range of molecular changes that includes biothiols synthesis as a protective defence against its damaging effects. As a consequence, cellular stress study could let us understand better the molecular bases of cell damage. More specifically, it is described oxidative stress induced by light exposition in photoreceptor-derived (661W) cells. It is shown that light exposure time is related with fluorescence intensity response and as a result, with the presence of biothiols and oxidative stress. This field could be extended to develop tests for antioxidants drugs to prevent from oxidative diseases or treat them.

Furthermore, we have focused our attention on acetate as a potential analyte that is related to several epigenetic alterations, fundamentally due to changes in chromatin acetylation. It has been designed and synthesized some fluorescent compounds, based on the family of the so-cold Tokyo green dyes, as acetate fluorescent probes thanks to an excited state proton transfer (ESPT) reaction mediated by acetate. In order to achieve this aim, it is necessary that the fluorophore has a similar pK_a value to acetate. Once the compounds were synthesized, some experiments allowed us to select the best candidate for acetate detection. It has been also studied the reaction in the excited state and calculated the rate constants that rule the process. Moreover, the study has been carried out further and it has been checked the selected compound functionality in synthetic serum in order to use this compound in a future as a probe for the diagnosis in biological samples of some

cancer in which acetate is involved. In order to conduct this research, steady-state and time-resolved measurements has been performed.

GENERAL INTRODUCTION

GENERAL INTRODUCTION

Chapter 1: Xanthene derivatives

Many human diseases cause variations in metabolism which induce changes in molecule physiological concentration in cells. Studying the evolution of these analytes is a basic research line that provides useful information to understand better the diseases that are involved and consequently to find new therapeutic targets for new drugs. For this reason, the development of low toxic sensing probes for clinically interesting analytes detection is a very active field of research. There are different methodologies for analyte detection that can be approached. However, optical methods have been demonstrated to be very convenient. Prominent amongst these techniques are measurements based on infrared spectroscopy, ultraviolet and visible spectroscopy, molecular fluorescence, and Raman scattering.[1] Optical imaging with fluorescent probes is especially remarkable because of lower cost, portability and real-time capabilities. Furthermore, optical probes have a unique characteristic: they can be designed that do not emit light when they are unbound but they generate light upon internalization. Consequently, there is no background signal from activatable agents and the only signal generated comes from the binding of the dye with the specific molecular target. [2, 3]

1.1. Requirements needed for fluorescent probes

Fluorogenic molecules find wide utilities in biology[4, 5] being used as reporters for enzyme activity, sensors for analytes and agents for sophisticated imaging experiments, including super-resolution microscopy. More specifically, organic fluorophores are considered invaluable tools for biological application, and changes in their chemical structure, allow tuning and controling optical properties of the fluorophores.

Moreover, fluorescent molecules are considered a fundamental tool for bioimaging, a technique to create structural or functional images of living systems that enables to visualize biological processes in real time. In order to obtain effective

reaction-based fluorescent-probes for bioimaging application, stringent requirements are needed. A useful probe should respond selectively to its intended target in a complex biological system that contains a host of competing analytes. However, this ideal case is often complicated or perturbed by the presence of interfering species that may have similar or closely related reactivity or even identical functional groups, and/or higher working concentrations. Furthermore, another critical consideration is biocompatibility. For a reaction to be a suitable trigger for detection and imaging applications, it must proceed with reasonable kinetics in water under biological constraints of physiological pH. Finally, a useful reaction-based probe should be fully bioorthogonal: it must not interfere with endogenous cellular and tissue processes, and must generate products that are inert and non-toxic to living systems. [5] Success in this approach requires an understanding of the intrinsic reactivity of the target analyte in its biological setting.

Furthermore, high optical brightness is important to reduce the amount of probe needed for bioimaging experiments, which minimizes the potential for interference from endogenous cellular analytes and reactions. A turn-on emission increase or a shift in excitation/emission profiles is preferred over a turn-off quenching response. A turn-on response gives a bright signal against a dark background, which maximizes spatial resolution.

An appropriate fluorophore scaffold should also be non-toxic and have excitation and emission profiles in the visible or near-infrared region, or be suitable for two-photon excitation, in order to minimize sample damage or interference from autofluorescence. Finally, the balance between hydrophobicity and hydrophilicity should be considered in the context of membrane permeability, cellular retention and water solubility.

As a resume, the utility of a particular fluorophore is dictated by its specific chemical properties (e.g. reactivity, lipophilicity, pK_a, stability) and photophysical properties (e.g. λ_{max}, $\lambda_{em,}$ τ, ϵ, Φ).

1.2. Xanthene derived molecules

The well-known xanthene **Fluorescein** molecule was first synthesized by Baeyer in 1871. Fluorescein remains one of the most widely used fluorophores in modern biochemical, biological and medicinal research. It has several interesting properties in aqueous solution and it is used as tracer for many applications owing to its good spectral characteristics: high molar absorptivity and excellent quantum yield (0.92 at pH 9 in NaOH 0.1M). It is a versatile core dye that can be modified further to tune properties such as pK_a or excitation and/or emission wavelengths. At present there is a wide repertoire of Fluorescein derived molecules that are extensively used as tools for cellular biology studies. It is described below its most remarkable characteristics.

Fluorescein structure (Figure 1) could be divided into two parts: the benzoic acid moiety, as a photoinduced electron transfer (PeT) donor and the xanthene ring as the fluorophore, in which PeT might determine the fluorescence quantum yield Φ_F. [6, 7]

Considering its chemical structure, Fluorescein has four prototropic forms; i.e. cation, neutral, monoanion and dianion. It was described the reaction in the steady-state and it was shown that the four prototropic forms of Fluorescein are in equilibrium with each other and they can be detected by optical absorption spectra measurements. Furthermore, the concentration of the different Fluorescein prototropic forms can be predicted at any pH from chemical equilibrium theory and from the pK_a values for these different species.

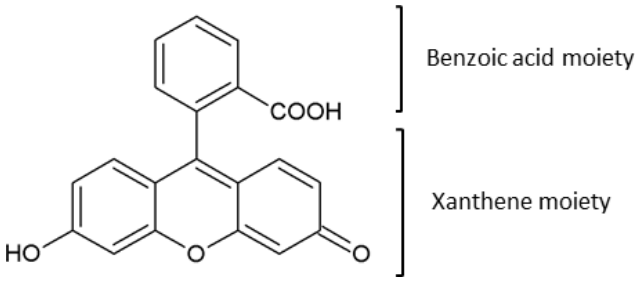

Figure1: Chemical structure of Fluorescein.

It is also really interesting the study of the excited state. When a Fluorescein solution is excited by a fast pulse of light the initial concentration of the different excited prototropic forms are not at equilibrium because of a preferential excitation of one of more of the forms and differences in the values of the equilibrium constants in the excited state (pK_a^*) compared to the ground state. Consequently, there is a tendency for the different excited forms to interconvert through excited-state proton reactions so as to achieve equilibrium during their lifetimes. Yguerabide and coworkers[8] showed that at low buffer concentrations the excited-state monoanion-dianion proton reaction of Fluorescein is too slow to have a significant effect on steady-state fluorescence intensity versus pH during the short lifetimes of theses anions. However, it was shown that in the presence of a suitable-proton donor acceptor, such as phosphate ions, the excited state monoanion-dianion proton transfer reaction occurs very efficiently and the decays of the excited monoanion and dianion become coupled.[9]

The presence of buffer mediated Excited State Proton Transfer (ESPT) reaction has important implications, since these excited-state reactions influence the decay traces from excited Fluorescein derivatives, showing complex kinetics and different decay times depending on both pH and buffer concentration. However, as

much Fluorescein in aqueous solution as in presence of a suitable buffer that promotes ESPT reaction, fluorescent decays of Fluorescein are biexponential at physiological pH what made difficult its application as a dye based on lifetime sensing, such as Fluorescence Lifetime measurement.[10, 11]

Other xanthene derivative frequently used as fluorescent indicator for near neutral pH measurements is **BCECF**, [2`,7`-bis-(2-carboxyethyl)-5-(and-6)-carboxyfluorescein]. In 2006, it was widely used as pH indicator for near-neutral intracellular detection because it was better retained in cells than Fluorescein. Because of its wide use, our group studied the excited-state dynamics of the molecular forms presented at near-neutral pH.[12] It was determined the rate constants of all excited-state processes and spectral parameters associated with excitation and emission. However, similar to Fluorescein, it presents a biexponential character of the fluorescence decays. This behaviour limits the use of BCECF dye as possible lifetime-based sensor because the close values of the two fluorescence decays prevent the use of the fluorescence lifetime imaging microscopy (FLIM) technique. Furthermore, while one of the coupled decay times depends on phosphate concentration, the other has practically no sensitiveness to phosphate. It was also reported that there was a critical influence of the ionic strength on the ground state apparent pK_a calculated through steady-state fluorescence measurements.

With the aim of getting beyond the limitation of Fluorescein, a big effort has been done with the objective of searching and developing new xanthenic dyes with improved spectral properties for specific purposes, for instance, the design probes for specific analyte detection. Accordingly, Urano and coworkers [13] discovered that the carboxylic group plays no role in the fluorescence properties of Fluorescein, contrary to what was believed to date, except to keep the benzene moiety and the fluorophore orthogonal to each other.

With this new knowledge, their first step was to synthesize a novel battery of Fluorescein derivatives in which the carboxylic was replaced with different groups. Here, they will be pointed some of them. Firstly the substitution by a methyl group (methyl **Tokyo Green**). Surprisingly, it showed similar fluorescent properties than Fluorescein with identical fluorescence quantum yield. Hence, this result suggested that the methyl group is sufficient to keep the benzene moiety and the fluorophore orthogonal to each other. Secondly, they synthesized also various derivatives whose electron density of the benzene moiety was tuned in a fine manner by introducing methyl and methoxy into the benzene moiety (2-Me-4-OMe TG and 2-OMe-5-Me TG). These group changes made Tokyo Green compounds reduced the number of prototropic species and consequently, the number of equilibria between them, but most interestingly of all, they made the new dyes have "on-off" character (i.e. one prototropic form has a negligible fluorescence and the other presents a high intensity). This is a very interesting and valuable behaviour and makes them very useful as biological fluorescent probes. Consequently, these two dyes were excellent candidates to be capable of under-going the characteristic buffer-mediated ESPT reaction with a single lifetime in the near neutral pH region due to the low quantum yield value of the neutral form, and therefore with an ESPT reaction analysis (mediated by a suitable proton donor acceptor) less complex than in Fluorescein.[14] After adding some electron-donating substituents on the pendant phenyl ring, they show a good advantage of being the construction of enzyme substrates with only one substrate moiety. These are the Tokyo Green substrates that show improved enzyme kinetics relative to di-substituted Fluorescein substrates and can be used for *in vivo* imaging. More specifically, they used a mouse tumor model to assess the practical utility of a Tokyo Green derived probe (AM-TG-Gal) which reacts with galactosidase. For this aim they labeled the tumors in the model with an avidin-galactosidase

conjugate. This conjugate was administered to the mice *in vivo* followed by AM-TG-Gal and subsequently they did *in ex vivo* fluorescence imaging.[15, 16]

As it has been mentioned previously the structure of Fluorescein can be modified farther to tune properties such as pK_a or excitation and/or emission wavelengths. For example 2`,7`-difluorofluorescein (**Oregon Green**) is less basic (pK_a=4.6) and maintains Fluorescein-like wavelengths and exhibits increased photostability relative to Fluorescein.[17] When other substituents are added such as chloride groups not only affects pH sensitivity but also elicits a bathochromic shift in excitation wavelength.[18] Examples of this include automated DNA sequencing dye 2`, 4, 7, 7`- tetrachlorohidrofluorescein (**TET**).

Moreover, Fluorescein is used as a tool for preparing indicator molecules, for example, it has been developed small molecule pH sensors based on Fluorescein sensitivity.[19] In order to report on the status of Fluorescein-labeled biomolecules, changes in the pK_a of Fluorescein have been used as index.[20] Adding to Fluorescein various chelating moieties creates sensors for important ions in biology: calcium,[21] sodium,[22] zinc,[23] palladium,[24] mercury,[25] fluoride ion [26] or nitric oxide.[27]

One molecule also interesting to describe and widely used as fluorophore is **Rhodamine** in which N-alkyl substitution can modify spectral characteristics. For instance, Rhodamine 110 (Rho_{110}) exhibits Fluorescein-like spectral properties. As it happened with Fluorescein, Rhodamine dyes have demonstrated to be useful for DNA sequencing. [28] Moreover, Rhodamine has been used to design indicators for ions such as sodium and calcium.[21, 29, 30]

Very recently synthesized molecule has been **Virginia Orange** which shows red-shifted wavelengths, shifted open closed equilibrium, and more physiologically suitable pK_a and could enable the design of smaller and single-input fluorogenic probes with fewer masking groups. This could help to solve size, hydrophobicity and solubility problems characteristics of some molecules.[31]

Finally, xanthene dyes that have only one added ring show interesting spectral properties. The asymmetry of these dyes can be engaged to construct ratiometric fluorescent pH and ion indicators.[32, 33]

As resume, taking Fluorescein and Rhodamine as model structures new and improved compounds have been synthesized during the last years that present varied photophysical characteristics. This work describes the specific design of some new “on-off” fluorescent dyes based on those previous works, their photophysical study and their use for analytes detection for different biological applications.

References

1. D. L. Andrews, in *The Optics Encyclopedia*, Wiley-VCH Verlag GmbH & Co. KGaA, 2007.
2. H. Kobayashi, M. Ogawa, R. Alford, P. L. Choyke and Y. Urano, *Chemical Reviews*, 2010, **110**, 2620-2640.
3. H. Kobayashi and P. L. Choyke, *Accounts of Chemical Research*, 2011, **44**, 83-90.
4. L. D. Lavis and R. T. Raines, *ACS Chem Biol*, 2008, **3**, 142-155.
5. J. Chan, S. C. Dodani and C. J. Chang, *Nat Chem*, 2012, **4**, 973-984.
6. T. Miura, Y. Urano, K. Tanaka, T. Nagano, K. Ohkubo and S. Fukuzumi, *J Am Chem Soc*, 2003, **125**, 8666-8671.
7. T. Ueno, Y. Urano, K. Setsukinai, H. Takakusa, H. Kojima, K. Kikuchi, K. Ohkubo, S. Fukuzumi and T. Nagano, *J Am Chem Soc*, 2004, **126**, 14079-14085.
8. J. Yguerabide, E. Talavera, J. M. Alvarez and B. Quintero, *Photochemistry and Photobiology*, 1994, **60**, 435-441.
9. J. M. Alvarez-Pez, L. Ballesteros, E. Talavera and J. Yguerabide, *J. Phys. Chem. A*, 2001, **105**, 6320-6332.
10. M. Bohmer, M. Wahl, H. J. Rahn, R. Erdmann and J. Enderlein, *Chemical Physics Letters*, 2002, **353**, 439-445.
11. J. Widengren, V. Kudryavtsev, M. Antonik, S. Berger, M. Gerken and C. A. M. Seidel, *Anal. Chem.*, 2006, **78**, 2039-2050.
12. N. Boens, W. Qin, N. Basaric, A. Orte, E. M. Talavera and J. M. Alvarez-Pez, *J. Phys. Chem. A*, 2006, **110**, 9334-9343.
13. Y. Urano, M. Kamiya, K. Kanda, T. Ueno, K. Hirose and T. Nagano, *Journal of the American Chemical Society*, 2005, **127**, 4888-4894.
14. L. Crovetto, J. M. Paredes, R. Rios, E. M. Talavera and J. M. Alvarez-Pez, *J. Phys. Chem. A*, 2007, **111**, 13311-13320.
15. Y. Urano, M. Kamiya, K. Kanda, T. Ueno, K. Hirose and T. Nagano, *J Am Chem Soc*, 2005, **127**, 4888-4894.
16. M. Kamiya, H. Kobayashi, Y. Hama, Y. Koyama, M. Bernardo, T. Nagano, P. L. Choyke and Y. Urano, *J Am Chem Soc*, 2007, **129**, 3918-3929.
17. W. C. Sun, K. R. Gee, D. H. Klaubert and R. P. Haugland, *J Org Chem*, 1997, **62**, 6469-6475.
18. N. O. Mchedlovpetrossyan, M. I. Rubtsov and L. L. Lukatskaya, *Dyes and Pigments*, 1992, **18**, 179-198.
19. M. L. Graber, D. C. DiLillo, B. L. Friedman and E. Pastoriza-Munoz, *Anal Biochem*, 1986, **156**, 202-212.
20. L. D. Lavis, T. J. Rutkoski and R. T. Raines, *Anal Chem*, 2007, **79**, 6775-6782.
21. A. Minta, J. P. Kao and R. Y. Tsien, *The Journal of biological chemistry*, 1989, **264**, 8171-8178.

22. V. V. Martin, A. Rothe and K. R. Gee, *Bioorganic & medicinal chemistry letters*, 2005, **15**, 1851-1855.
23. K. Kikuchi, K. Komatsu and T. Nagano, *Current opinion in chemical biology*, 2004, **8**, 182-191.
24. F. Song, A. L. Garner and K. Koide, *J Am Chem Soc*, 2007, **129**, 12354-12355.
25. S. Yoon, E. W. Miller, Q. He, P. H. Do and C. J. Chang, *Angew Chem Int Ed Engl*, 2007, **46**, 6658-6661.
26. X. F. Yang, S. J. Ye, Q. Bai and X. Q. Wang, *Journal of Fluorescence*, 2007, **17**, 81-87.
27. M. H. Lim and S. J. Lippard, *Accounts of Chemical Research*, 2007, **40**, 41-51.
28. L. G. Lee, S. L. Spurgeon, C. R. Heiner, S. C. Benson, B. B. Rosenblum, S. M. Menchen, R. J. Graham, A. Constantinescu, K. G. Upadhya and J. M. Cassel, *Nucleic acids research*, 1997, **25**, 2816-2822.
29. V. V. Martin, A. Rothe, Z. Diwu and K. R. Gee, Bioorganic & medicinal chemistry letters, 2004, 14, 5313-5316.
30. Y. Koide, Y. Urano and T. Nagano, Free Radical Bio Med, 2007, 43, S16-S16.
31. J. B. Grimm, T. D. Gruber, G. Ortiz, T. A. Brown and L. D. Lavis, Bioconjug Chem, 2016, 27, 474-480.
32. J. E. Whitaker, R. P. Haugland and F. G. Prendergast, Analytical Biochemistry, 1991, 194, 330-344.
33. C. J. Chang, J. Jaworski, E. M. Nolan, M. Sheng and S. J. Lippard, Proc Natl Acad Sci U S A, 2004, 101, 1129-1134.

GENERAL INTRODUCTION

Chapter 2: Interesting Analytes Detection

Multiple interesting analytes are involved on physiological and pathological processes. Their detection could help the study of some unknown metabolic and pathologic pathways. New discoveries on this field can make progress in the development of the design of new drugs. Fluorescence probes are excellent sensors for biomolecules, being sensitive, fast responding and capable of affording high spatial resolution via microscopic imaging. In this work, we have focused our attention on three clinically relevant analytes detection: phosphate, biothiols and acetate.

2.1 Phosphate

Phosphate is a charged particle that contains the mineral phosphorus. The body needs phosphorus to build and repair bones and teeth, help nerves function, and make muscles contract. Most (about 85%) of the phosphorus contained in phosphate is found in bones. The rest of it is stored in tissues throughout the body. Phosphate abnormal levels are related with disease. It is described that Hyperphosphatemia for example, has been independently linked with calcification of the coronary arteries and aorta,[1-3] as well as cardiovascular diseases and all-cause mortality in the setting of ESRD (end-stage renal-disease).[3] Intracellular phosphate is mostly bound or complexed to proteins and lipids and kinases and phosphatases make phosphate ions attach and detach from different molecules. The ability of cells to transport phosphate has long been recognised a requirement for mineralization in bone.[4] Phosphate ions play important roles in signal transduction and energy storage in biological systems and hence, the detection and quantification in cells and extracellular media are profitable parameters.[5-7]

2.2. Biothiols

Biothiols are some essential molecules for cell and tissue growth in living systems. Cysteine (Cys), Homocysteine (Hcy) and Glutathione (GSH) play important roles in cell defence that they act as antioxidants. Altered values of these biothiols are related to numerous diseases and hence, their detection in cells could be of interest to establish the relationship between their levels and these diseases.

Glutathione (GSH) is a water tripeptide composed of the amino acids gluthamine, cysteine, and glycine. GSH, the most abundant intracellular small molecule thiol, is an important antioxidant. Furthermore, GSH plays a role in other cellular reactions, including the glyoxalase system, reduction of ribonucleotides to deoxyribonucleotides, regulation of protein and gene expression via thiol: disulphide exchange reactions.[8] It is the principal non protein thiol component of the antioxidant defence system in the living cells. It protects the cellular constituents from the damaging effect of hydroperoxides formed during the normal metabolism.[9] Free glutathione is present mainly in its reduced form, which can be converted to the oxidized form during oxidative stress, and can be reverted to the reduced form by the action of the enzyme glutathione reductase. The redox status depends on the relative amounts of the reduced and oxidized forms of glutathione (GSH/GSSG) and appears to be a critical determinant in cells.[10] A deficiency of GSH puts the cell at risk for oxidative damage and an imbalance of GSH is observed in a wide range of pathologies, including, cancer, neurodegenerative disorders, cystic fibrosis, HIV and aging.

On the other hand, cysteine plays many important roles in living systems. The deficiency of this compound causes many diseases, such as slowed growth in children, depigmentation of hair, edema, lethargy, liver damage, skin lesions and weakness.[11] Cysteine controls nitrogen balance and maintains body cell mass. A

dysregulation of the cysteine catabolism is associated with excessive urea production and it also decreases plasma glutamine levels, development of skeletal muscle wasting and immuno-deficiencies in several diseases of unrelated etiology.[12] Cysteine has a cytotoxic effect in vitro against several cell types. Cysteine supports superoxide-mediated modification of LDL which may facilitate foam cell formation. Finally, cysteine forms an adduct with nitric oxide and may thereby impair endothelial function.[13]

Cysteine, homocysteine and other amino thiols exist in plasma in reduced oxidized and protein-bound forms interacting with each other through redox and disulphide exchange reactions. High levels of total Homocysteine cause complex changes in total Cysteine and the overall aminothiol status in plasma.[14] It is also reported that increased concentration of homocysteine induce secondary effects on redox status and protein binding of other aminothiols.[15] An elevated level of total homocysteine in blood is a prevalent and strong risk factor for atherosclerotic vascular disease in the coronary, cerebral and peripheral vessels, and for arterial and venous thromboembolism.[16] It is related to pregnancy complications,[17] neural tube defects[18] and cognitive impairment in the elderly.[19] Furthermore, there are studies that provide ample evidence that an elevated total Homocysteine level is a common cardiovascular risk factor in the general population. [20, 21]

2.3. Acetate

Acetate is a type of anion, salt or ester derived from the compound acetic acid. Acetate is easily taken up by cells and converted by acetyl-CoA synthetase 2 enzyme (ACSS2) to acetyl-CoA, a common metabolic intermediate for synthesis of cholesterol and fatty acids which are the principal components of the cell membrane in mammals.[22] Acetate has been reported to be a promising imaging tracer for tumors, in prostate cancer [23] but also in one of the most prevalent cancer in the

world, colorectal cancer. It is described that acetate induces apoptosis and inhibits cell proliferation in colorectal cancer cells.[24] Furthermore, some data suggest that the ability to oxidize acetate is either a unique adaptation to the brain microenvironment or a more general property of tumor cells. Under normal resting conditions, circulating acetate levels may contribute up to 10%-15% of the basal energy demands of brain astrocytes.[25] In order for the tumor cell to metabolize acetate the cell must upregulate acetyl-CoA synthetase 2 enzyme. The upregulation of this enzyme is linked to an increase in acetate oxidation by the tumor.[26]

References

1. P. Raggi, A. Boulay, S. Chasan-Taber, N. Amin, M. Dillon, S. K. Burke and G. M. Chertow, Journal of the American College of Cardiology, 2002, 39, 695-701.
2. W. G. Goodman, J. Goldin, B. D. Kuizon, C. Yoon, B. Gales, D. Sider, Y. Wang, J. Chung, A. Emerick, L. Greaser, R. M. Elashoff and I. B. Salusky, New Engl J Med, 2000, 342, 1478-1483.
3. G. A. Block, T. E. Hulbert-Shearon, N. W. Levin and F. K. Port, American journal of kidney diseases : the official journal of the National Kidney Foundation, 1998, 31, 607-617.
4. G. R. Beck, B. Zerler and E. Moran, Proceedings of the National Academy of Sciences of the United States of America, 2000, 97, 8352-8357.
5. N. Majed, Y. Li and A. Z. Gu, Current opinion in biotechnology, 2012, 23, 852-859.
6. S. Khoshniat, A. Bourgine, M. Julien, P. Weiss, J. Guicheux and L. Beck, Cellular and molecular life sciences : CMLS, 2011, 68, 205-218.
7. C. Bergwitz and H. Juppner, Adv Chronic Kidney D, 2011, 18, 132-144.
8. D. M. Townsend, K. D. Tew and H. Tapiero, Biomedicine & pharmacotherapy = Biomedecine & pharmacotherapie, 2003, 57, 145-155.
9. C. Perricone, C. De Carolis and R. Perricone, Autoimmunity reviews, 2009, 8, 697-701.
10. A. Pastore, G. Federici, E. Bertini and F. Piemonte, Clinica chimica acta; international journal of clinical chemistry, 2003, 333, 19-39.
11. S. Shahrokhian, Anal Chem, 2001, 73, 5972-5978.
12. W. Droge and E. Holm, FASEB journal : official publication of the Federation of American Societies for Experimental Biology, 1997, 11, 1077-1089.
13. L. El-Khairy, P. M. Ueland, H. Refsum, I. M. Graham, S. E. Vollset and P. European Concerted Action, Circulation, 2001, 103, 2544-2549.
14. M. A. Mansoor, A. B. Guttormsen, T. Fiskerstrand, H. Refsum, P. M. Ueland and A. M. Svardal, Clinical chemistry, 1993, 39, 980-985.
15. P. M. Ueland, Clinical chemistry, 1995, 41, 340-342.
16. H. Refsum, P. M. Ueland, O. Nygard and S. E. Vollset, Annual review of medicine, 1998, 49, 31-62.
17. R. P. Steegers-Theunissen, G. H. Boers, H. J. Blom, F. J. Trijbels and T. K. Eskes, Lancet, 1992, 339, 1122-1123.
18. R. P. Steegers-Theunissen, G. H. Boers, F. J. Trijbels, J. D. Finkelstein, H. J. Blom, C. M. Thomas, G. F. Borm, M. G. Wouters and T. K. Eskes, Metabolism: clinical and experimental, 1994, 43, 1475-1480.

19. S. Seshadri, A. Beiser, J. Selhub, P. F. Jacques, I. H. Rosenberg, R. B. D'Agostino, P. W. Wilson and P. A. Wolf, The New England journal of medicine, 2002, 346, 476-483.
20. O. Nygard, S. E. Vollset, H. Refsum, L. Brattstrom and P. M. Ueland, Journal of internal medicine, 1999, 246, 425-454.
21. C. J. Boushey, S. A. Beresford, G. S. Omenn and A. G. Motulsky, Jama, 1995, 274, 1049-1057.
22. M. Yoshimoto, A. Waki, Y. Yonekura, N. Sadato, T. Murata, N. Omata, N. Takahashi, M. J. Welch and Y. Fujibayashi, Nuclear medicine and biology, 2001, 28, 117-122.
23. R. L. Wahl, J. Harney, G. Hutchins and H. B. Grossman, The Journal of urology, 1991, 146, 1470-1474.
24. C. Marques, C. S. Oliveira, S. Alves, S. R. Chaves, O. P. Coutinho, M. Corte-Real and A. Preto, Cell death & disease, 2013, 4, e507.
25. G. A. Dienel and N. F. Cruz, Neurochemistry international, 2006, 48, 586-595.
26. T. Mashimo, K. Pichumani, V. Vemireddy, K. J. Hatanpaa, D. K. Singh, S. Sirasanagandla, S. Nannepaga, S. G. Piccirillo, Z. Kovacs, C. Foong, Z. Huang, S. Barnett, B. E. Mickey, R. J. DeBerardinis, B. P. Tu, E. A. Maher and R. M. Bachoo, Cell, 2014, 159, 1603-1614.

GENERAL INTRODUCTION

Chapter 3: Buffer mediated Excited State Proton Transfer (ESPT) Reaction

Fluorophores can undergo chemical reactions while in the excited state. Such reactions occur because light absorption frequently changes the electron distribution within a fluorophore, which in turn changes its chemical or physical properties.[1] These interactions are not restricted to ionization. Many dynamic processes that affect fluorescence can be interpreted in terms of excited-state reactions. These processes include resonance energy transfer and excimer formation. Excited-state processes display characteristic time-dependent decays that can be unambiguously assigned to the presence of an excited-state process. Previously studies concluded that perhaps the most dominant type of an excited-state reaction is the loss or gain of protons.[2-9]

3.1. Excited State Proton Transfer (ESPT) reaction in the presence of a proton donor/acceptor

3.1.1. Background

Since the works of Föster *(1949)* and Weller *(1961)*, the study of ESPT reactions has been reviewed multiple times. Most of these reviews have described dyes than can undergo reversible ESPT processes in aqueous solution based on photoacids or photobases. However, very few have considered the need for a suitable proton donor/acceptor for the reaction to progress. In previous pioneering works it was described phosphate-mediated ESPT reaction of fluorescein. It was shown that in the presence of 1M phosphate buffer that behaves as a suitable proton donor-acceptor and at near-neutral pH, the proton donor reaction between two prototropic forms (monoanion and dianion) of fluorescein occurs very efficiently in the excited state, and their fluorescence decays become coupled. In contrast, at low buffer concentrations (5mM Phosphate buffer or less) the excited monoanion and dianion are not coupled via ESPT and hence decay independently of each other.[10, 11] As fluorescein has strong spectral that overlaps over absorption and emission spectra

of the two anionic forms and due to the fact that fluorescence pK_a values in the excited and ground state are very similar, the study of ESPT reactions between the mono and dianion of fluorescein is challenging. The method of choice to full characterize the ESPT is Global Compartment Analysis (GCA), an advanced method of analysis that allows the determination of the rate constants of the full ESPT kinetic scheme and the associated absorption and emission spectral parameters.[12] Global Compartment Analysis permits the establishment of a rational design for the experimental conditions to ensure full characterization of the kinetic system.[13]

As it has been described in *Chapter 1 "Xanthene derivatives"*, Urano and coworkers[14] replaced the carboxylic group of fluorescein with different groups because they discovered that it showed similar fluorescent properties than fluorescein with identical fluorescence quantum yield. Furthermore, they synthesized some derivatives called **2-Me-4-OMe TG** and **2-OMe-5-Me TG** that presented "on-off" behaviour. These two probes were able to undergo with a single lifetime the buffer-mediated ESPT reaction near neutral pH.

To fully understand the complex photophysics of these new "on-off" derivatives, our group expound on the excited state dynamics of the prototropic forms present at near physiological pH of these two TG compounds (2-Me-4-OMe TG and 2-OMe-5-Me TG) in the presence of phosphate buffer in the pH range between 5 and 10.[15, 16] The results showed that both undergo the characteristic ESPT reaction, in which the coupled fluorescence decay exhibits a phosphate-sensitive component on the order of nanoseconds and a second component on the order of subnanoseconds whose values become negligible at pH and buffer concentration greater than 6 and 0.02M respectively. Furthermore, around physiological pH, the larger decay time (only measurable at that conditions) was sensitive to the phosphate concentration, while the presence of other ions not involved in the proton transfer reaction had a

negligible on the fluorescence decay time.[17] Therefore, the changes in the fluorescence were considered a possible direct means of investigating the environmental phosphate concentration in a small volume at near neutral pH.

The ability of 2-Me-4-OMe TG to undergo phosphate-mediated ESPT was used to investigate the intracellular phosphate concentration at physiological pH in live cells.[18] Despite this remarkable achievement, the low pK_a of this dye (around 6.00) provided a limited sensitivity in physiological conditions. It was known that the dependence of the recovered long decay times from aqueous solutions of 2-Me-4-OMe TG on the phosphate concentration increases when the pH of the medium is near to the pK_a of the dye. To solve this issue, it is necessary to increase the pK_a of the probe. One strategy to achieve this is to incorporate other aliphatic electron donating groups without modifying the optical properties of the dye. Fluorescein, pK_a 6.43; BCECF, pK_a 6.98; DHCF, pK_a 6.60; and DEF, 6.61 were taking as reference to add alkyl groups to the xanthene core.

In 2004 our group designed **9-alkyl xanthenones** with different aliphatic pendant groups and studied their photophysical characteristics[19] and some of them retained similar properties to those of fluorescein including the characteristic phosphate-mediated ESPT reaction and higher pK_a values (6.20-6.67) compared with TGs (5.97-6.04).

All these studies helped to design **Granada Green** compound [9-1-(4-tert-butyl-2-methoxyphenil)]-6-hydroxy-3H-xanthen-3-one, a tailor-made TG-type fluorescein that shows low acidity with a pH closer to physiological pH (pK_a 7.39) for the neutral and anion equilibrium.[20] This compound also showed the same phosphate-mediated reaction in the excited state as done fluorescein and its derivatives, giving rise to fluorescence decay traces that are dependent on the phosphate concentration in the medium. It had also the ability to detect a wider

range of phosphate concentrations along with additional slight increase in sensitive so it was probed in cells and it showed intracellular phosphate concentration changes.

Apart from phosphate mediated ESPT reactions Orte et al also studied acetate mediated ESPT reactions and it helped to characterize the species involved.[21] The compound used for this aim was 2`,7`-difluorofluorescein (**Oregon Green 488, OG488**). Two fluorine atoms imparted higher polarity to the molecule, lessening pK_a value achieving the optimal situation for ESPT reaction in which the buffer and the dye have a similar pK_a. Unfortunately, OG488 does not presents "on-off" properties, and previously reported xanthene-based dyes with this remarkable characteristic present an unsuitable pK_a value of around 7 for acetate sensing for an ESPT reaction. In 2006[22] it was reported the synthesis of a fluorophore called Pennsylvania Green. This compound melted the pH insensitivity and photostability of Oregon Green with the hydrophobicity of Tokyo Green. Based on Pennsylvania Green compound, we have designed in this work some new compounds and do their full photophysical study with the purpose of selecting a candidate that best described the reaction with acetate in the excited state.

3.1.2. Excited State Proton Transfer Reaction scheme

Introducing a proton acceptor/donor transfer in an ESPT reaction kinetic scheme involves considerable changes in the equations. The mentioned kinetic scheme is showed below (scheme 3.1) and it is based on a compartmental system for two states ESPT reaction and promoted by a proton donor/acceptor.

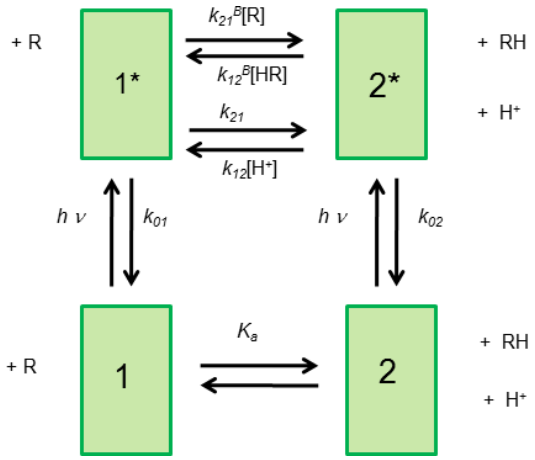

Figure 2: The kinetic scheme of the buffer-mediated ESPT reaction.

Species 1 and 2 are the molecules in the ground-state. Photoexcitation creates the excited-state species 1* and 2*. The composite rate constants for these processes are denoted by $k_{01}(= k_{F1} + k_{NR1})$ and $k_{02}(= k_{F2} + k_{NR2})$. k_{12} and k_{21} represent the excited-state deprotonation and protonation rate constants, respectively. The buffer acid and base species are denoted by HR and R, respectively, and may act as suitable proton donors/acceptors for the buffer-mediated excited-state protonation (k_{21}^{B}) and deprotonation (k_{21}^{B}).

We consider an intermolecular, dynamic, linear and time-independent system which consists of two types of species of the compound of interest in the ground state, with their corresponding species in the excited state.

Electromagnetic radiation excitation creates the excited species 1* and 2* which can decay via fluorescence (*F*) and non-radiative (*NR*) processes which include internal conversion and intersystem crossing. The composite rate constants for these processes are denoted by $k_{01}(= k_{F1} + k_{NR1})$ and $k_{02}(= k_{F2} + k_{NR2})$. The rate constant of the deactivation processes for 1* specie is given by $k_{01} = k_{F1} + k_{NR1}$.

k_{21} represents 1* → 2*+ H^+ unimolecular dissociation kinetic constant, while k_{12} represents the second order constant for the association 2*+ H^+ → 1*. k_{21}^B and k_{12}^B are the kinetic constants for the excited state proton transfer reaction mediated by the proton donor-acceptor. k_{21}^B is the second order constant for 1*+ R → 2*+ RH and k_{12}^B is the second order constant for the inverse reaction 2*+ RH → 1*+ R. All these constants are positive. Acid and basic proton donor/acceptor forms which are represented by RH and R respectively do not affect 1 and 2 ground state balance.

Once the rate constants are known the model equations permit the prediction of the fluorescence decay times as a function of the pH and total buffer concentration and the comparison of these predicted values with the experimental values.[23]

3.1.3. Rate constants calculation

The convolution integral used for the analysis of experimental decay curves is the following one:

$$F(t) = \int_o^t L(t-t')I(t')dt' \quad (1)$$

Where $F(t)$ is the experimentally measured decay curve, $L(t)$ is the time profile of the exciting light pulse, and $I(t)$ is the law of decay of the sample when excited by an instantaneous pulse of light. We assume that $I(t)$ can be expressed as a sum of n exponential functions with n lifetimes as shown in the following expression.

$$I\,(t) = A + \sum_i^n \alpha_i e^{-(t+\delta t)/\tau_i} \quad (2)$$

Where τ_i is the i^{th} lifetime, α_i is the preexponential or weighting coefficient, *A* is a background term, and δt is a temporal shift term. The temporal shift δt is used

to compensate for a small time shift in the leading edge of the decay curve, relative to the recorded lamp time profile, due to differences in the wavelengths of the emission and excitation wavelengths. The equations described above are curve fitted to the different experimental $F(t)$ vs t graphs by non-linear least-squares analysis using the Marquardt algorithm.

In order to increase the precision of the analysis of $F(t)$ graphs it is very common to apply the method of "global" analysis in which more than one fluorescence decay graph is used simultaneously in the nonlinear analysis with eqs (1) and (2). This method of analysis significantly increases the reliability of the evaluated weighting coefficients and lifetimes.

We denote the first-order rate constant for the dissociation of 2* into 1* and H^+ by k_{21} and the bimolecular rate constant for the reverse reaction by k_{12}. The solution of the coupled differential rate equations are the well-known biexponential expressions:

$$[1^*] = \beta_{1S} e^{\gamma_S t} + \beta_{1L} e^{\gamma_L t} \tag{3}$$

$$[2^*] = \beta_{2S} e^{\gamma_S t} + \beta_{2L} e^{\gamma_L t} \tag{4}$$

Where

$$\gamma_{S,L} = \frac{(-\mathrm{a}+\mathrm{c}) \pm \sqrt{(\mathrm{c}-a^2)+4bd}}{2} \tag{5}$$

And $a = k_1 + k_{21} + \mathrm{k}_{21}^{B}[R]$; $b = k_{12}[H^+] + \mathrm{k}_{12}^{\mathrm{B}}[RH]$; $c = k_2 + k_{12}[H^+] + \mathrm{k}_{12}^{B}[RH]$; $d = k_{21} + \mathrm{k}_{21}^{B}[R]$. [*R*] and [*RH*] are related to total buffer concentration, $C_{RH} = [R] + [RH]$, by the expressions $RH = C_{RH}[H^+]/([H^+] + K_{RH})$ and $[R] = C_{RH}K_{RH}/([H^+] + K_{RH})$ where K_{RH} is the dissociation constant for reversible reaction $RH \leftrightarrows [R] + [H^+]$.

The γ factors are related to the lifetimes τ_s and τ_L by the expression:

$$\tau_{S,L} = \frac{-1}{\gamma_{S,L}} \quad (6)$$

Where S and L refer to short and long lifetimes.

References

1. J. R. Lakowicz, *Principles of Fluorescence Spectroscopy*, 3rd edn., Springer, 2006.
2. L. M. Tolbert and K. M. Solntsev, *Acc Chem Res*, 2002, **35**, 19-27.
3. B. Cohen, D. Huppert and N. Agmon, *J Phys Chem A*, 2001, **105**, 7165-7173.
4. R. Yang and S. G. Schulman, *Journal of Fluorescence*, 2001, **11**, 109-112.
5. P. Leiderman, L. Genosar, N. Koifman and D. Huppert, *J Phys Chem A*, 2004, **108**, 2559-2566.
6. A. Mironczyk, A. Jankowski, A. Chyla, A. Ozyhar and P. Dobryszycki, *J Phys Chem A*, 2004, **108**, 5308-5314.
7. B. Cohen and D. Huppert, *J Phys Chem A*, 2001, **105**, 7157-7164.
8. M. H. Kleinman, J. H. Flory, D. A. Tomalia and N. J. Turro, *Journal of Physical Chemistry B*, 2000, **104**, 11472-11479.
9. P. Wan and D. Shukla, *Chemical Reviews*, 1993, **93**, 571-584.
10. J. Yguerabide, E. Talavera, J. M. Alvarez and B. Quintero, *Photochemistry and Photobiology*, 1994, **60**, 435-441.
11. J. M. Alvarez-Pez, L. Ballesteros, E. Talavera and J. Yguerabide, *J. Phys. Chem. A*, 2001, **105**, 6320-6332.
12. L. Crovetto, A. Orte, E. M. Talavera, J. M. Alvarez-Pez, M. Cotlet, J. Thielemans, F. C. De Schryver and N. Boens, *J. Phys. Chem. B*, 2004, **108**, 6082-6092.
13. N. Boens, N. Basaric, E. Novikov, L. Crovetto, A. Orte, E. M. Talavera and J. M. Alvarez-Pez, *J. Phys. Chem. A*, 2004, **108**, 8180-8189.
14. Y. Urano, M. Kamiya, K. Kanda, T. Ueno, K. Hirose and T. Nagano, *J Am Chem Soc*, 2005, **127**, 4888-4894.
15. J. M. Paredes, L. Crovetto, R. Rios, A. Orte, J. M. Alvarez-Pez and E. M. Talavera, *Phys. Chem. Chem. Phys.*, 2009, **11**, 5400-5407.
16. L. Crovetto, J. M. Paredes, R. Rios, E. M. Talavera and J. M. Alvarez-Pez, *J. Phys. Chem. A*, 2007, **111**, 13311-13320.
17. J. M. Paredes, A. Garzon, L. Crovetto, A. Orte, S. G. Lopez and J. M. Alvarez-Pez, *Physical Chemistry Chemical Physics*, 2012, **14**, 5795-5800.
18. J. M. Paredes, M. D. Giron, M. J. Ruedas-Rama, A. Orte, L. Crovetto, E. M. Talavera, R. Salto and J. M. Alvarez-Pez, *Journal of Physical Chemistry B*, 2013, **117**, 8143-8149.
19. A. Martinez-Peragon, D. Miguel, R. Jurado, J. Justicia, J. M. Alvarez-Pez, J. M. Cuerva and L. Crovetto, *Chemistry*, 2014, **20**, 447-455.
20. A. Martinez-Peragon, D. Miguel, A. Orte, A. J. Mota, M. J. Ruedas-Rama, J. Justicia, J. M. Alvarez-Pez, J. M. Cuerva and L. Crovetto, *Organic & biomolecular chemistry*, 2014, **12**, 6432-6439.

21. A. Orte, R. Bermejo, E. M. Talavera, L. Crovetto and J. M. Alvarez-Pez, *J. Phys. Chem. A*, 2005, **109**, 2840-2846.
22. L. F. Mottram, S. Boonyarattanakalin, R. E. Kovel and B. R. Peterson, *Org Lett*, 2006, **8**, 581-584.
23. M. J. Ruedas-Rama, J. M. Alvarez-Pez, L. Crovetto, J. M. Paredes and A. Orte, in *Advanced Photon Counting: Applications, Methods, Instrumentation*, eds. P. Kapusta, M. Wahl and R. Erdmann, Springer International Publishing, Cham, 2015, pp. 191-223.

GENERAL INTRODUCTION

Chapter 4: Fluorescence Lifetime Imaging Microscopy

Fluorescence Lifetime Imaging Microscopy (FLIM) is a technique for producing an image based on the measurements of the decay rate of the emission from a fluorescent sample. Thus, in contrast with the intensity-based fluorescent images, FLIM is a fluorescence imaging technique based on the lifetime of individual fluorophores rather than their emission spectra. The fluorescence lifetime is defined as the time a molecule remains in the excited state before returning to the ground state by emitting a photon and it is characteristic for every dye and its environment. FLIM produces an image based on the differences in the excited state decay rate from a fluorescent sample. The local environment determines the fluorescence lifetime, in which is then used to calculate an image. FLIM is an excellent alternative to fluorescence intensity and fluorescence ratiometric measurements because overcome some limitations from the intensity-based methods, like it is concentration independent and only a single excitation wavelength/emission interval is required.[1] Supposing that the lifetime of a probe changes in response to pH or some analyte, when the lifetime is measured this value can be used to determine the analyte concentration, and the determination will be independent of probe concentration.[2] As the fluorescence lifetime does not depend on concentration, absorption by the sample, sample thickness, photo-bleaching and/or excitation intensity it is more robust than intensity based methods. Additionally, fluorescence lifetime measurements have the advantage to be not influenced by internal settings of the instrument like laser intensity or detector gain. At the same time, the fluorescence lifetime depends on a wealth of environmental parameters such as pH, ion or oxygen concentration, molecular binding or the proximity of energy acceptors making it the technique of choice for functional imaging of many kinds.

The images produced by the microscope are converted into digital form for storage, analysis, or processing prior to display and interpretation.[3] Digital processing is used to extract quantitative information about the specimen from the microscope

image, and it transforms an image so that a displayed version is much more informative than it would otherwise be.[4, 5] It is not only a natural extension but is proving to be essential to the success of subsequent data analysis and interpretation of the new generation of microscope images. There is some microscope imaging modalities in which any suitable image for viewing is only available after digital image processing. Digital processing of microscope images has opened up new realms of medical research and brought about the possibility of advanced clinical diagnostic procedures.[6]

In order to determine the fluorescence lifetime, Time-Correlated Single Photon Counting (TCSPC) is used. In TCSPC, it is measured the time between the sample excitation by a pulsed laser and the arrival of the emitted photon at the detector. TCSPC requires a defined “start”, provided by the electronics steering the laser pulse or a photodiode, and a defined “stop” signal, realized by detection with single-photon sensitive detectors (e.g. Single Photon Avalanche Diodes, SPADs). The measurement of this time delay is repeated many times to account for the statistical nature of the fluorophores emission.

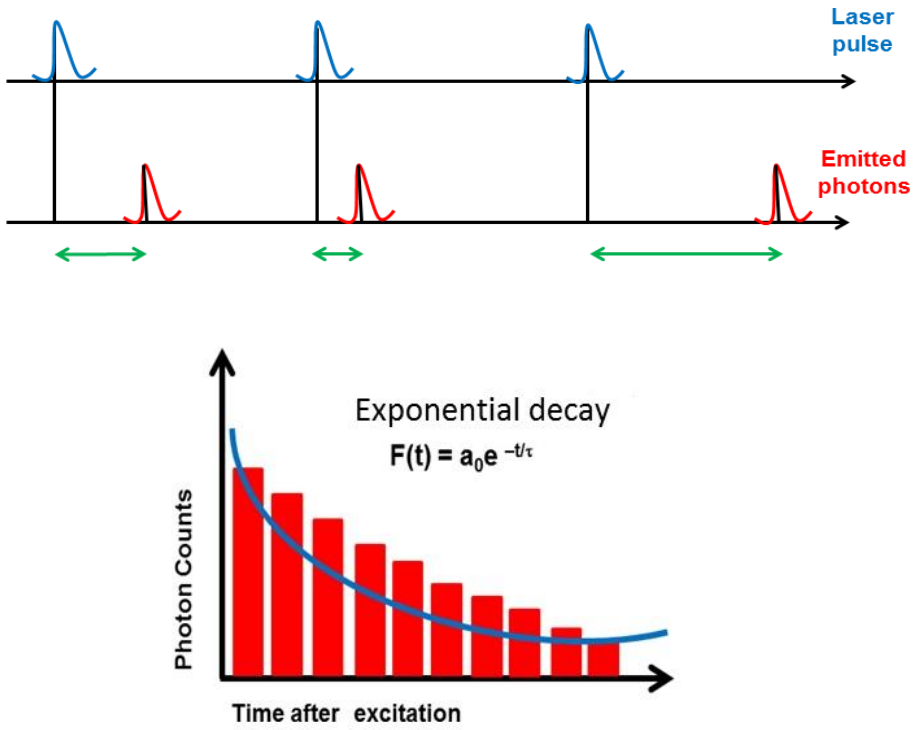

Figure 3: Time-Correlated Single Photon Counting (TCSPC) procedure scheme.

The emission of a fluorescence photon from a fluorophore does not occur at a fixed time (green arrows). Instead it is observed some moment distribution that can be described by an exponential decay function. The time constant characteristic of the decay is the time fluorescence. The delay times are sorted into a histogram that plots the occurrence of emission over time after the excitation pulse.

As it has been said, FLIM combines fluorescence lifetime measurements with images obtaining. In order to acquire a fluorescence lifetime image, the photons have to be attributed to the different pixels and it is done by storing the absolute arrival times of the photons additionally to the relative arrival time in respect to the laser pulse. Line and frame marker signals from the scanner of the confocal microscope are

additionally recorded in order to sort the time stream of photons into the different pixels. By this form, FLIM provide information about the space distribution of the fluorescence molecule with information about its nanoenviroment.

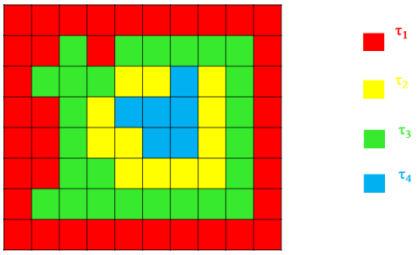

Figure 4: FLIM image example. Fluorescence lifetimes are codified by colours producing an image.

Consequently the essential components of a FLIM set-up are:

- Pulsed laser source (diode lasers or multi-photon excitation)
- Single photon sensitive detector
- Dichroic mirror (to separate fluorescence signal from excitation light)
- Objective (to focus the excitation light into the sample and collect fluorescence signal)
- TCSPC unit to measure the time between excitation and fluorescence emission

References

1. M. Y. Berezin and S. Achilefu, *Chem. Rev.*, 2010, **110**, 2641-2684.
2. J. R. Lakowicz, *Principles of Fluorescence Spectroscopy*, 3rd edn., Springer, 2006.
3. G. Sluder and D. E. Wolf, *Method Cell Biol*, 2013, **114**, Xix-Xx.
4. P. Kapusta, *Advanced Photon Counting*, 2015.
5. A. Diaspro, *Confocal and Two-Photon Microscopy: Foundations, Applications and Advances*, 2001.
6. K. R. Castleman and I. T. Young, in *Microscope Image Processing*, Academic Press, Burlington, 2008, pp. 1-9.

AIM OF THE THESIS AND SPECIFIC OBJECTIVES

The aim of this thesis is the design, synthesis and photophysical study of new fluorescent dyes for biologically relevant molecules detection. The analytes of interest are phosphate, biothiols and acetate and these are the specific objectives for the dyes designed capable to detect the mentioned molecules:

Biological thiols and Phosphate anions probe:

- Do the photophysical study (absorption and fluorescence spectroscopy, fluorescence lifetime measurements).
- Check the efficiency for detecting phosphate and biothiols in human epithelioid cervix carcinoma (HeLa) cell line.

Biological thiols probe for oxidative stress detection

- Do the photophysical study (absorption and fluorescence spectroscopy).
- Check the efficiency in photoreceptor cells for stress detection through biothiols response under light exposure condition.

Acetate Probe:

- Do the photophysical study (absorption and fluorescence spectroscopy, quantum yield and acid dissociation constant in the ground state calculation, fluorescence lifetime measurements).
- Study the Excited State Proton Transfer reaction (ESPT) and calculate the kinetic constants that rule the process.
- Check the capability of the dye for detecting acetate changes in synthetic serum.

INSTRUMENTATION

In this section it is described the instrumentation used for the experiments done in this work.

1. pH Meter

pH measurements have been done with a pH-meter Crison pH-Meter BASIC 20+ that permits measurements from -2 to 16, mV: ±2000, -20-150° temperature. For its calibration they have been used Crison standard tampons: 4.01, 7 and 9.21. Measure error (± 1 digit): ≥ 0.01 pH, ≥ 1mV, ≥ 0.2°.

2. Balance

It has been used an electronic analytical Sartorious Balance A-120 S model provided with an internal and external calibration system. It has a standard deviation ± 0.1 mg and 3s time-response.

3. Absorption Spectrophotometer

Absorption spectra were recorded on a Perkin-Elmer Lambda 650 UV/Vis spectrophotometer with a temperature-controlled cell and it has a 0.17 nm UV/Vis resolution. It is a dual sampling compartment spectrophotometer and it is compatible with transmission and reflectance measurements. It is possible to work from 190-900 nm wavelengths. It has an automated polarizer/depolarizer drive in the large sample compartment that provides further depolarization or allows of oriented samples with polarized light. It is equipped with a beam depolarizer that corrects instruments bias. It has a deuterium and tungsten halogen light source which is prealigned and prefocused for quick replacement and maximum uptime and there are double holographic grating monochromators for ultra-low stray light performance. The system and all the components that are part of it are controlled by a computer that is provided of some software to control the system.

4. Steady State Spectrofluorometer

Steady state fluorescence spectra were recorded using a Jasco FP-8300 Spectrofluorometer. It is specifically designed for bio-applications and it is controlled by external software called Spectra Manager.

Synchronization of the spectra is possible with a wavelength or constant energy difference. The light source is a Xenon lamp with shielded lamp house of 150 W. The detector is a silicon photodiode for excitation and a photomultiplier for emission with a wavelength covering from 200 to 900 nm. Measurements repeatability is $\pm$ 1 nm and a signal to noise ratio for Raman peak of water higher than 170:1 (peak to peak) and higher than 680:1 (rms) at 350 nm excitation wavelength, 2 s response time and 5 nm excitation and emission monochromator bandwidths. It is possible to select the slit band width between these values: 1, 2.5, 5, 10, 20 nm for excitation and emission. Wavelength scan speed is also a controllable parameter, speed from 20 to 20000 nm/min, it depends on the response and sensitivity selected. It is also possible to select filters for different wavelengths or transmittance attenuator. It has a 10 mm rectangular cell holder as sample compartment and it is nitrogen purgeable. For spectral correction there is a beam splitter that passes part of the incident current though a reference photodiode for excitation correction in contrast, some fields provided by the manufacturer itself by the software correct the emission.

5. Time-Resolved Fluorometer

Time-resolved fluorescence measurements were done in FluoTime 200 instrument (PicoQuant GmbH) based on Time-correlated single photon counting (TCSPC) and provided with an excitation laser. In the next lines are described the laser excitation source and TCPC system.

- Laser excitation source: the excitation source consists of a pulsed high-power picosecond diode laser (LDH-485, PicoQuant GmbH; LDH-440, PicoQuant GmbH). The laser source provides a pulse train of up to 40MHz and a pulse-width with a minimum amplitude of 40 ps. The emission wavelength of the laser is 483 nm and 438 nm respectively thanks to the generation of the second harmonic of the primary laser source. The excitation source is accompanied by a controller system PDL 800 B (PicoQuant GmbH), which has a crystal oscillator that generates fluctuations lower than the mother frequency. Hence, allows the frequency of repetition of the laser pulse to be divided between binary factors (1, 2, 4, 8 or 16) it allows generating a range of pulse frequencies of 40, 20, 10, 5 and 2.5 MHz.
In order to have stability on the measurements the room temperature is controlled by a thermostat that keeps the temperature in the laser source stable.

- TCSPC system: using the time-correlated individual photon counting technique (TCSPC), fluorescence decay curves are acquired by performing a histogram of individual photon arrival times over many excitation / emission cycles. The arrival times are recorded in the histogram through relative times between the generation of the excitation laser pulse and arrival of the emission photons corresponding to the mentioned excitation. This technique was carried out on a time-resolved fluorescence spectrophotometer, Fluotime 200 is based on an L-geometry, and controlled by a computer equipped with the TCSPC TimeHarp 200 data acquisition card (PicoQuant GmbH).

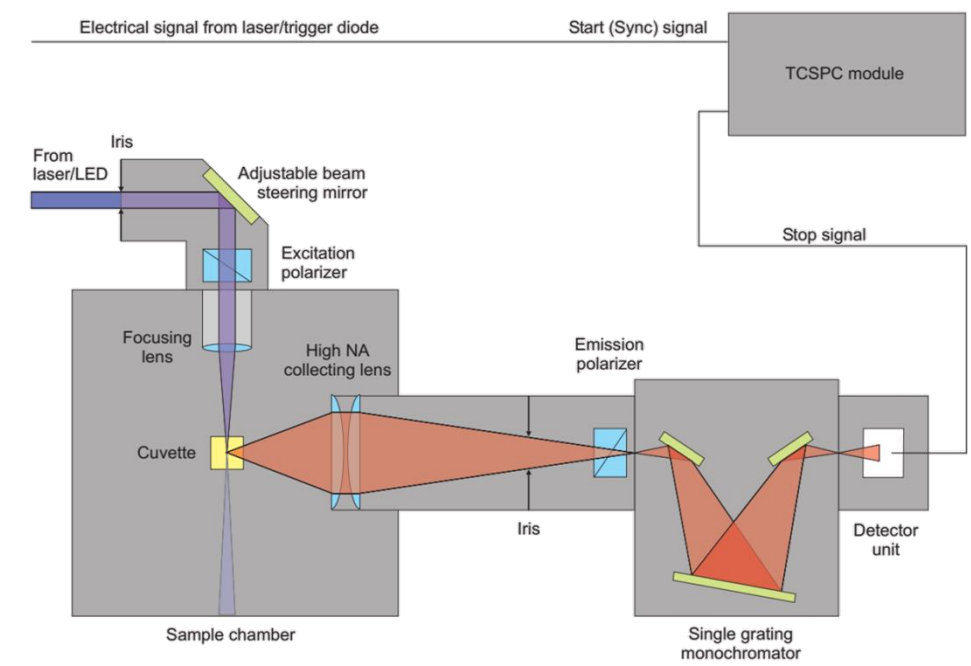

Figure 1: Time-resolved fluorometer Fluotime 200 (PicoQuant Inc) disposition.

The pulsating excitation radiation of the laser is directed to the sample chamber through an optical fibre, there, by means of a lens the beam is focused towards the sample. The emission of the excited sample is collected and collimated through lenses at right angles to the excitation. In order to eliminate the effects of the rotational diffusion of the fluorophores in the fluorescence decays, the emitted light passes through a laminar polarizer at an angle of 54.7° respect to the direction of polarization of the excitatory light. Subsequently, the emitted light is focused on a monochromator (Science Tech 9030 Model, f / 3.5, 1200 lines / mm concave holographic diffraction grating, 8 nm / mm angular dispersion and a spectral range from 350 to 800 nm). After passing through two slits of adjustable width, the detection of the emitted photons is carried out in a microchannel plate photomultiplier. This signal serves as a START pulse, and is connected, alongside the STOP pulse from the pulse-activated PDL 800 B oscillator, to a computer equipped

with the TimeHarp 200 card and a control software which has integrated the two modules constant fraction discrimination (CFD), time-amplitude converter (TAC) and analog-digital converter (ADC). The fluorescence decay histograms are collected over 1036 channels.

6. Inverse Time-Resolved Confocal Microscope

The system used to perform Fluorescence Lifetime Imaging Microscopy (FLIM) measurements is based on a confocal microscope with pulsed laser excitation (MicroTime 200, PicoQuant GmbH), capable of fluorescence life-time measurements, FLIM, Fluorescence Correlation Spectroscopy (FCS) and single-molecule sensitivity detection.

MicroTime 200 consists of 4 parts:

- **Olympus IX71 Microscope**, it is an inverted microscope that includes the infinity-corrected optical system (UIS), which allows not compromising the path of vision when intermediate accessories are added. It is equipped with WHN10x optical lenses and lenses: Plan-N-x40, Plan-N-x60, and immersion U-Plan-S-Apo-x100, being the last one used with immersion oil type DF that has a refraction index of 1.515. The general characteristics of the microscope can be observed in figure 2.

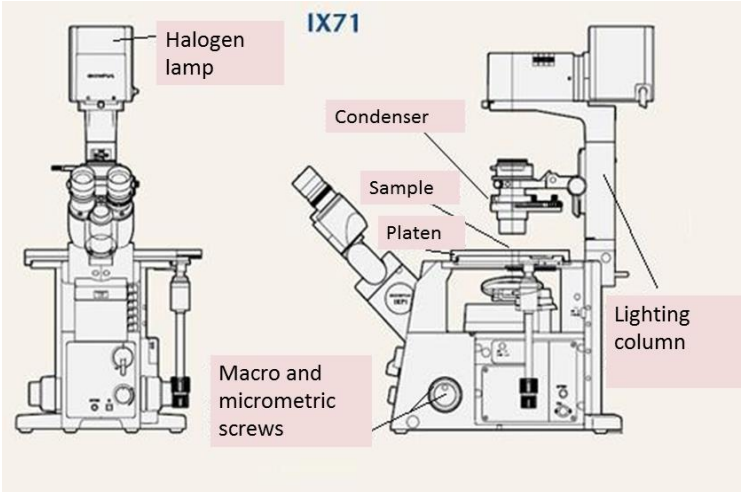

Figure 2: Olympus IX71 inverted microscope structure.

- **Excitation system,** it is previously described.
- **Main Optical Unit (MOU),** it is a set of subunits in which there are:

· The excitation segment: It is the part where the laser light beam that comes from the excitation system enters into the Main Optical Unit. It is incorporated by an optical fibre by means of an FC / APC connector and after reflection in mirror, it passes through the excitation shutter (which can be controlled either by software, or manually). Once the beam passes through the shutter 10-20% of the intensity is directed to the photodiode that measures the excitation intensity.

· Basic confocal unit: after passing through the excitation segment the light beam passes to the dichroic in a 45° geometry that redirects the light to the Olympus IX7 microscope, which has been described above, when it is targeted to the sample through the target.

· The fluorescence emission as well as the reflected excitation light are picked up again by the lens and redirected back to the dichroic filter, which is optimized to let mainly pass the fluorescence emission

radiation. The light transmitted in the dichroic is directed towards an achromatic lens that focuses on an aperture of 50 µm diameter. The distance between the lens and the aperture is easily controllable to optimize the confocal plane. After the aperture, the beam is re-collimated by a second lens and guided to the detectors, which we will see later. On the other hand, the excitation light reflected and redirected to the dichroic is in turn reflected by it towards the diagnostic segment of the focal plane.

- Focal plane diagnosis: the optical design of the MicroTime 200 allows a continuous analysis of the excitation light, which makes it possible to control the position and quality of the focal plane and the excitation volume in the sample. There is a CCD camera (GANZ ZC-F10C2, with 500 x 582 pixels (1/3 ")) that allows the diagnosis and it permanently monitors the image seen by the lens. The obtained images are displayed on the computer. The light arriving at the camera can be regulated by filters of different optical density.
- Detection channels: The collimated beam of the fluorescent emission reaches the detectors through the basic confocal unit. 50/50 radiation separator at 45° geometry separates the fluorescence emission into two equivalents detection channels. Each detection channel has a mechanical shutter and a lens to focus the incident radiation on the sensitive section of the detectors. The detectors used are individual photon avalanche diodes (SPAD) SPCM-AQR-14 (PerkinElmer). They have a detection wavelength range from 400 to 1100 nm, and they have high detection efficiency (more than 70% at 630 nm).

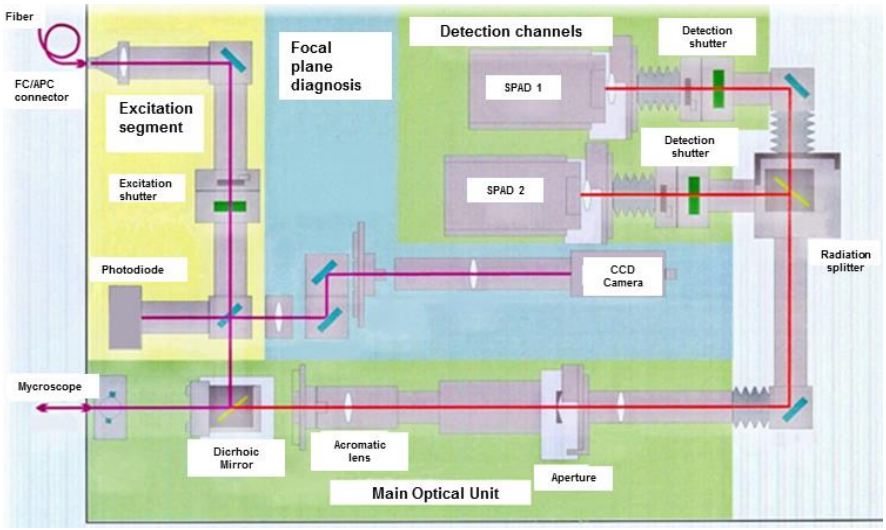

Figure 3: Main Optical Unit Scheme.

- **Data acquisition and electronic control:** it is the place where 2 TimeHarp 200 data collection targets are (each one for each detection channel). It is a TCSPC system that can operate in several ways, the most important is Time-Tagged-Time-Resolved.

The Time-Tagged Time-resolved (TTTR) methodology is performed for the analysis of individual molecules.

This method allows the recording of the arrival times to the individual photon detectors. On the one hand, the START-STOP times of each photon with picosecond resolution are determined, more specifically it is the time elapsed between the excitation pulse (START) and the arrival of the photon (STOP signal), as the fluorescence time resolved by TCSPC mode is done. On the other hand, the arrival of the photons is recorded by an independent clock that measures the total time of each experiment and it labels each photon to its global time of

arrival to the detector. This allows identifying photons that come from the same molecule and also discriminating fluorescence blinking which is a feature of single molecule fluorescence experiments. Therefore, the most outstanding applications are: the detection of single molecule diffusion, FCS, and single molecule blinking that is obtained by integrating fluorescence lifetimes.

Histograms are not performed in TTTR mode. Instead the START-STOP time of each event is always recorded with a time tag of a separate clock, assigned at the time of arrival of the STOP photon. As a result, recordings made by TTTR mode occupy 12 bits for the START-STOP time and 16 bits for time tag. These 16 bits with the clock at 100 ns will cover a maximum range of 6.5536 ms. It should be noted that it is not possible to combine the START-STOP time of picoseconds and the time tag in the same figure, since the two times are not synchronized. The aim of these two times is, rather, to examine physical processes with two very different time scales and time references. However, analysis sophisticated methods use both times to extract as much information as possible from such physical processes, for example, the diffusion of individual molecules to a measure.

It is often desirable to synchronize TCSPC measurements with other information or with other records. In order to perform, for example, images of fluorescence times, it is also necessary to record the spatial location of the photons. To achieve this, a mechanism is needed that assigns the external synchronization information to the TCSPC data collected independently. To solve this problem, the data set generated by the TimeHarp 200 may contain markers for the synchronization

information derived from the captured images. Figure 4 shows how the signal of the external marker signal is recorded in the data sequence.

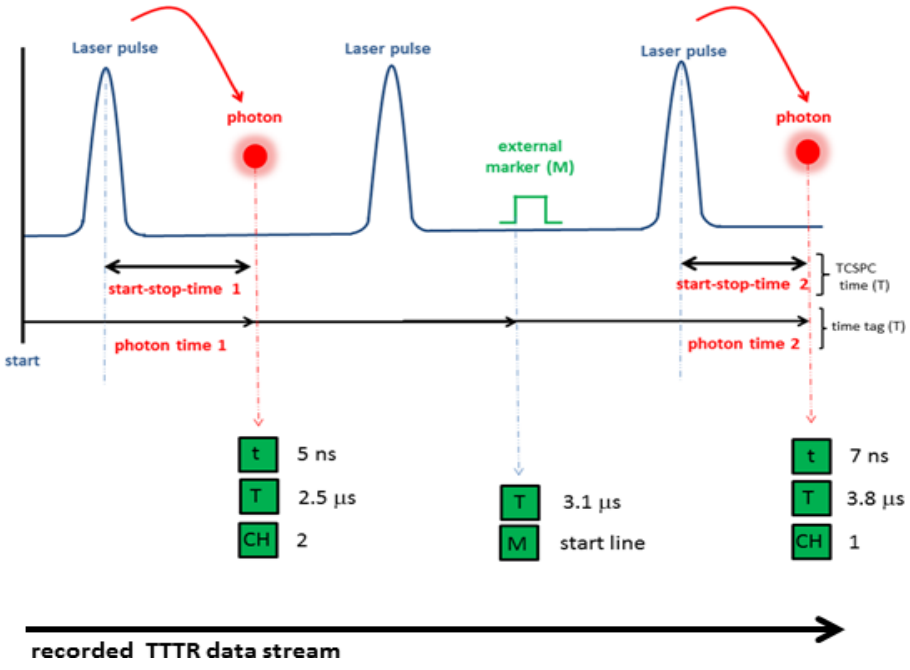

Figure 4: Measurement scheme of the Time-Tagged-Time-Resolved (TTTR).

Like in classical TCSPC the time difference between the moment of excitation and the arrival of the first fluorescence photon at the detector is measured. This TCSPC time (t) is stored into the TTTR data stream along with a global tag (T) and the information about the detection channel (CH). Additional external synchronization signals (markers, M) can be included in the data stream for imaging.

RESULTS

RESULTS

Chapter 1: New Dual Fluorescent Probe for Simultaneous Biothiol and Phosphate Bioimaging

NEW DUAL FLUORESCENT PROBE FOR SIMULTANEOUS BIOTHIOLS AND PHOSPHATE BIOIMAGING

ABSTRACT

The simultaneous detection of relevant metabolites in living organisms by using one molecule introduces an approach to understand the relationships between these metabolites in healthy and deregulated cells. Fluorescent probes of low toxicity are remarkable tools for this type of analysis of biological systems in vivo. As a proof of concept, different naturally occurring compounds, such as biothiols and phosphate anions, were the focus for this work. The 2,4-dinitrobenzenesulfinate (DNBS) derivative of 9-[1-(4-tertbutyl-2-methoxyphenyl)]-6-hydroxy-3H-xanthen-3-one (Granada Green; GG) were designed and synthesized. This new sulfinyl xanthene derivative can act as a dual sensor for the aforementioned analytes simultaneously. The mechanism of action of this derivative implies thiolysis of the sulfinyl group of the weakly fluorescent DNBS-GG by biological thiols at near-neutral pH values, thus releasing the fluorescent GG moiety, which simultaneously responds to phosphate anions through its fluorescence-decay time. The new dual probe was tested in solution by using steady-state and time-resolved fluorescence and intracellularly by using fluorescence-lifetime imaging microscopy (FLIM) in human epithelioid cervix carcinoma (HeLa) cells.

INTRODUCTION

Fluorescent probes of low toxicity for multiplex sensing are remarkable tools for the analysis of biological systems.[1, 2] To this end, different properties of the sensor must be related to unrelated bioanalytes, which is a difficult task. Within this context, we focused on very different naturally occurring compounds, such as biothiols and phosphate anions. Both of these compounds are widely present in living organisms

and are relevant because their deregulation is related to cellular dysfunction. Biological thiols play crucial roles in biological systems; thus, in the last two decades, there has been a great effort to develop new methods to detect them. Among the methods for detecting and quantifying biological thiols, fluorescence approaches have proved to be the most suitable due to their advantages derived from their high sensitivity, simplicity and low cost.[3] Phosphate ions play important roles in signal transduction and energy storage in biological systems; thus, their detection and quantification inside the cell and in the extracellular media are relevant parameters in biological studies.[4-6] Measurement of intracellular phosphate as a marker of osteoblast differentiation and bone deposition combined with the assay of biothiol levels as marker of oxidative stress would be a useful tool to address pathological processes that combine alterations of bone metabolism with increased oxidative stress as obesity and diabetes.[7]

To our knowledge, no fluorescent probes with the ability to simultaneously measure both of these parameters have been described to date. Therefore, we believe that a fluorescence-based multiplexed probe that can jointly sense biological thiols and inorganic phosphates, both inside and outside the cell, would be of broad interest and utility.

The key point in this study is the careful selection of the fluorophore. In recent years, fluorescein-based compounds have evolved to yield simple structures that can retain their striking photophysical properties. Thus, for example, some aryl-[8] and alkyl-substituted xanthenones[9] have simplified the original prototropic equilibrium in fluorescein, improving the analysis of photophysical data (Figure 1). Therefore, they have been used as fluorescent probes for many biologically relevant analytes, such as β-galactosidase,[8, 10] hydrogen peroxide,[11] nucleotide pyrophosphatases/phosphodiesterases,[12] UDP-glucuronosyltransferase,[13] and BlaC

hydrolase of Mycobacterium tuberculosis[14] as well as in western blot analysis.[15] Within this context, a new methodology based on the dependence of the fluorescence decay time of these xanthene-based dyes on the phosphate buffer concentration at near physiological pH was recently developed in our laboratories.[16] The highest sensitivity was obtained with a customized compound, called Granada Green (GG), with a fine-tuned p*K*a value of 7.3.[17]

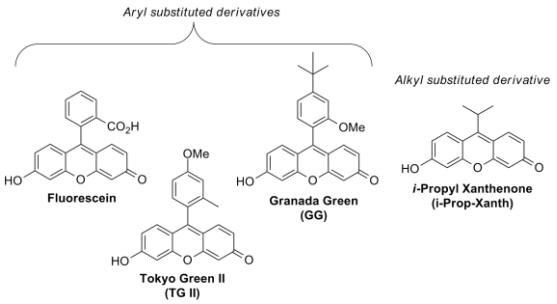

Figure 1: Xanthenone-based fluorescent compounds.

Considering the remarkable properties of these compounds, we decided to demonstrate their selective “on-off” fluorogenic behaviour towards biological thiols. In this manner, the liberated fluorophore could be used for dual purposes, as follows: a) for detecting the presence of biothiols and b) for providing information on the local phosphate concentration (Scheme 1).

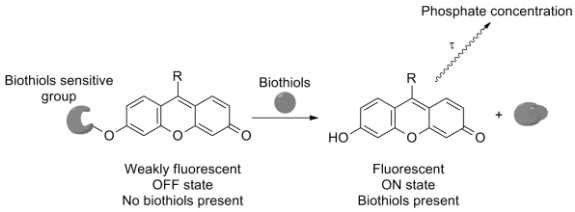

Scheme 1: Xanthenone-based fluorescent compounds and proposed function of the simultaneous probe.

In 2005, Maeda et al. reported that 2,4-dinitrobenzenesulfonyl fluorescein derivatives can act as "on-off" fluorescent probes towards thiols because of the highly selective aromatic nucleophilic addition of thiols to the highly electron-deficient aromatic ring.[18, 19] These seminal studies allowed the extension of the reactive 2,4-dinitrobenzenesulfonyl derivatives to new fluorescent compounds, such as cyanine,[20]merocyanine,[21] boron-dipyrromethene (BODIPY),[22]benzothiazol[23] and coumarin.[24-26] Remarkably, despite the excellent properties of xanthene-based dyes, the corresponding 2,4-dinitrobenzenesulfonyl derivatives have not been described to date. We then prepared the corresponding 2,4-dinitrobenzenesulfonates of 9-[1-(2-methyl-4-methoxy-phenyl)]-6-hydroxy-3H-xanthen-3-one (TG II), 9-[1-(4-tert-butyl-2-methoxyphenyl)]-6-hydroxy-3H-xanthen-3-one (Granada Green, GG, compound 1 in SI), and 6-hydroxy-9-isopropyl-3H-xanthen-3-one (i-Prop-Xanth) which, unfortunately, presented a fast and unselective hydrolysis reaction in aqueous or methanolic solutions. Moreover, the poor solubility in pure water was also limiting for in vivo bioimaging purposes. One possible reason for this undesirable solvolysis reaction is the low p*K*a value of the starting hydroxyxanthenones, which enhances their properties as nucleofuges in a direct substitution reaction at the electron deficient sulfur center.

After obtaining these unfruitful results, we thought that the undesirable hydrolysis reaction (Scheme 2, path a) could be changed to the desired reaction if it is transformed in a selective thiolysis[27-29] reaction (Scheme 2, path b).[30] Therefore, a new biothiol-sensitive group could be developed if the thiolysis reaction takes place in aqueous solution without the interference of oxigenated nucleophiles. In this study, we present the synthesis of the 2,4-dinitrobenzenesulfinate (**DNBS**) derivative of **GG**, **DNBS-GG**, a new sulfinate-based[31] biothiol-sensitive group based on such selective thiolysis reaction. This compound presents an excellent performance in terms of avoiding undesirable hydrolysis reactions, thus increasing the specificity of the fluorogenic probe towards biothiols. Moreover, **DNBS-GG** shows an excellent behavior as a dual probe for biothiols and phosphate anions at near-neutral pH in vitro and in extracellular medium.

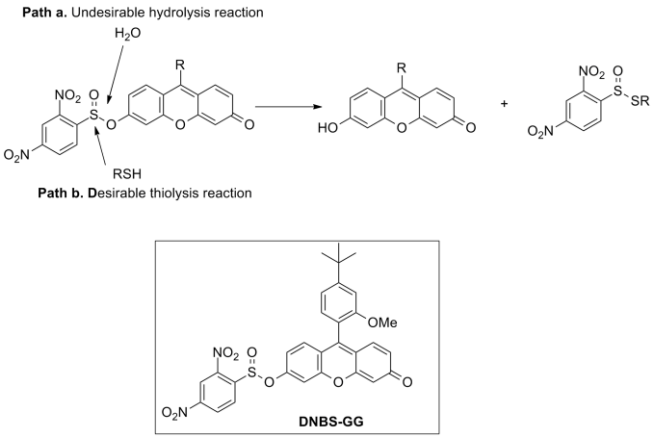

Scheme 2: Working hypothesis and structure of DNBS-GG.

RESULTS AND DISCUSSION

For our purposes, the fluorescent probe should fulfill three primary conditions: i) the nucleophilic aromatic substitution reaction should be turned off, ii) the water-

promoted hydrolysis reaction should be diminished and iii) the thiolysis reaction should be selective. To this end, less deactivated aromatic sulfonates were prepared, but they were unreactive towards any of the previously mentioned reactions. One solution would be the use of other less electrophilic functional groups, such as sulfinates (R1-SO-O-R2). Additionally, the dipolar moment of the resulting molecule could increase its water solubility. The required sulfinate moiety must also be in a carefully balanced equilibrium between the undesirable hydrolysis and the desirable thiolysis reactions. Thus, the probe must be sufficiently robust to resist hydrolysis but must also react with sulfur nucleophiles.

After some experimentation, we found that both the xanthene dye and the substitution of the sulfinate group are key factors for the success of the approach. Only the combination of GG as a xanthene dye and the 2,4-dinitro substitution of the benzene sulfinate in DNBS-GG was shown to be appropriate for this application, being stable and soluble in water and presenting the expected selective reactivity towards biothiols. However, the corresponding DNBS derivatives of TG II and iso-Prop-Xanth were labile towards water. The reason for this different reactivity is unclear but could be related to the higher p*K*a value of GG.

The primary synthetic problem in this study is that the required 2,4-dinitrobenzenesulfinyl chloride has not been described to date.[32] Therefore, we used an unusual reaction of electron-deficient sulfonyl chlorides, which allows the in situ reduction of the sulfur atom from S(+6) to S(+4) using triethylamine as a reductant (Scheme 3).[33]

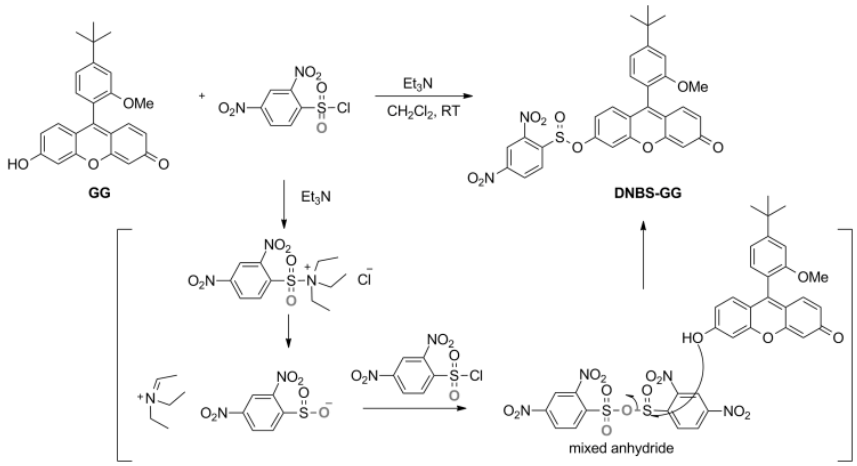

Scheme 3: Synthesis of DNBS-GG.

To explore the use of the new fluorescent probe to detect biologically relevant substances containing a thiol group (e.g., cysteine, homocysteine and glutathione), the temporal dependence of the DNBS-GG fluorescence emission in the presence of these biothiols was investigated at the pH values of 9 (at which DNBS-GG shows the highest sensitivity to biothiols due to the influence of the pK_a value of the aliphatic thiols on the reaction), 4.80 (to check there are not undesirable hydrolysis under acidity conditions, ruling out any potential interference of lysosomal actions in the use of the dye in cells), and 7.35 (interesting for physiological applications). The fluorescence emission of DNBS-GG in the absence of biothiols was very weak. However, in presence of biothiols, an emission band centered at 520 nm, characteristic of GG, gradually increased over time. This fluorescence increase indicates the cleavage of DNBS-GG and its separation into two moieties, releasing the fluorescent compound GG from the electron-withdrawing 2,4-dinitrobenzene-sulfinate moiety. Figure 2 shows representative fluorescence emission spectra at different reaction times of DNBS-GG in the presence of glutathione (GSH) at pH 7.35. Similar reactions were found upon reaction with cysteine (Cys) and homocysteine

(Hcy) (Figure 3 and Figure S1). The absorption spectra of DNBS-GG (Figure S2 in Supporting Material) exhibits a clear change upon reaction with thiols in which from a dual absorption band with maxima at 436 and 461 nm, the reaction gave rise to the spectral profile characteristic of free GG (absorption maximum at 495 nm).

We then attempted to analyse the fate of the DNBS-based fragment. Control experiments using sodium propiolate as a nucleophile showed that the nucleophilic attack does not occur in the aromatic ring, as expected. The S-nucleophile attacks the sulfur electron-deficient center, initially leading to the thiolysis of DNBS-GG. After the hydrolysis of the resulting propyl 2,4-dinitrobenzenethiosulfinate[34, 35] we were able to isolate the 2,4-dinitrobenzenesulfinic acid. This result is relevant because the S-nucleophile can be slowly regenerated over time and can influence the overall kinetics of the process.

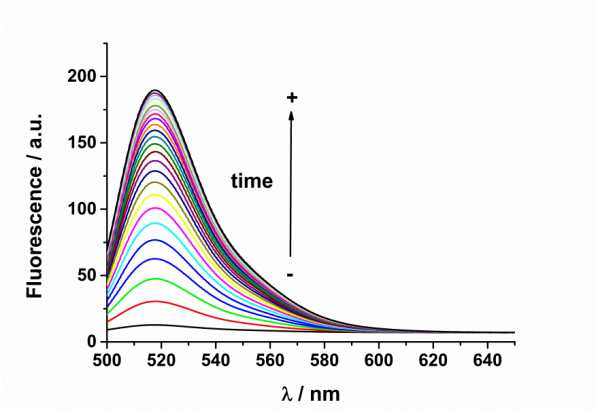

Figure 2: Fluorescence emission spectra (λex=485 nm) of DNBS-GG (6.5 µM) in the presence of 6.5 µM Cys at pH=7.35 in 10 mM Tris solution, recorded every five minutes until reaching 1300 minutes.

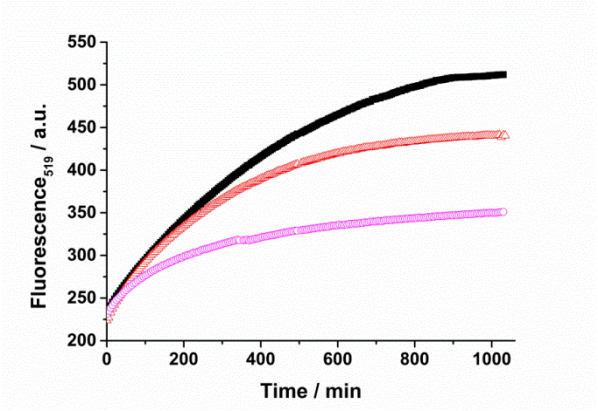

Figure 3: Fluorescence intensity at λex=485 nm and λem=519 nm vs. time of DNBS-GG (6.5 µM) in the presence of 6.5 µM GSH (■), Cys (Δ), or Hcy (O) at pH=9 and 40 º C.

To optimize the experimental conditions to use the DNBS-GG in biothiol detection, we further investigated the effects of the probe concentration and reaction time in the temporal generation of the fluorescent signal. First, we studied the limit in the linearity of the fluorescence signal with the concentration of the free dye (Fig. S5 and

S7). The maximum suitable concentration of the probe was selected as 6.5 μM. Because we intend to perform the detection inside living cells, biological experimental conditions were established for the reaction at 37 ºC and pH = 7.35. Figure 3 shows the fluorescence intensity of DNBS-GG in the presence of Cys, Hcy or GSH at 519 nm, increasing sharply with the reaction time from 0 h to 3 h and then reaching a nearly constant value at approximately 3 h. Figure S6 shows the relative response of DNBS-GG towards Cys, Hcy and GSH after 2 h of reaction under physiological experimental conditions. The results confirm a highly similar sensitivity of the probe towards the three biothiols.

To study the specific response of the probe to biothiols, we also investigated the potential interference by the presence of other amino acids (lacking a thiol group) or by reactive oxygen species (ROS). The increase in the fluorescence emission intensity of DNBS-GG in the presence of L-alanine, L-serine, H2O2, or Fe(II) was low (Figure S6). The low response to ROS indicates that the probe would be a good candidate for thiol detection in cases of cellular stress due to high levels of ROS in which the thiols are the first to respond to oxidative stress.

In previous studies, we demonstrated the fluorescence decay time of GG to be a good estimator of the phosphate ion concentration.[17] Given that the product of the reaction between DNBS-GG and thiols is the free GG, the measurements of the fluorescence decay time must provide the basis for a dual sensor. To test the capability of the DNBS-GG dye to jointly estimate the concentrations of phosphate and biothiols, we studied the reaction between 6.5 μM DNBS-GG and GSH in the presence of phosphate buffer at different concentrations over the range of 0 to 0.4 M and at pH = 7.35. Experimental measurements were completed in the time-resolved regime, and Figure 4 shows the recovered results. As can be observed, the recovered lifetimes show a decrease with the phosphate concentration, revealing

that the product of the DNBS-GG cleavage is the free GG, which is sensitive towards phosphate ions via an excited-state proton transfer reaction (scheme 4 in the Supporting Material).

The recovered fluorescence lifetimes after the reaction with the thiols are in excellent agreement with those previously published for free GG in the presence of phosphate ions (Figure 5).[17]

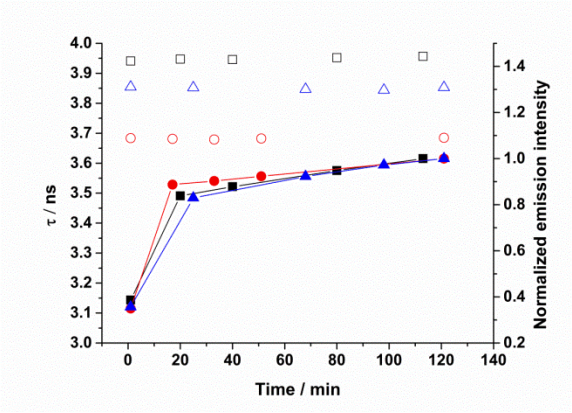

Figure 4: Fluorescence decay time (open symbols, left y-axis) and normalized emission intensity (closed symbols, right y-axis) of DNBS-GG (6.5×10^{-6} M) in the presence of GSH (6.5×10^{-6} M) at pH=7.35 and 0 (open squares), 200 (open triangles), and 400 mM (open circles) total phosphate concentration.

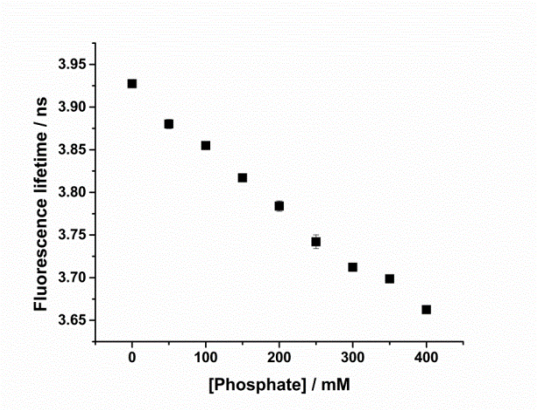

Figure 5: Average of the fluorescence decay time of DNBS-GG (6.5×10^{-6} M) in the presence of GSH (6.5×10^{-6} M) at pH=7.35, collected every 10 minutes for 1 h of reaction in the presence of different amounts of total phosphate ranging between 0 and 400 mM.

The innovative dual probe for the detection of thiols and phosphate ions was also tested intracellularly by fluorescence lifetime imaging microscopy (FLIM). DNBS-GG was added to the extracellular medium of HeLa cell cultures, and FLIM images were collected at different times. The evaluation of the fluorescence intensity changes displayed with time due to their own biological thiols shows that the probe is cell membrane-permeable and can selectively detect thiols in living cells (Figure 6A and C). To verify this statement, an excess of N-methyl maleimide (NMM) was added to the extracellular medium to block the cellular thiols. The fluorescence signal of the probe did not appreciably change with time (Figure 6B and C).

To verify the phosphate sensitivity using changes in the fluorescence lifetime, the cells were incubated with α-toxin, a non-specific ionophore that opens membrane pores to allow a free flow of small ions, including the phosphate buffer added to the extracellular media. Along with the increase in the fluorescence emission due to reaction with the internal thiols, the FLIM images show the changes in the fluorescence lifetime of the probe because of the changes in the total phosphate

concentration (Figure 7A and B). Previously, it was reported the kinetic rate constant of the buffer-mediated proton-transfer reaction in the ground state in different buffers by using Fluorescence Correlation Spectroscopy (FCS) and showed that only suitable buffer, like phosphate, makes the reaction fast enough to compete with fluorescence emission; therefore, we could assign these changes in lifetime to phosphate ESPT among other cell species. Although Δτ shows a large error bar, this is intrinsic to cell to cell variation. Nevertheless, in previous articles we have shown the excellent feasibility and specificity of this method for following variations of phosphate concentration in living cells between 10 mM to 600 mM.[17, 36]

We show that this dye is capable of detecting thiols and phosphate at a time. The combined sensing of inorganic phosphate and glutathione has a clear biological relevance. In bone tissue, regulation of bone synthesis and degradation is modulated by oxidative stress. The molecular bases of these interactions have been proposed and the role of specific genes that promote oxidative stress in the development of osteoporosis has been described (for example NOX4 gene promotes oxidative stress and osteoporosis[37] while FoxO1 gene expression exerts a protective effect).[38] In addition, sensing of phosphate based energy-rich compounds and oxidative stress is relevant in biology in pathological processes that include alteration of the energetic metabolism combined with an increase in oxidative stress. Examples of these situations are cancer,[39] obesity, diabetes[7] and hypoxia.[40] Studies to use our dye in some of these biological diseases and sensibility against phosphate compounds are in progress.

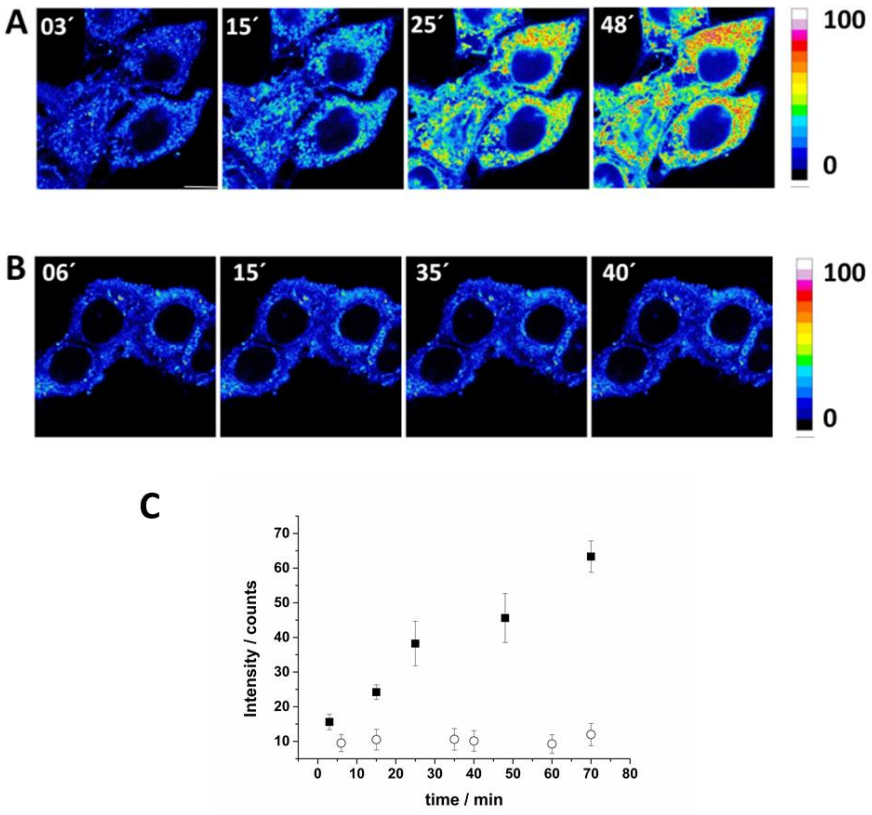

Figure 6: Fluorescence intensity images of cell cultures with DNBS-GG (1×10^{-7} M) at different reaction times (in minutes). (A) Physiological conditions with natural thiols present; (B) cells incubated with an excess of NMM. (C) Average number of photons per pixel containing the fluorescence of the probe (cell cytoplasm) from cells under physiological conditions (black squares) or incubated with an excess of NMM (open circles). Error bars represent standard deviations from the measurements of at least five different cells.

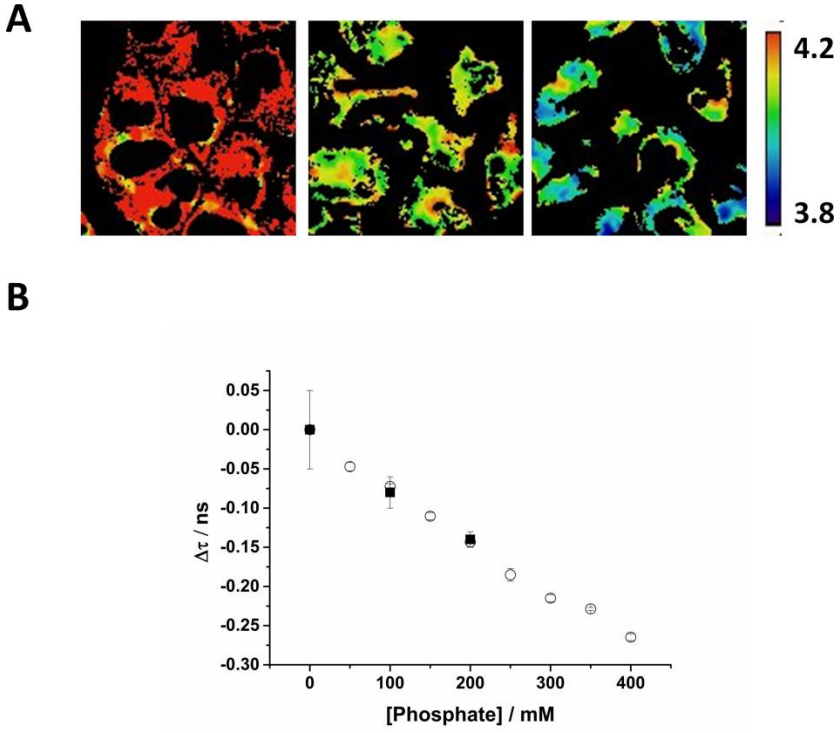

Figure 7: A) FLIM images of cells incubated with α-toxin and with DNBS-GG (1×10-7 M) at pH=7.35 with phosphate concentrations of 0, 100 and 200 mM, applying an arbitrary color scale. FLIM images were collected after 30 minutes to allow the reaction of DNBS-GG with the intrinsic thiols. B) Recovered lifetime of DNBS-GG in α-toxin-treated cells in the presence of different phosphate concentrations. Error bars represent standard deviations from the measurements of at least five different images containing multiple cells.

CONCLUSIONS

We designed and synthesized a new sulfinyl xanthene derivative that can act as a simultaneous dual sensor of different analytes, such as biological biothiols and phosphate anion. Its mechanism of action implies thiolysis of the sulfinyl group of the weakly fluorescent DNBS-GG by biological biothiols, releasing a fluorescent GG moiety that simultaneously responds to phosphate anions through its fluorescence

decay time. The efficiency of this new dye as a dual sensor was probed in in vitro experiments at two significant pH values: pH = 9, where the probe is faster and more sensitive to biothiols, and pH = 7.35, required for biological applications. In both cases, we could detect the presence of cysteine, homocysteine or glutathione and determine phosphate concentration at a time. Note that this probe is suitable for thiol detection in cases of cellular stress due to its low response to ROS. Moreover, this new dye was tested intracellularly by FLIM in HeLa cells, showing permeability through the cell membrane. Again, the increase in the fluorescence intensity confirms its ability to detect thiols, and the changes in the fluorescence lifetime enable its behaviour as a phosphate concentration sensor.

EXPERIMENTAL SECTION

General information

All reactions were performed in dry glassware under air atmosphere. All of the commercially available reagents (2,4-dinitrobenzenesulfonyl chloride and 2,4-dinitrobenzenesulfonic acid) and solvents (triethylamine, dichloromethane and methanol) were used without further purification. TLC was performed on aluminium-backed plates coated with silica gel 60 (230-240 mesh) with F254 indicator. The spots were visualized with UV light (254 nm) and/or staining with Ce/Mo reagent or phosphomolybdic acid solution and subsequent heating. NMR spectra were measured at room temperature. 1H NMR spectra were recorded at 500 or 600 MHz.

Synthesis and spectroscopic data of DNBS-GG

Granada Green (GG, 20 mg, 0.056 mmol) was dissolved in 2 mL of Et3N and 2 mL of CH2Cl2. Then, 2,4-dinitrobenzenesulfonyl chloride (29 mg, 0.11 mmol) was added (Scheme 3). The reaction was monitored by TLC, and 29 mg of the chloride were added every 60 minutes until no starting material was observed. The solvent was then evaporated, and the residue was purified by flash chromatography (CH2Cl2:MeOH mixtures) to give the corresponding DNBS-GG (16 mg, 50%) as a dark orange solid: 1H-NMR (600 MHz, Acetone-d6) δ 8.95 (d, J = 2.7 Hz, 1H), 8.60 (dd, J = 9.2, 2.8 Hz, 1H), 7.66 (d, J = 9.2 Hz, 1H), 7.35 (s, 1H), 7.34 (d, J = 2.4 Hz, 1H), 7.29 – 7.25 (m, 3H), 7.17 (dd, J = 8.8, 2.4 Hz, 1H), 7.08 (d, J = 9.8 Hz, 1H), 6.44 (dd, J = 9.8, 1.7 Hz, 1H), 6.16 (d, J = 1.7 Hz, 1H), 3.82 (s, 3H), 1.44 (s, 9H). 13C-NMR (151 MHz, Acetone- d6) δ 187.1 (C), 161.1 (C), 160.9 (C), 159.5 (C), 157.9 (C), 156.2 (C), 148.1 (C), 146.1 (C), 143.7 (C), 133.7 (CH), 133.2 (CH), 133.0 (CH), 132.8 (CH), 132.1 (CH), 130.2 (C), 124.8 (CH), 124.6 (CH), 123.2 (C), 121.0 (C), 120.9 (C), 120.5 (CH), 118.3 (CH), 111.7 (CH), 109.4 (CH), 107.9 (CH), 57.8 (CH3), 37.7 (C), 33.3 (CH3).LSIMS (FAB) m/zcalcd. for C30H24N2O9S [M+]: 588.12; obtained: 588.12.

Preparation of Solutions

Tris buffer solutions were prepared by mixing the required amounts of Trizma base and Tris-HCL (both from Sigma) to obtain the desired pH.

For the preparation of phosphate buffer (pK_a^B = 6.8) solutions, NaH_2PO_4·H2O and Na_2HPO_4·7H2O (both from Fluka, puriss. p.a.) were used. All of the solutions were prepared using Milli-Q water as a solvent. All of the chemicals were used as received without further purification.

A stock solution of DNBS-GG (10^{-4} M) in ethanol was prepared. Using this stock solution, water solutions with a final concentration of 1×10^{-5} M of dye and pH =7.35 in Tris buffer were prepared.

The required amounts of this solution and thiol stock solution were added to obtain the desired concentrations of DNBS-GG and thiol in Tris buffer (20 mm) at pH=7.35.

Solutions of all of the compounds for time-resolved fluorescence measurements were prepared so that the absorbance of the final solutions at λ_{ex} was lower than 0.1. Solutions were kept cool in the dark when not in use to avoid possible deterioration by exposure to light and heat. The solutions were not degassed.

Cell culture

The human epithelioid cervix carcinoma (HeLa; ATCC No CCL-2) cell line was provided by the Cell Culture Facility, University of Granada. HeLa cells were grown in Dulbecco's modified Eagle's medium (DMEM) supplemented with 10% (v/v) fetal bovine serum (FBS), 2 mM glutamine, 100 U/mL penicillin, and 0.1 µg/mL streptomycin in a humidified 5% CO_2 incubator.

For the FLIM microscopy experiments, HeLa cells were seeded onto 25 mm coverslips in 6-well plates at a density of 11 250 cells/cm^2. On the day of the experiment, cells were washed twice with Krebs-Ringer phosphate medium (118 mM NaCl, 5 mM KCl, 1.2 mM $MgSO_4$, 1.3 mM $CaCl_2$, 1.2 mM KH_2PO_4, 30 mM Hepes, pH 7.4) and incubated in the same medium with effectors. When N-methyl maleimide (NMM) was used to block the intracellular thiols, the cells were pre-incubated with 1 mM NMM for 20 minutes. NMM was maintained in the medium during the FLIM experiments.

Cell Permeabilization

Cells were permeabilized as described in the literature.[17] Briefly, HeLa cells were seeded onto coverslips in 12-well plates. On the day of the experiment, the cells were washed twice with phosphate buffered saline (PBS) and were perforated by incubation for 15 minutes at 37 °C with 2 μg/mL α-toxin in permeabilization buffer (20 mM potassium MOPS, pH 7.0, 250 mM mannitol, 1 mM potassium ATP, 3 mM $MgCl_2$, and 5 mM potassium glutathione). Subsequently, the cells were washed twice with PBS and were analysed by FLIM in the presence of different concentrations of phosphate in the assay medium.

References

1. C. Ding, A. Zhu and Y. Tian, *Accounts of Chemical Research*, 2014, **47**, 20-30.
2. P. D. Howes, R. Chandrawati and M. M. Stevens, *Science*, 2014, **346**.
3. X. Chen, Y. Zhou, X. Peng and J. Yoon, *Chemical Society Reviews*, 2010, **39**, 2120-2135.
4. N. Majed, Y. Li and A. Z. Gu, *Current Opinion in Biotechnology*, 2012, **23**, 852-859.
5. S. Khoshniat, A. Bourgine, M. Julien, P. Weiss, J. Guicheux and L. Beck, *Cell. Mol. Life Sci.*, 2011, **68**, 205-218.
6. C. Bergwitz and H. Jüppner, *Advances in chronic kidney disease*, 2011, **18**, 132-144.
7. T. Yokota, S. Kinugawa, M. Yamato, K. Hirabayashi, T. Suga, S. Takada, K. Harada, N. Morita, N. Oyama-Manabe, Y. Kikuchi, K. Okita and H. Tsutsui, *Diabetes Care*, 2013, **36**, 1341-1346.
8. Y. Urano, M. Kamiya, K. Kanda, T. Ueno, K. Hirose and T. Nagano, *J. Am. Chem. Soc.*, 2005, **127**, 4888-4894.
9. A. Martinez-Peragon, D. Miguel, R. Jurado, J. Justicia, J. M. Alvarez-Pez, J. M. Cuerva and L. Crovetto, *Chem. - Eur. J.*, 2014, **20**, 447-455.
10. M. Kamiya, D. Asanuma, E. Kuranaga, A. Takeishi, M. Sakabe, M. Miura, T. Nagano and Y. Urano, *Journal of the American Chemical Society*, 2011, **133**, 12960-12963.
11. D. Srikun, A. E. Albers, C. I. Nam, A. T. Iavarone and C. J. Chang, *Journal of the American Chemical Society*, 2010, **132**, 4455-4465.
12. M. Kawaguchi, T. Okabe, S. Okudaira, K. Hanaoka, Y. Fujikawa, T. Terai, T. Komatsu, H. Kojima, J. Aoki and T. Nagano, *Journal of the American Chemical Society*, 2011, **133**, 12021-12030.
13. T. Terai, R. Tomiyasu, T. Ota, T. Ueno, T. Komatsu, K. Hanaoka, Y. Urano and T. Nagano, *Chemical Communications*, 2013, **49**, 3101-3103.
14. Y. Cheng, H. Xie, P. Sule, H. Hassounah, E. A. Graviss, Y. Kong, J. D. Cirillo and J. Rao, *Angewandte Chemie International Edition*, 2014, **53**, 9360-9364.
15. M. Kamiya, Y. Urano, N. Ebata, M. Yamamoto, J. Kosuge and T. Nagano, *Angewandte Chemie International Edition*, 2005, **44**, 5439-5441.
16. J. M. Paredes, M. D. Giron, M. J. Ruedas-Rama, A. Orte, L. Crovetto, E. M. Talavera, R. Salto and J. M. Alvarez-Pez, *Journal of Physical Chemistry B*, 2013, **117**, 8143-8149.
17. A. Martinez-Peragon, D. Miguel, A. Orte, A. J. Mota, M. J. Ruedas-Rama, J. Justicia, J. M. Alvarez-Pez, J. M. Cuerva and L. Crovetto, *Org. Biomol. Chem.*, 2014, **12**, 6432-6439.

18. H. Maeda, H. Matsuno, M. Ushida, K. Katayama, K. Saeki and N. Itoh, *Angewandte Chemie International Edition*, 2005, **44**, 2922-2925.
19. H. Maeda, K. Yamamoto, I. Kohno, L. Hafsi, N. Itoh, S. Nakagawa, N. Kanagawa, K. Suzuki and T. Uno, *Chemistry – A European Journal*, 2007, **13**, 1946-1954.
20. D. Maity and T. Govindaraju, *Org. Biomol. Chem.*, 2013, **11**, 2098-2104.
21. S.-P. Wang, W.-J. Deng, D. Sun, M. Yan, H. Zheng and J.-G. Xu, *Org. Biomol. Chem.*, 2009, **7**, 4017-4020.
22. X. Li, S. Qian, Q. He, B. Yang, J. Li and Y. Hu, *Org. Biomol. Chem.*, 2010, **8**, 3627-3630.
23. W. Sun, W. Li, J. Li, J. Zhang, L. Du and M. Li, *Tetrahedron Letters*, 2012, **53**, 2332-2335.
24. J. Li, C.-F. Zhang, Z.-Z. Ming, W.-C. Yang and G.-F. Yang, *RSC Advances*, 2013, **3**, 26059-26065.
25. J. Bouffard, Y. Kim, T. M. Swager, R. Weissleder and S. A. Hilderbrand, *Organic Letters*, 2008, **10**, 37-40.
26. M. Li, H. Ge, R. L. Arrowsmith, V. Mirabello, S. W. Botchway, W. Zhu, S. I. Pascu and T. D. James, *Chemical Communications*, 2014, **50**, 11806-11809.
27. A. K. Chakraborti, M. K. Nayak and L. Sharma, *The Journal of Organic Chemistry*, 1999, **64**, 8027-8030.
28. T. Okuyama, H. Takano and K. Senda, *Bulletin of the Chemical Society of Japan*, 1996, **69**, 2639-2644.
29. T. Okuyama, *Bulletin of the Chemical Society of Japan*, 1996, **69**, 3281-3287.
30. H. Maeda, K. Yamamoto, Y. Nomura, I. Kohno, L. Hafsi, N. Ueda, S. Yoshida, M. Fukuda, Y. Fukuyasu, Y. Yamauchi and N. Itoh, *Journal of the American Chemical Society*, 2005, **127**, 68-69.
31. S. R. Malwal, A. Labade, A. S. Andhalkar, K. Sengupta and H. Chakrapani, *Chemical Communications*, 2014, **50**, 11533-11535.
32. C. Lee and L. Field, *Synthesis*, 1990, **1990**, 391-397.
33. T. Netscher and P. Bohrer, *Tetrahedron Letters*, 1996, **37**, 8359-8362.
34. T. Takata, Y. H. Kim and S. Oae, *Bulletin of the Chemical Society of Japan*, 1981, **54**, 1443-1447.
35. S. Oae and T. Takata, *Tetrahedron Letters*, 1980, **21**, 3213-3216.
36. J. M. Paredes, M. D. Giron, M. J. Ruedas-Rama, A. Orte, L. Crovetto, E. M. Talavera, R. Salto and J. M. Alvarez-Pez, *J. Phys. Chem. B*, 2013, **117**, 8143-8149.
37. C. Goettsch, A. Babelova, O. Trummer, R. G. Erben, M. Rauner, S. Rammelt, N. Weissmann, V. Weinberger, S. Benkhoff, M. Kampschulte, B. Obermayer-Pietsch, L. C. Hofbauer, R. P. Brandes, Schr, xF and K. der, *The Journal of Clinical Investigation*, 2013, **123**, 4731-4738.
38. M.-T. Rached, A. Kode, L. Xu, Y. Yoshikawa, J.-H. Paik, R. A. DePinho and S. Kousteni, *Cell Metabolism*, 2010, **11**, 147-160.

39. J. A. Hess and M. K. Khasawneh, *BBA Clinical*, 2015, **3**, 152-161.
40. A. Almeida, M. Delgado-Esteban, J. P. Bolaños and J. M. Medina, *Journal of Neurochemistry*, 2002, **81**, 207-217.

SUPPLEMENTARY MATERIAL

General information

NMR spectra were measured at room temperature. ^{1}H NMR spectra were recorded at 500 or 600 MHz. Chemical shifts are reported in ppm using a residual solvent peak as a reference ($CHCl_3$: δ7.26). Data are reported as follows: chemical shift, multiplicity (s: singlet, d: doublet, dd: doublet of doublets), coupling constant (*J* in Hz) and integration. ^{13}C-NMR spectra were recorded at 126 or 151 MHz using broadband proton decoupling, and chemical shifts are reported in ppm using residual solvent peaks as a reference ($CDCl_3$: δ 77.16). Carbon multiplicities were assigned by distortionless enhancement by polarization transfer (DEPT) techniques.

High-resolution mass spectra (HRMS) were recorded on a Micromass AutoSpec using electron impact (EI) at 70 eV or fast atom bombardment (FAB).

Synthesis of sulfonyl derivative I:

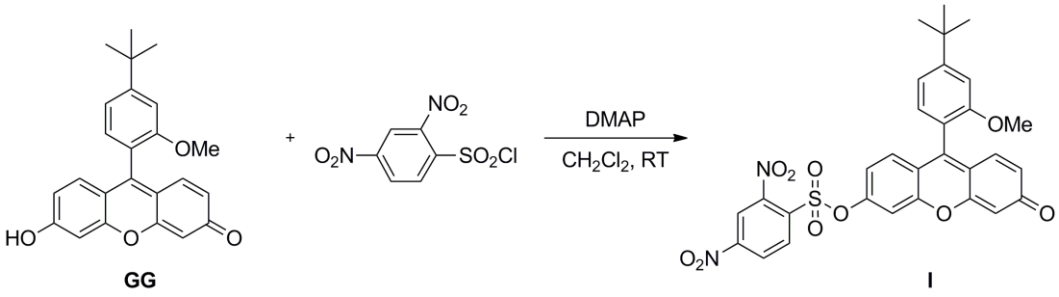

Granada Green (GG, 67 mg, 0.179 mmol) and 4-dimethylaminopyridine (DMAP) (33 mg, 0.269 mmol) were dissolved in 2 mL of dry CH2Cl2. Then, 2,4-dinitrobenzenesulfonyl chloride (57 mg, 0.215 mmol) was added. The reaction was monitored by TLC and stirred at room temperature until no starting material was observed. The solvent was then evaporated, and the residue was purified by flash

chromatography (CH2Cl2: MeOH mixtures) to give the corresponding product I (96 mg, 89%) as a brown solid.

1H NMR (500 MHz, Acetone-d6) δ 8.99 (d, J = 2.3 Hz, 1H), 8.72 (dd, J = 8.7, 2.3 Hz, 1H), 8.44 (d, J = 8.7 Hz,1H), 7.43 (d, J = 2.4 Hz, 1H), 7.33 (d, J = 1.6 Hz, 1H), 7.26 (dd, J = 7.9, 1.6 Hz, 1H), 7.23 (d, J = 7.9 Hz, 1H), 7.20(d, J = 8.8 Hz, 1H), 7.13 (dd, J = 8.8, 2.4 Hz, 1H), 7.08 (d, J = 9.8 Hz, 1H), 6.44 (dd, J = 9.8, 1.9 Hz, 1H), 6.16 (d, J= 1.9 Hz, 1H), 3.78 (s, 3H), 1.42 (s, 9H).

13C NMR (126 MHz, Acetone-d6) δ 185.4 (C), 158.9 (C), 157.8 (C), 156.3 (C), 153.5 (C), 152.9 (C), 152.0 (C), 149.8 (C), 145.5 (C), 135.0 (CH), 132.8 (C), 131.9 (CH), 131.5 (CH), 131.3 (CH), 131.1 (CH), 128.2 (CH), 122.5 (C), 122.0 (CH), 121.5 (C), 119.0 (CH), 118.8 (C), 118.7 (CH), 111.5 (CH), 110.0 (CH), 106.4 (CH), 56.1 (CH3), 36.0 (C),31.6 (3 CH3).

LSIMS (FAB) m/z calcd. for C30H25N2O10S [M++H]: 605.12; obtained: 605.12.

Synthesis of 2,4-dinitrobenzenesulfinic acid II by thiolysis of DNSB-GG:

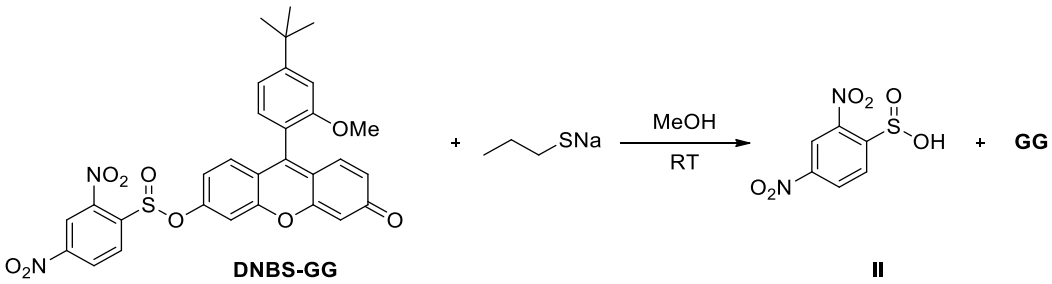

DNBS-GG (16 mg, 0.027 mmol) was dissolved in 1 mL of MeOH, and sodium propiolate (2.6 mg, 0.027 mmol) was added. The reaction was stirred at room

temperature, and 2.6 mg of sodium propiolate was added every 24 h until no starting material was observed by TLC (2-3 eq, 48-72 h was required to consume starting material). The solvent was then removed, and the residue was purified by flash chromatography (CH_2Cl_2:MeOH mixtures) to give the corresponding 2,4-dinitrobenzenesulfonic acid **II** as a white solid.

^{1}H-NMR (600 MHz, CD_3OD) δ 8.72 (d, *J* = 2.8 Hz, 1H), 8.50 (dd, *J* = 9.3, 2.8 Hz, 1H), 7.50 (d, *J* = 9.3 Hz, 1H).

^{13}C-NMR (151 MHz, CD_3OD) δ 158.5 (C), 141.5 (C), 130.1 (CH), 122.3 (CH), 115.6 (CH).

IR (KBr) *cm^{-1} (%T)* 3116 (97.28), 3119 (97.45), 1604 (81.4), 1534 (80.38), 1348 (78.29),1303 (82.41), 1095 (85.11)

All of the techniques employed afforded fragmentations in the high-resolution mass spectra.

Data of commercially available 2,4-dinitrobenzenosulfonic acid **III**:

^{1}H-NMR (600 MHz, CD_3OD) δ 8.52 (d, *J* = 2.3 Hz, 1H), 8.49 (dd, *J* = 8.6, 2.3 Hz, 1H), 8.27 (d, *J* = 8.6 Hz, 1H).

^{13}C-NMR (151 MHz, CD_3OD) δ 150.0 (C), 149.5 (C), 144.0 (C), 132.3 (CH), 126.9 (CH), 120.0 (CH).

IR (KBr): *cm^{-1} (%T)* 3407 (80.33), 2509 (79.74), 1535 (35.42), 1354 (41.37), 1200 (39.1), 1113 (43.88), 1025 (32.35).

Copies of IR spectra of 2,4-dinitrobenzenesulfonic acid **II** and 2,4-dinitrobenzenesulfonic acid **III**

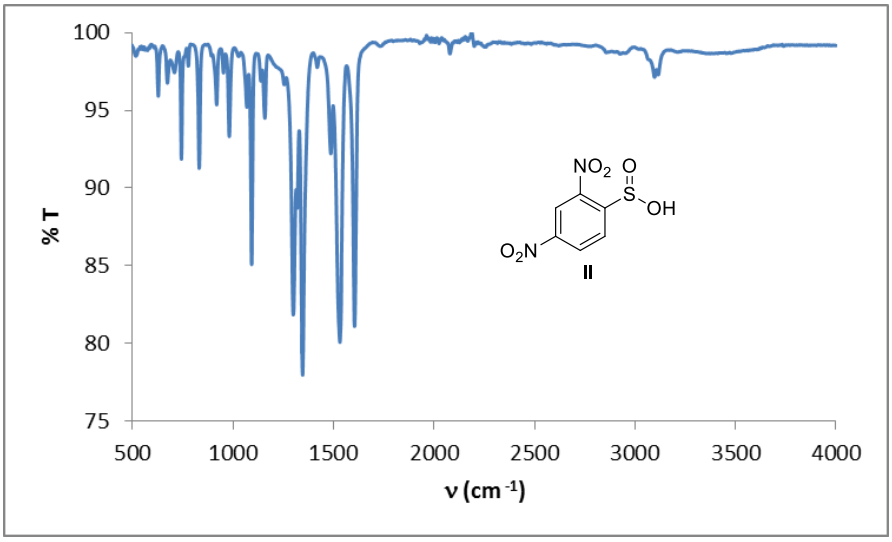

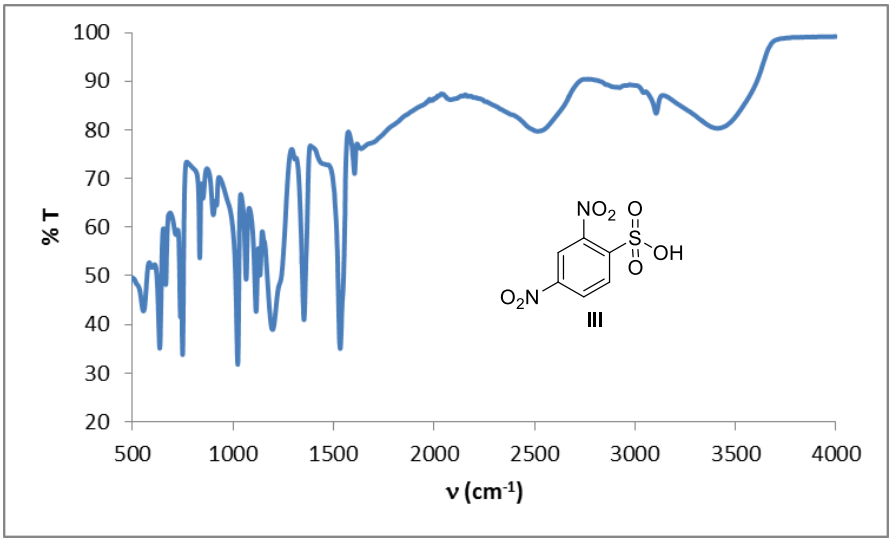

Copies of ^{1}H-NMR and ^{13}C-NMR of compounds **I**, **DNBS-GG,** 2,4-dinitrobenzenesulfonic acid **II** and 2,4-dinitrobenzenesulfonic acid **III**:

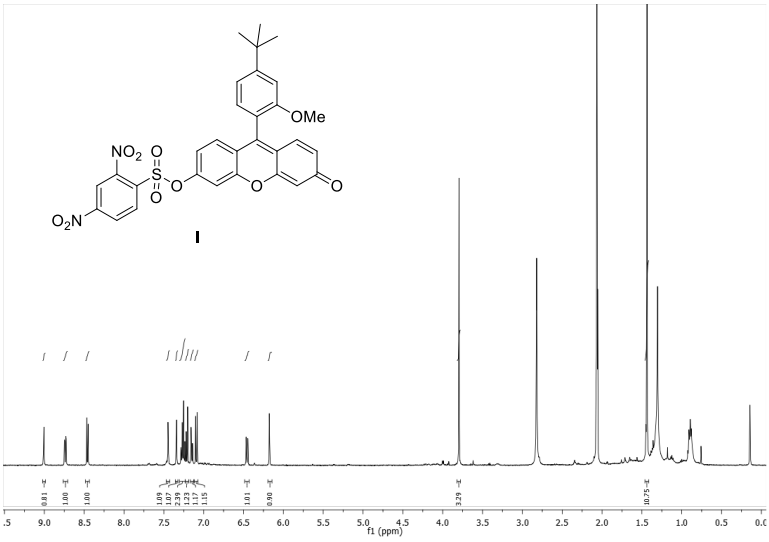

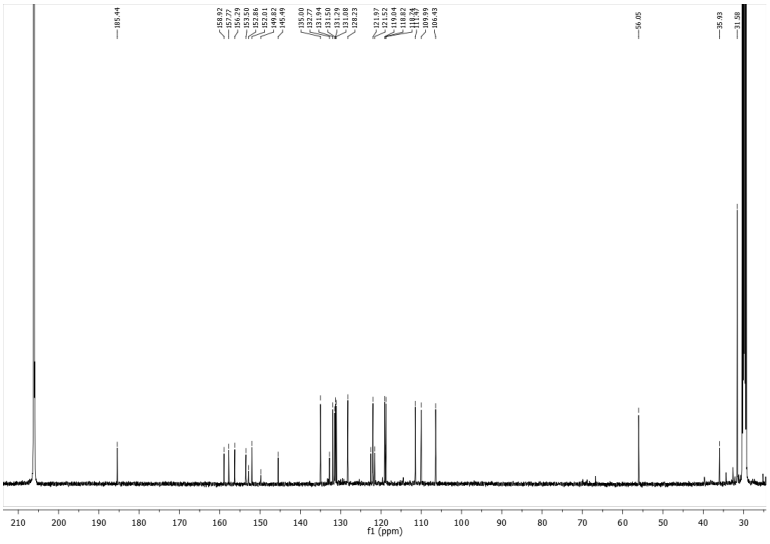

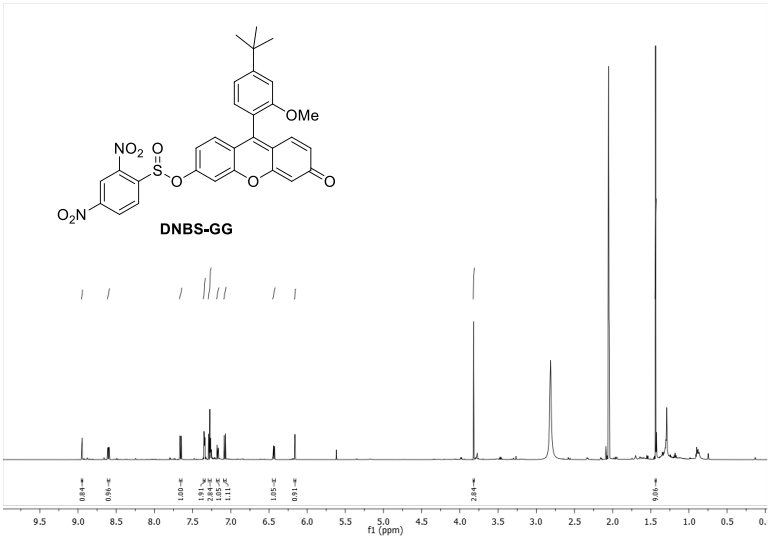
OMe
NO2
O
S
O
O
O
O2N
DNBS-GG
f1 (ppm)

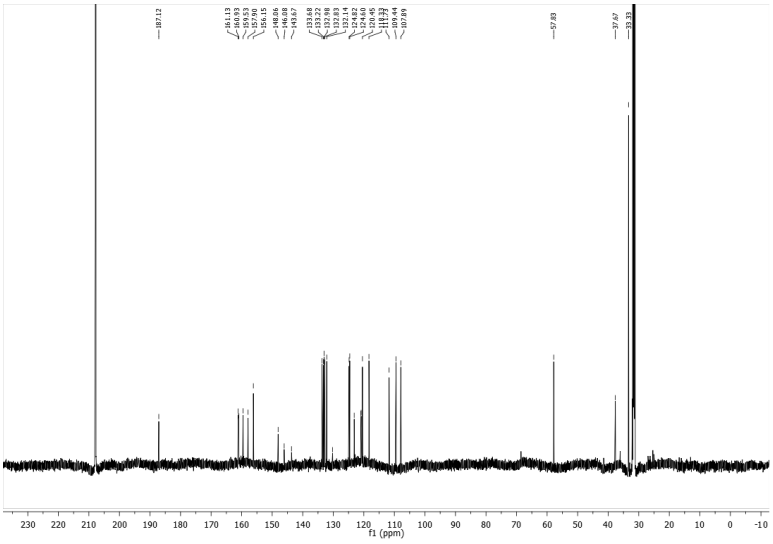
187.12
161.13
160.93
159.53
157.70
156.15
148.86
146.08
143.67
57.83
37.67
33.33
f1 (ppm)

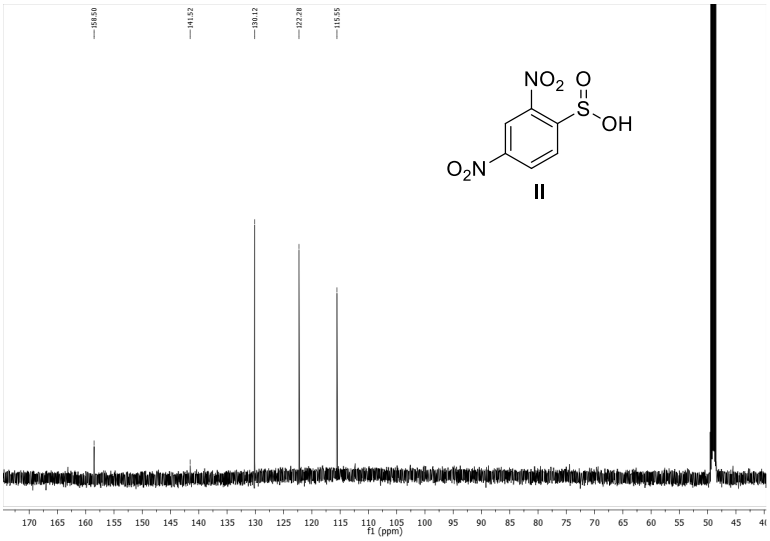
168.50
141.52
130.12
122.28
115.55
NO2
O
S
OH
O2N
II
f1 (ppm)

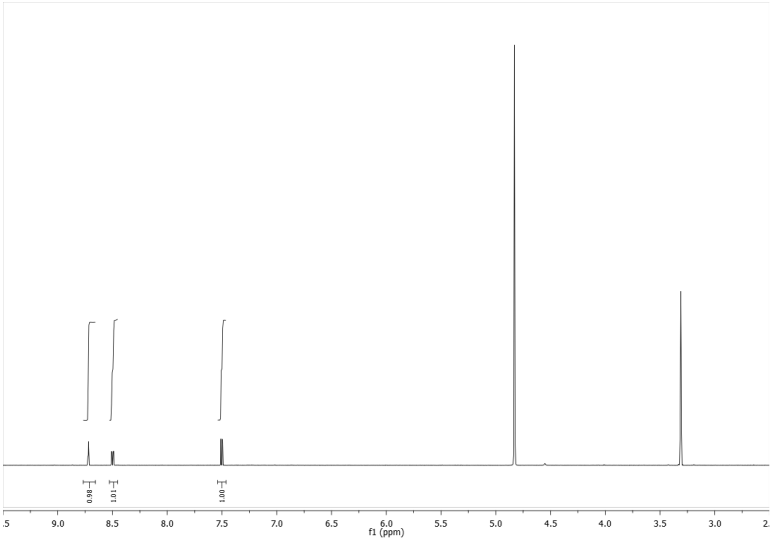
0.98
1.01
1.00
f1 (ppm)

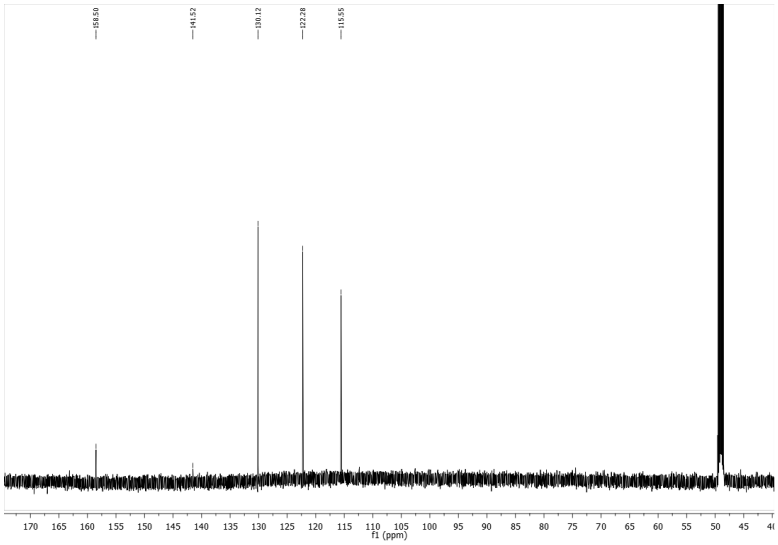

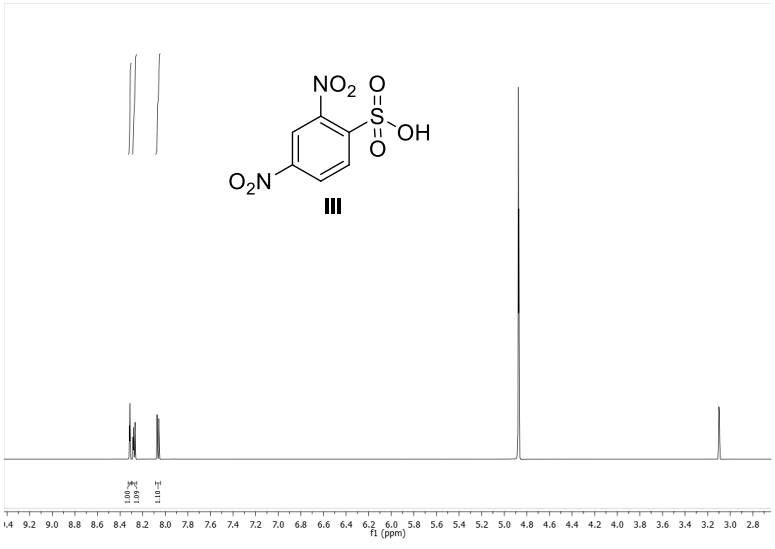

III

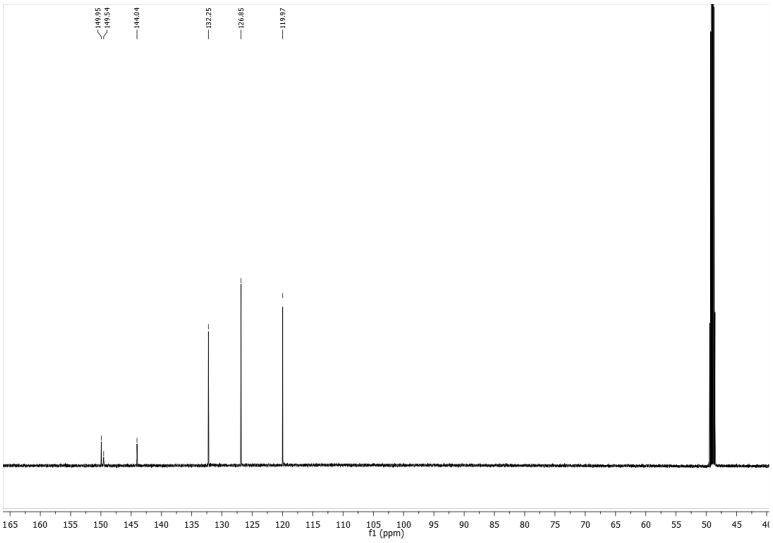

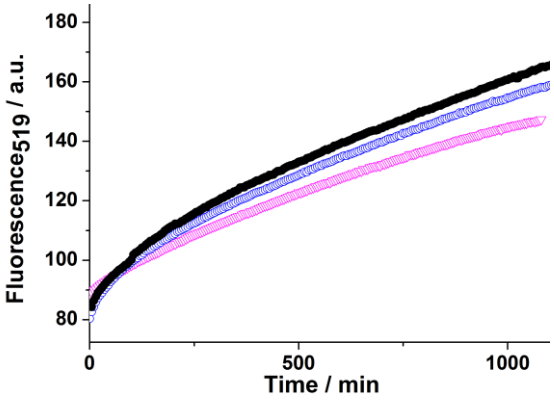

Figure S1: Fluorescence intensity at λ_{ex}=485 nm and λ_{em}=519 nm vs. time of DNBS-GG (6.5 µM) in the presence of 6.5 µM of GSH (black), Cys (red), or Hcy (pink) at pH=7.35 and 37°C.

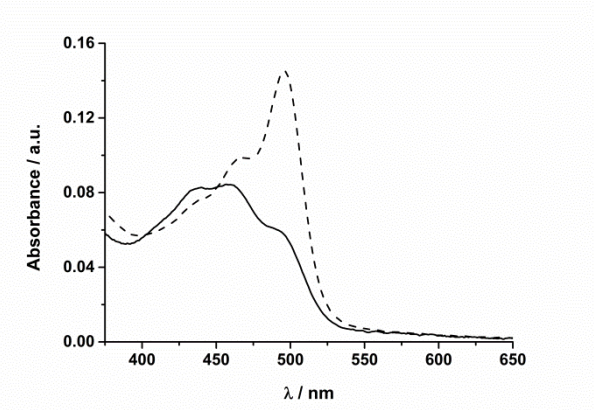

Figure S2: Absorption spectra of DNBS-GG (6.5×10^{-6} M) in Tris (20 mM) solution at pH=7.35, without thiol (▬) and with thiol (1×10^{-5} M) after 24 h (····).

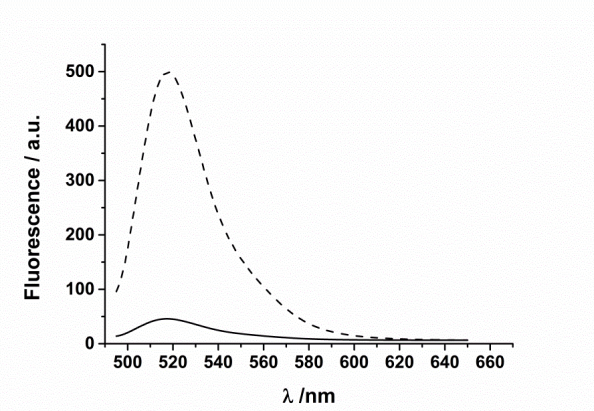

Figure S3: Fluorescence emission spectra of DNBS-GG (1×10^{-6} M) in Tris (20 mM) solution at pH=7.35, without thiol (▬) and with thiol (1×10^{-6} M) after 24 h (····).

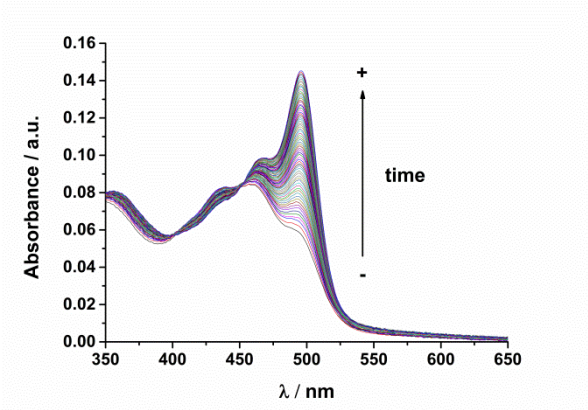

Figure S4: Absorption spectra of DNBS-GG (6.5×10^{-6} M) in Tris (20 mM) solution at pH=7.35, (**—**) in the presence of thiol (1×10^{-6} M) recorded every 5 minutes.

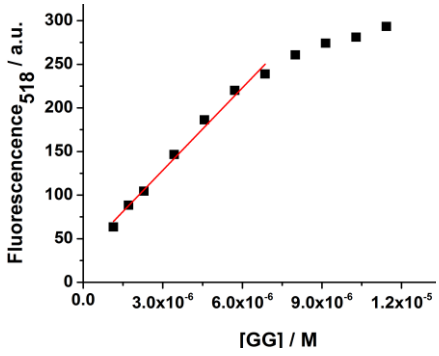

Figure S5: Kavanagh law of GG at λ_{ex}=485 nm and λ_{em}=518 nm.

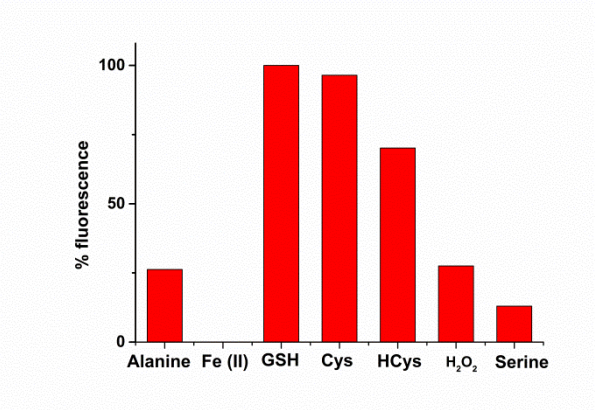

Figure S6: Relative increase in fluorescence after 2 h of DNBS-GG 6.5×10^{-6} M in the presence of glutathione, cysteine, homocysteine, different amino acids, Fe(II) and H_2O_2 at pH=7.35.

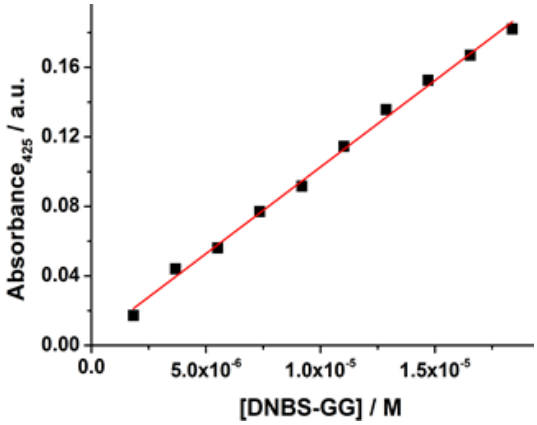

Figure S7: Beer's law of DNBS-GG at 461 nm.

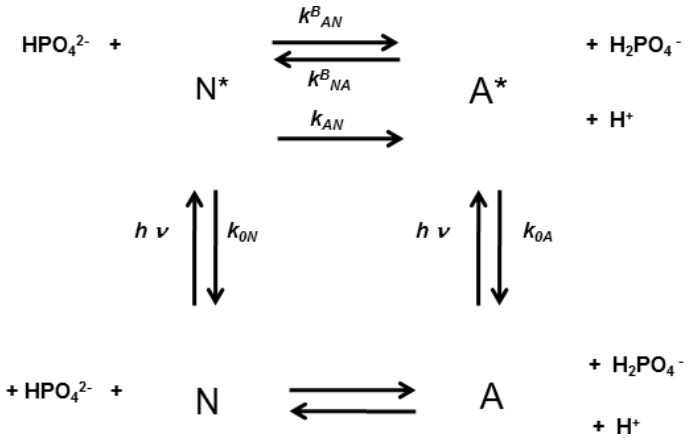

Scheme 4: Kinetic Model of an Excited-State Proton Transfer Reaction, Promoted by a Suitable Proton Acceptor or Donor.

Scheme 4 represents the dynamic, linear, time-invariant, intermolecular system studied. It consists of two distinct types of ground-state species and their corresponding excited-state species (N neutral, A anion). Both species are two different prototropic forms of the considered dye at neutral pH. Thus, the ground-state species are related through the acid-base equilibria, determined by the corresponding p*K*a. Excited-state species N* and A* are created upon photoexcitation, and they can decay by fluorescence (F) and non-radiative (NR) processes. We include those decay processes in rate constant k_{0i} (equal to $k_{Fi} + k_{NRi}$) for species i*. In this study, we consider the excited-state process promoted by species of an added buffer, $H_2PO_4^-$ and HPO_4^{2-}. Hence, $H_2PO_4^-$ could promote an excited-state protonation with **A***, represented by rate constant k_{AN}^B. Likewise, HPO_4^{2-} could react with **N*** resulting in an excited-state deprotonation, whose rate constant is denoted by k_{AN}^B. We also include the deprotonation of excited state **N*** (represented by rate constant k_{AN}).

The fluorescence decay traces should be influenced by the presence of ESPT reactions, if kinetic rate constant of buffer mediated proton transfer are fast enough to compete with fluorescence emission, causing the decay times to be dependent on the pH and on the buffer concentration.[1-4]

We show in previous paper that GG undergoes an ESPT reaction, which interconverts the neutral and anion forms in the presence of phosphate at near neutral pH and which strongly alters the fluorescence emission signal.[5]

References

1. J. M. Alvarez-Pez, L. Ballesteros, E. M. Talavera and J. Yguerabide, J. Phys. Chem. A, 2001,105, 6320.

2. L. Crovetto, A. Orte, E. M. Talavera, J. M. Alvarez-Pez, M. Cotlet, J. Thielemans, F. C.De Schryver and N. Boens, J. Phys. Chem. B, 2004, 108, 6082.

3. A. Orte, L. Crovetto, E. M.Talavera, N. Boens and J. M. Alvarez-Pez, J. Phys. Chem. A, 2005, 109, 734. d) N. Boens, W. Qin, N.Basaric, A. Orte, E. M. Talavera and J. M. Alvarez-Pez, J. Phys. Chem. A, 2006, 110, 9334.

4. A. Martinez-Peragon, D. Miguel, A. Orte, A. J. Mota, M. J. Ruedas-Rama, J. Justicia, J. M. Alvarez-Pez, J. M. Cuerva, L. Crovetto, Organic & Biomolecular Chemistry 2014,

RESULTS

Chapter 2: A new Fluorescent Dye for Oxidative Stress through Thiol Detection in vivo in Cell Culture

A NEW FLUORESCENT DYE FOR OXIDATIVE STRESS THROUGH THIOL DETECTION IN VIVO IN CELL CULTURES

ABSTRACT

It has been synthesized a new xanthene derivative, Granada Green Dinitrophenyl sulfonate (GGDNPS), for the assay of cellular oxidative stress based on biothiols concentration changes. The dye is able to react with biological thiols by a thiolysis reaction that promotes fluorescence intensity variations. To demonstrate the usefulness of GGDNPS for the in vivo measurement of oxidative stress, 661W photoreceptor derived cells were exposed to light to induce ROS generation and the changes of GGDNPS fluorescence was measured. In these cells, GGDNPS fluorescence correlated with the biothiols levels measured by an enzymatic method. Therefore GGDNPS allows single-cell bioimaging to monitor changes in biothiols levels associated with ROS generation.

INTRODUCTION

Cells damages promoted by unfavorable external factors like temperature changes, light exposure or/and extreme pH values usually result in the presence of some kind of cellular stress. Such stresses have been associated with the production of high levels of undesirable reactive oxygen species (ROS).[1, 2] Within this context, a wide range of physiological processes at molecular level have been raised as protective defence against the damaging effects of oxidative stress.[3] Among them, a common response is the increase of the biothiols levels in cellular media and, therefore, one of the most successful methods to measure the oxidative stress is to determine the biothiols concentration.

New methods to measure biothiols are continuously being developed.[4, 5] Among them, fluorescence approaches are the most interesting ones taking into account the

advantages derived from their high sensitivity, simplicity and low cost.[6] Recently, it has been done a considerable effort to develop new biothiols probes with improved features, like the simultaneous detection of biothiols and phosphate[7] or a reversible fluorescent biothiols probe[8]. In this work, we have synthesized a new fluorescent dye, Granada Green Dinitrophenyl sulfonate (GGDNPS), carefully designed to optimize the intracellular biothiols sensitivity and fast response for its use in bioimaging. As a proof of concept to demonstrate its biomedical applications, we have used this probe for the measurement of ROS due to light irradiation on photoreceptors cells.

Degeneration of photoreceptors due to oxidative stress[9-11] is one of the main causes of the loss of vision in diseases such as age-related macular degeneration (AMD) or diabetic retinopathy.[11-14] A well-established model of oxidative-stress-induced photoreceptor death is exposition to light of the mouse-derived photoreceptor cell line 661W in culture[15] since it has been demonstrated that short periods of light exposure induces ROS generation and cell death in this cone cell line.

The use of this new fluorescent dye has allowed us to evaluate the rapid generation of ROS in response to the light as well as a precise quantitation of biothiols in this experimental setting. As expected, our results indicate that there is dependence between the light exposure period and the intracellular biothiols levels, in response to the oxidative stress. The use of this fluorescent dye could be optimal for the development of an automated, high throughput method for the screening of new antioxidant drugs for photoreceptor oxidative related diseases or other diseases that are associated with an increase in the intracellular ROS concentrations.

EXPERIMENTAL SECTION

Instrumentation

Steady-state fluorescence emission spectra were performed on a JASCO FP−8300 spectrofluorometer equipped with a 150 W xenon lamp for excitation.

Fluorescence Imaging Microscopy (FIM) was performed on a Pico Quant MicroTime 200 microscope system with an excitation source of LDH-485 laser. The light beam was directed onto a dichroic mirror (510dcxr, Chroma) and passed through the oil immersion objective (1.4 NA, 100×) specific to an inverted microscope system (IX-71, Olympus). After passing the immersion objective, the fluorescence light was filtered by a long-pass filter (500LP, AHF/Chroma) and directed to a 75-µm confocal aperture. The light was transmitted to a FF01-520/35 bandpass filter (Thorlabs) and focused on single-photon avalanche diodes (SPCM-AQR 14, Perkin Elmer). The data were collected by a TimeHarp 200 TCSPC module (PicoQuant). Raw Fluorescence intensity images were acquired by a scanner with 512 x 512 pixels resolution, exported as matrix data by SymPhoTime software and analysed by Fiji ([Fiji Is Just] ImageJ)[16].In order to obtain the fluorescence intensity of the cells, output matrix data were exported and Gaussian smoothing function was applied (s.d. = 2, in pixels). In addition, the background (extracellular pixels) was removed for the calculation.

Synthesis of GGDNPS

The synthesis of Granada Green Dinitrophenyl sulfonate (GGDNPS) derivative was carried out starting from Granada Green probe, previously synthesized by our group.[7] Following the procedure we have previously described (Scheme S1), Granada Green (GG, 67 mg, 0.179 mmol) and DMAP (33 mg, 0.269 mmol) were dissolved in 2mL of dry CH_2Cl_2 and then commercially available 2,4-dinitrobenzenesulfonyl chloride (57 mg, 0.215 mmol) was added. The reaction was stirred at room temperature and

monitored by TLC. When no starting material was observed, the solvent was then evaporated and residue was purified by flash chromatography (CH_2Cl_2: MeOH mixtures). The corresponding product (96 mg, 89%) was obtained as pure sample and showed NMR and HRMS spectra matching with the reported one.[7]

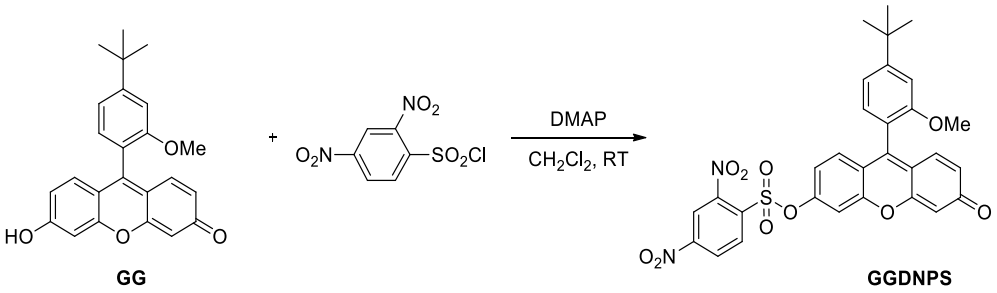

Scheme 1: Synthesis of GGDNPS.

Sample preparation

A stock solution of GGDNPS (3.4×10^{-4}M) was prepared using ethanol as solvent. From this stock solution, an aqueous (Mili-Q water) solution at 1×10^{-5}M concentration was prepared to get a final concentration of the dye of 2.43×10^{-7}M at pH 7.35 in KRP media for cell and aqueous solution samples. Stock solution of GSH (100mM) was prepared using diluted $HClO_4$ or NaOH to adjust to the desired pH. No further purification was done on chemicals that they were used as received. In order to avoid possible deterioration caused by light and heat exposure, all the solutions were kept cool in the dark when not in use.

KREBS Ringer Phosphate (KRP) buffer was prepared by mixing the require amounts of different salts. The salts used were the following ones with the respective concentrations mentioned in brackets: NaCl (118mM), KCl (5mM), $CaCl_2$ (1.3mM), $MgSO_4$ (1.2mM), KH_2PO_4 (1.2mM), Hepes (30mM). It was checked that the solution had a pH around 7.35.

CHO-k1, HepG2 and 661WCell cultures

Chinese hamster ovary cells (CHO-k1; ATCC no.CCL-61) and human hepatocellular carcinoma HepG2 (ATCC no. HB-8065™) were provided by the Cell Culture Facility of the University of Granada. The mouse retinal cone-cell line 661W, is a transformed cell line derived from mouse retinal tumors and was a gift from Dr. Enrique de la Rosa (CIB, CSIC, Madrid, Spain). All these cells were grown at 37ºC in Dulbecco's Modified Eagle's Medium (DMEM) supplemented with 10% (v/v) fetal bovine serum (FBS), 2 mM glutamine plus 100 U/ mL penicillin, and 0.1 mg/mL streptomycin. Cells that were submitted to Fluorescence Imaging Microscopy (FIM), were seeded onto coverslips at a density of 2.3 10^5 cells per well into 6-well plates.

661W cells exposure to light.

661W cells were seeded at a density of 2.3 10^5 cells per well into 6-well plates, and then incubated for 24 h under a humidified atmosphere of 5% CO_2 at 37ºC. Then, cells were exposed to 0.64mW/cm^2 of white light from above the 6-well plates for the indicated period of time. Incubations were carried out in a humidified atmosphere of 5% CO_2 at 37ºC. Controls cells were kept in the dark in the same incubator to eliminate any effects due to temperature fluctuations.

Quantitation of light induced cells death

661W cells were seeded at 1.5 10^4 cells per well into a p48 plate and 24 h later were exposed to white light for several periods of time as described. Cytotoxicity was assayed by determining the percentage of cell viability (with respect to unexposed cells) using the 3-(4,5-dimethylthiazol-2-yl)-2,5-diphenyl-2H-tetrazolium bromide (MTT)[17]method which correlates the cellular metabolic activity with the number of viable cells in culture. Results are reported as % viability based on the untreated control cells at 24 h normalized to 100% viable.

ROS assay in light exposed 661W cells

For the assay of light induced ROS generation in 661W cells, cells were seeded at 1.5 10^4 cells per well into a p48 plate and 24 h later were exposed to white light for several periods of time as described. Then, cells were incubated with 10 µM 2´,7´-dichlorodihydrofluorescein diacetate (DCFDA) for 30 minutes, washed twice in PBS, lysed in 50 µl passive lysis buffer (Promega) and diluted with 150 µl PBS. The fluorescence generated by the ROS dependent oxidation of the fluorophore was measured in a JASCO FP−8300 spectrofluorometer at 485 nm excitation and 535 nm emission wavelengths. Protein content was assayed using the Bio-Rad protein assay kit and results were shown as relative fluorescence units / mg proteins for each sample.

GSH determinations

For the assay of GSH content in the 661W cells, cells were seeded at 4.5 10^5 cells per p60 plate and 24 h later were treated with white light as described above. At selected time points, cells were trypsinized and washed with ice cold 1X PBS twice and centrifuged at 500 xg. Immediately, the pellets were re-suspended with 200 µL ice-cold 5% metaphosphoric acid, mixed, sonicated and centrifuged at 12000 xg for 5 minutes at 4ºC. Supernatants were used for the assay of GSH, using a using enzymatic recycling method.[18] Protein pellets were washed with ethanol, re-suspended in 0.1% SDS in 400 mM Tris-HCl pH8 buffer and assayed for protein content using the Bio-Rad protein assay kit.

RESULTS AND DISCUSSION

We have recently explored the photophysical properties of Granada Green (GG), a xanthenic structure developed in our lab, and their derivatives for the in vivo detection of different analytes, including biothiols.[19] Within this context, we now describe a new use of a GG derivative (Figure 1), a 2,4-dinitrosulfonate (DNS),

Granada Green Dinitrophenyl sulfonate (GGDNPS) with excellent kinetic and photophysical characteristics for the *in vivo* intracellular detection of biothiols, in which mainly the photostability of the derivative was significantly improved.

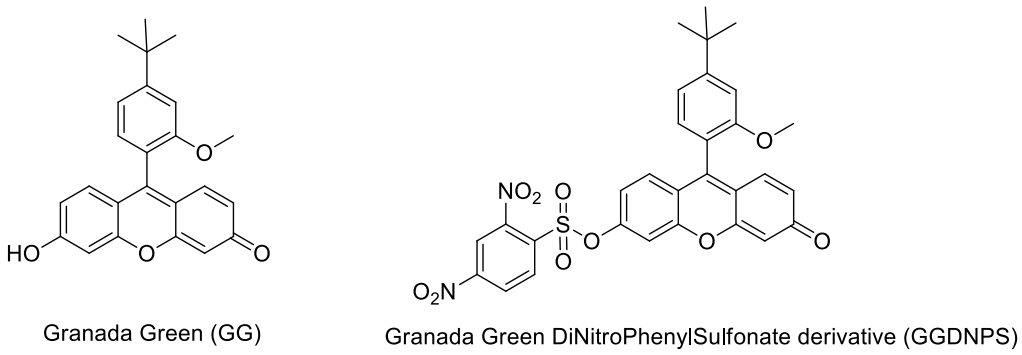

Figure 1. Chemical structures of GG (left) and GGDNPS (right).

In this case, a fast response of the dye is required to keep the cells in good conditions during the measure (see Supplementary Material). This fast response is obtained at the cost of using of a highly activating group such as DNS, instead of a less activated dinitrosulfinate one. [7] Control experiments show that GGDNPS is reasonable stable towards hydrolysis in the presence and absence of N-Methyl-D-maleimide (NMM), a well-known scavenger for biothiols. Nevertheless, taking into account the high reactivity of GGDNPS these results do not exclude that other nucleophiles present in the complex cellular media could give a background signal.

As expected, in the presence of glutathione (GSH) (ratio GGDNPS:GSH, 1:100) a notable increase in fluorescence intensity (×7.5 times Figure 2-A) was observed. Moreover, the increase observed was linear (R^2=0.997, see Figure S2). Next, we asseverate that the fluorescence increases over time was due to the presence of GSH; for this purpose, we prepared solutions of NMM and biothiols and afterward, GGDNPS was added. The use of different GSH:NMM ratios resulted in a dose-

response decrease in fluorescence of the dye. As can be observed in Figure 2-B, GSH:NMM ratios 2:1 and even 1:1 ratios blocked the increase in fluorescence due to a lower level of biothiols availability and consequently less reaction with the dye. Therefore, these results in aqueous solution predict an excellent behavior for the potential use of GGDNPS as intracellular probe in short periods of time.

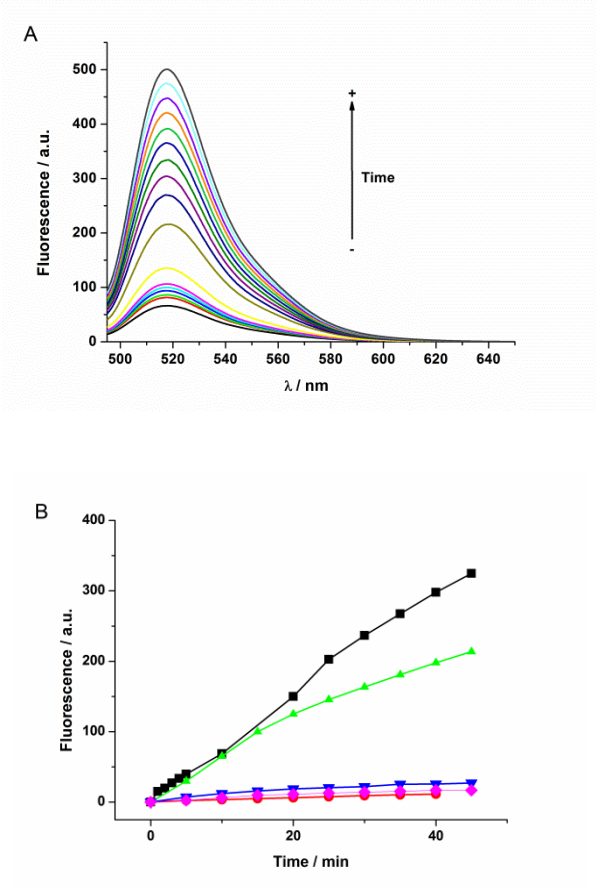

Figure 2: A) Fluorescence spectra at 0, 1, 5, 7, 15, 20, 25, 30, 35, 40, 45, 50, 55 and 60 minutes after GSH addition. B) Kinetics of increase of GGDNPS fluorescence adding GSH (square), GSH + 1 mM NMM (ratio 10:1) (triangle), GSH + 5 mM NMM (ratio 2:1) (invert triangle), GSH + 10 mM NMM (ratio 1:1) (diamond)and NMM (circle).

With these results in hands, we examined the GGDNPS response in live cells. Cell membrane permeability of GGDNPS allowed the direct use of this compound without needs of any treatment (see Figure 3). This is probably because its lipophilicity allows it to cross the plasma membrane and this is a common behavior for other xanthenic dyes.[20, 21] We have measured the increase in the fluorescence intensity using a control fibroblast cell line CHO-K1 (Chinese Hamster Ovary Cell line), a human hepatoma cell line, HepG2 and a mouse retinal cone-cell line, 661W. Figure 3 shows FIM of the control (CHO-K1) (up), HepG2 (middle) and 661W (down) cells. As can be observed, at the same measure times, a significant response is produced in HepG2 and 661W cells. However, as expected in the fibroblast cells, where the biothiols levels are lower, it is only observed an almost negligible increase. The result confirms a higher presence of biothiols in the reservoir pool of HepG2 and 661W cells to protect themselves from the higher production of ROS, which is characteristic of these cell lines.[15] Therefore, up to this point the GGDNPS probe shows an adequate sensibility to discriminate biothiols content in different cells lines.

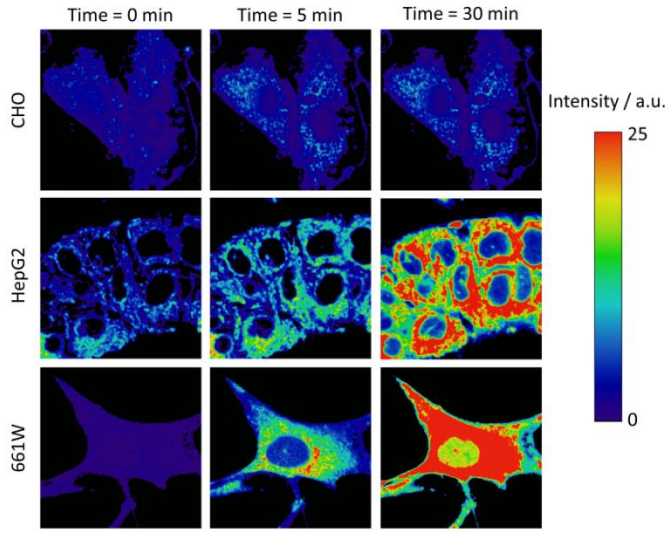

Figure 3: FIM images of CHO-k1, HepG2 and 661W cells at different incubation times (0 min, 5 min and 30 min).

Next, to confirm the use of GGDNPS as a dynamic biothiols probe in live cells, we studied its response in liver hepatocellular carcinoma (HepG2) cells. As described above, this cellular line contains enough biothiols levels in its reservoir pool to achieve a correct answer of GGDNPS. As it can be observed in Figure 4, to confirm the selectivity of the probe towards biothiols in this cell line, we added a thiol−blocking reagent, NMM, to them. The kinetics of the fluorescence increase of HepG2 cells in absence (open circle) and in presence of NMM (square) is represented in Figure 4. NMM quenched the increase in fluorescence upon addition of GGDNPS with only a slight increase upon time in the fluorescence signal, and therefore, the selectivity of GGDNPS through the intracellular biothiols could be confirmed.

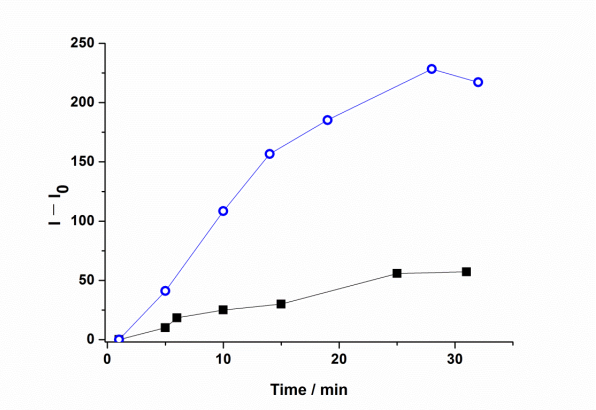

Figure 4: HepG2 cells fluorescence Intensity in presence (squares) and in absence (open circles) of NMM (ratio 1:1).

In order to demonstrate the validity of GGDNPS to detect fast changes in biothiols levels caused by oxidative stress, we introduced the dye into 661W cells. This cell line is used as a model for photoreceptor−like cellular pathologies associated with retinal degenerations caused by light exposure.[22] It has been reported that in this cell line, oxidative stress produces a severe damage through photochemical reactions that leads to lipid peroxidation and accumulation of ROS.[15] Therefore, we have studied the light−induced cellular stress to 661W cells. For this purpose, we exposed them to light during different periods of time (0 min, 15min, 45 min, 60 min, 100 min, 120 min, 150 min and 180 min), and after light−exposition, we added GGDNPS into cells and the fluorescence intensity was measured by FIM every 5 minutes during 30 minutes. Some of these FIM images are represented in Figure 5. From each image the average of fluorescence intensity values were calculated. As can be observed, in Figure 5 the kinetic of the increase in the fluorescence intensity depends on the time cells have been exposed to light.

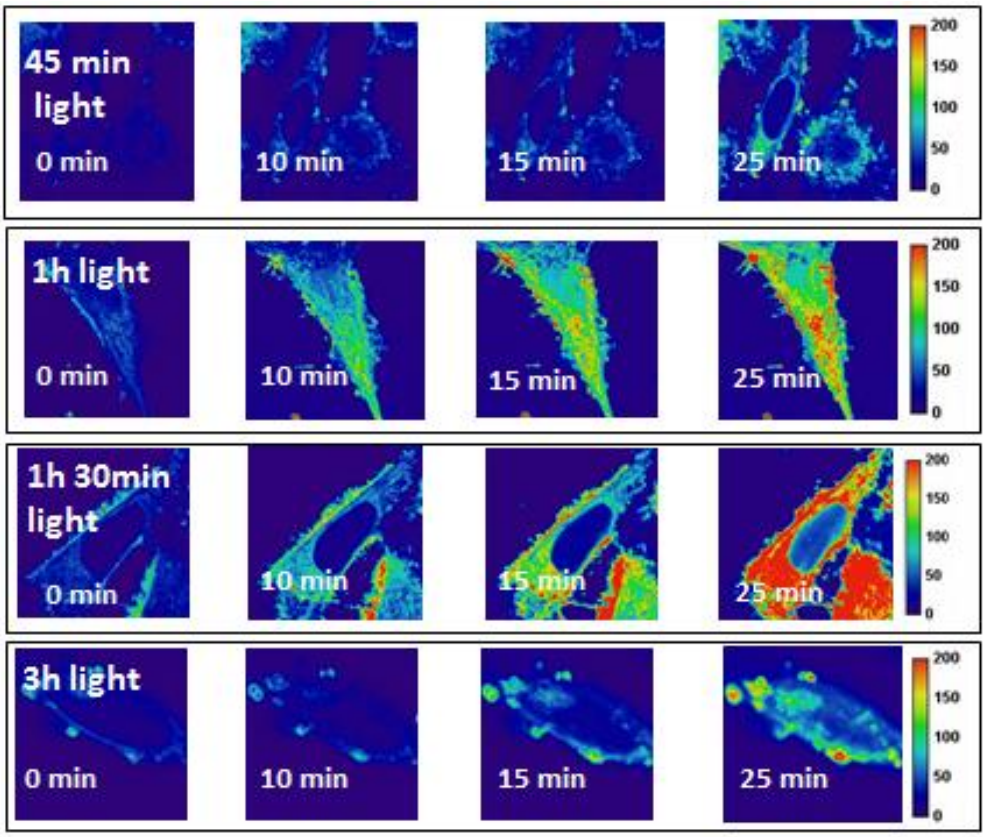

Figure 5: FIM cell images at different light time exposure (45 min, 60 min, 90 min and 180 min). The images show fluorescence intensity changes depending on the light time exposure through time.

In order to study deeply the dependence of light exposure time on oxidative stress, cell viability and ROS content (assayed using a 2´,7´-dichlorodihydrofluorescein diacetate probe) were measured at selected time points (Figure 6A). At the same time points, the area under the curve (AUC) of the kinetic obtained from each light exposure time using the GGDNPS probe was calculated and compared with the GSH content of the cells, measured using an enzymatic method (Figure 6B). As expected, Figure 6A shows a strong dependence of the cell viability and ROS generation on the

light exposure time. When the AUC for the GGDNPS probe is depicted (Figure 6B), it can be observed that, at short light exposure times (until ~40 min) a decrease in the AUC recovered from the fluorescence kinetics is detected. This decrease is probably due to an increase in ROS, produced by the light-induced cellular oxidative stress, and as a consequence a decrease in the reservoir pool of biothiols. During this initial period there was almost not observed changes in cell viability. After this initial period and until ~120 min, it is observed a fast increase in the AUC of fluorescence intensity values in the kinetics. Albeit in this cell line, a time course of biothiols concentration upon light exposure has not been previously described; our results suggest an intracellular synthesis of biothiols as a defence mechanism to the high light-induced stress. This period coincides with a slight decrease in the viability of the cells. Finally, we observed a final period after ~120 min with a decrease in the AUC. This is coincident with a dramatically decrease in the viability of the cells. Here, we hypothesized that after a long exposure time to light and ROS generation, cellular capability to restore biothiols pool is exhausted and then ROS induced cellular stress translates into a massive cellular death. When the data obtained with the GGDNPS probe is compared with the GSH content of the cells measured by an enzymatic method, a clear resemblance is obtained. Remarkably, detection of biothiols by GGDNPS presents a higher sensitivity than enzymatic method. Probably, this is because the enzymatic method is based on an average value of all the cells (live and dead) however, the single-cell biothiols detection using GGDNPS is obtained selecting only live cells.

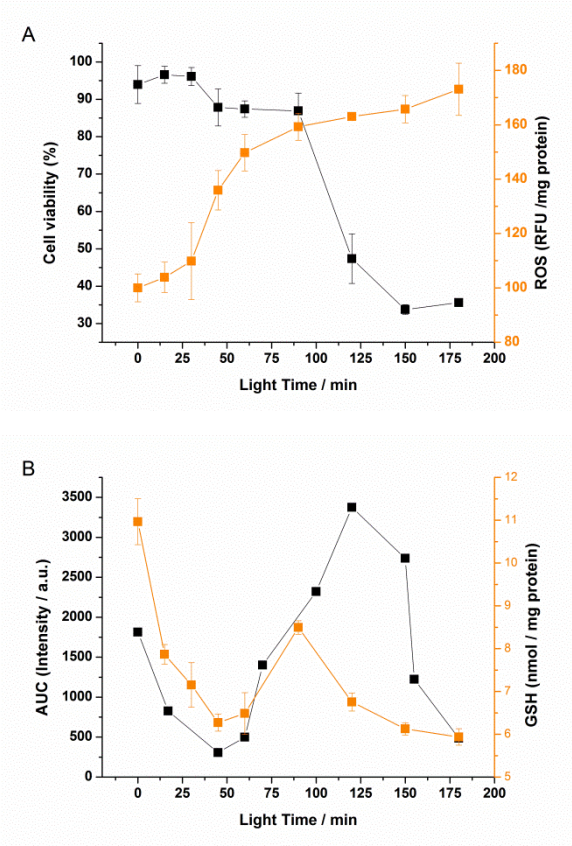

Figure 6: A) ROS measurement (orange) and 661W cell viability B) GSH enzymatically measurement (orange) and Area Under the Curve Fluorescence intensity data at different light exposure time.

CONCLUSIONS

We have designed and synthesized a new compound optimized as biothiols sensor for fluorescence imaging microscopy. The mechanism of action implies the thiolysis of the sulfinyl group by biothiols and producing a fast increase of the fluorescence intensity.

Our experiments confirm that GGDNPS is an excellent tool for detecting rapid occurring changes in intracellular biothiols levels as a response of cellular oxidative stress. We performed measurements using Hepatocelullar Carcinoma cells (HepG2) and a photoreceptor-derived cell line (661 W) and the results confirm the ability of this new dye to detect intracellular biothiols variations as a consequence of cellular stress induced by ROS. Photoreceptor−like cells show a biothiols reservoir to protect themselves from light induced ROS that are consumed after a period of ~40 minutes of light exposure time. After this initial period it is detected an intracellular synthesis of biothiols as a response of cells to defend from ROS. Finally, it is observed cell death and consequently, biothiols decrease promoted by the excess of light−induced oxidative stress.

The simplicity of this approach could be easily extended to develop high-throughput tests for new antioxidant drugs to prevent and/or treat photoreceptor oxidative related diseases.

References

1. L. F. Mottram, S. Boonyarattanakalin, R. E. Kovel and B. R. Peterson, *Org Lett*, 2006, **8**, 581-584.
2. G. A. Block, T. E. Hulbert-Shearon, N. W. Levin and F. K. Port, *American journal of kidney diseases : the official journal of the National Kidney Foundation*, 1998, **31**, 607-617.
3. N. Majed, Y. Li and A. Z. Gu, *Current opinion in biotechnology*, 2012, **23**, 852-859.
4. P. C. White, N. S. Lawrence, J. Davis and R. G. Compton, *Electroanalysis*, 2002, **14**, 89-98.
5. J. R. Winther and C. Thorpe, *Biochimica Et Biophysica Acta-General Subjects*, 2014, **1840**, 838-846.
6. L. El-Khairy, P. M. Ueland, H. Refsum, I. M. Graham, S. E. Vollset and P. European Concerted Action, *Circulation*, 2001, **103**, 2544-2549.
7. M. A. Mansoor, A. B. Guttormsen, T. Fiskerstrand, H. Refsum, P. M. Ueland and A. M. Svardal, *Clinical chemistry*, 1993, **39**, 980-985.
8. P. M. Ueland, *Clinical chemistry*, 1995, **41**, 340-342.
9. P. N. Youssef, N. Sheibani and D. M. Albert, *Eye*, 2011, **25**, 1-14.
10. G. Sluder and D. E. Wolf, *Method Cell Biol*, 2013, **114**, Xix-Xx.
11. P. Raggi, A. Boulay, S. Chasan-Taber, N. Amin, M. Dillon, S. K. Burke and G. M. Chertow, *Journal of the American College of Cardiology*, 2002, **39**, 695-701.
12. W. G. Goodman, J. Goldin, B. D. Kuizon, C. Yoon, B. Gales, D. Sider, Y. Wang, J. Chung, A. Emerick, L. Greaser, R. M. Elashoff and I. B. Salusky, *New Engl J Med*, 2000, **342**, 1478-1483.
13. C. Bergwitz and H. Juppner, *Adv Chronic Kidney D*, 2011, **18**, 132-144.
14. D. M. Townsend, K. D. Tew and H. Tapiero, *Biomedicine & pharmacotherapy = Biomedecine & pharmacotherapie*, 2003, **57**, 145-155.
15. R. P. Steegers-Theunissen, G. H. Boers, H. J. Blom, F. J. Trijbels and T. K. Eskes, *Lancet*, 1992, **339**, 1122-1123.
16. J. Schindelin, I. Arganda-Carreras, E. Frise, V. Kaynig, M. Longair, T. Pietzsch, S. Preibisch, C. Rueden, S. Saalfeld, B. Schmid, J. Y. Tinevez, D. J. White, V. Hartenstein, K. Eliceiri, P. Tomancak and A. Cardona, *Nature Methods*, 2012, **9**, 676-682.
17. T. Mosmann, *Journal of Immunological Methods*, 1983, **65**, 55-63.
18. I. Rahman, A. Kode and S. K. Biswas, *Nature Protocols*, 2006, **1**, 3159-3165.
19. A. Martinez-Peragon, D. Miguel, A. Orte, A. J. Mota, M. J. Ruedas-Rama, J. Justicia, J. M. Alvarez-Pez, J. M. Cuerva and L. Crovetto, *Organic & biomolecular chemistry*, 2014, **12**, 6432-6439.

20. J. M. Paredes, M. D. Giron, M. J. Ruedas-Rama, A. Orte, L. Crovetto, E. M. Talavera, R. Salto and J. M. Alvarez-Pez, *Journal of Physical Chemistry B*, 2013, **117**, 8143-8149.
21. L. Crovetto, A. Orte, J. M. Paredes, S. Resa, J. Valverde, F. Castello, D. Miguel, J. M. Cuerva, E. M. Talavera and J. M. Alvarez-Pez, *J Phys Chem A*, 2015, **119**, 10854-10862.
22. H. Refsum, P. M. Ueland, O. Nygard and S. E. Vollset, *Annual review of medicine*, 1998, **49**, 31-62.

SUPPLEMENTARY MATERIAL

Water stock solutions of both dyes (GGDNPS and DNBS-GG) without thiols were irradiated continuously by means of a Xe lamp in order to afflict maximum damage and test their photostability. Figure S1 shows the resulting steady-state fluorescence signal versus time. As can be observed, GGDNPS (up) retains almost no fluorescence signal after 4 days while DNBS-GG dye has an increase of the signal after 1 day (botton).

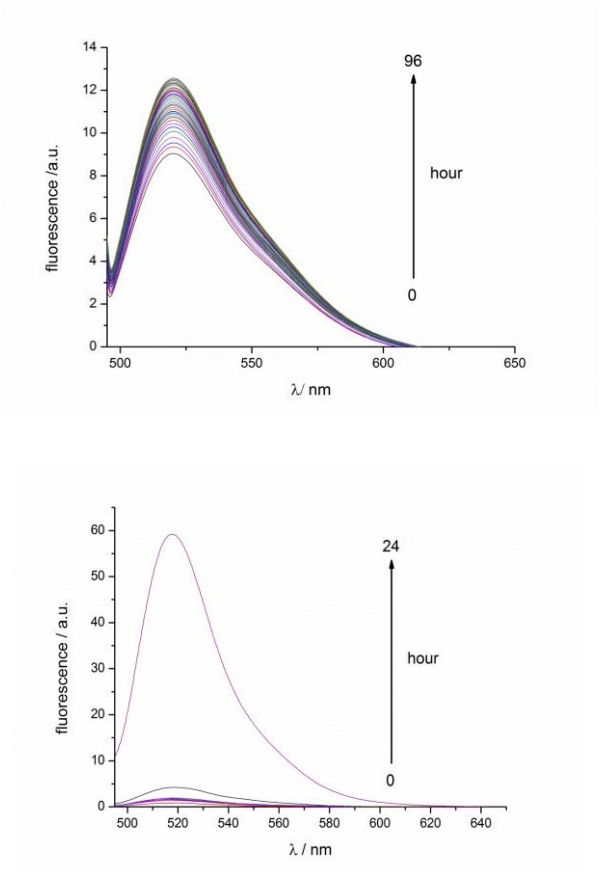

Figure S1: Steady-state fluorescence signal of GG-DNPS (up) and DNBS-GG (down) versus time.

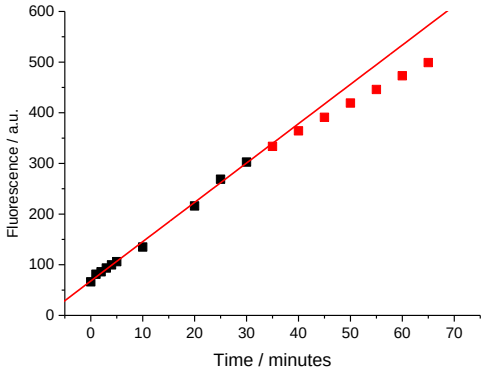

Figure S2: Increase in Fluorescence intensity of the dye in the presence of GSH.

RESULTS

Chapter 3: Efficient Acetate Sensor in Biological Media based on a Selective Excited State Proton Transfer (ESPT) Reaction

Efficient Acetate Sensor in Biological Media Based on a Selective Excited State Proton Transfer (ESPT) Reaction

ABSTRACT

We have synthesized a new fluoride−containing xanthenic dye able to dynamically and quantitatively detect acetate anion, a biologically relevant analyte, in water. We studied deeply the photophysical properties of the compound and verified its use as an acetate probe in synthetic serum.

INTRODUCTION

Acetate, the ionized form of acetic acid, is a critical metabolite in fatty acids and carbohydrate metabolism.[1] The importance of acetate in the metabolism goes further than a physiological process as it is directly and/or indirectly involved in cancer metabolism,[2, 3] and consequently several acetate role studies about different cancer types can be found in literature. [4, 5] In particular, it is relevant in the colorectal tumor, one of the most prevalent cancers in the world nowadays. One of the roles acetate has in cancer is that it participates in cancer cells apoptosis[6] and its detection and study could help to achieve a better understanding of cell death mechanism and could also help to discover new tools for colorectal cancer prevention. [1, 7]

Due to its biological and physiopathological importance, the availability of new probes to detect acetate *in situ* in biological samples is essential for metabolism research in which acetate is involved. A very successful approach in this field has been the interaction between the probe and the acetate anion by complementary hydrogen bonding. [8] Nevertheless, such kind of interactions can also occur with other anions such as phosphate, iodine, bromide or fluoride. [9] Moreover the nature of this interaction precludes, in general, the use of pure water as solvent owing to the undesirable competition of water with the hydrogen-bond based interaction. [10, 11] To

the best of our knowledge there are only two strategies in literature in which water is exclusively used as solvent. First implies chemical derivatization of acetate in basic media followed by gas chromatography analysis.[12] The second one is the use of commercially available kits. These can be based on kinetic processes or the use of enzymes. Nevertheless, they present some drawbacks related with the necessity of clear samples, interferences with either compounds (i.e. –SH containing reagents) or other enzymes present in the samples. Moreover, in all the cases the total acetate anion is determined by derivatization of the compound, which prevents from measuring changes in acetate concentration during the analysis in dynamic samples. In this sense it would be interesting to base the analysis in a parameter which is not affected by turbidity and/or the sample composition and that allows a dynamic detection in real time. Therefore, the challenge in this field is to retain the acetate sensitivity and selectivity in water in a dynamic way. To this end a very different approach is required.

A common feature of all the anions is the acid-base characteristics in water, which in principle can be used to discriminate between them. Within this context, it is known that Excited State Proton Transfer (ESPT) reactions [13] promote changes in fluorescent molecules, which can be detected and related with the presence of the corresponding proton donor/acceptor. ESPT reaction is faster than fluorescence emission and depends on the proton donor/acceptor concentration. Therefore, fluorescence decay lifetime (τ) can be used to monitor the analyte concentration. [14] This fluorescent parameter (τ) presents several advantages over fluorescence intensity such as independence on the dye concentration or easily differentiation of autofluorescence interferences. [15] Moreover, this approach is fully compatible with water and the selectivity of the transfer process is based on the similarities in pK_a between the dye and the analyte (proton donor/acceptor), which precludes any

interference of anions with different acid-base characteristics. [16] The approach is only limited by the existence of the suitable dye with the required pK_a.

Xanthene-based dyes seem to be ideal for this purpose owing to the remarkable photophysical properties they present and the possibility of a fine-tuning of the pK_a. In particular, Tokyo [13, 14, 17, 18] and Granada Green derivatives [19] had previously shown remarkable "on-off" properties and possibility of ESPT, but they present an unsuitable pK_a value of 6-7. Fluorinated Oregon Green xanthenes [20] present a lower pK_a, achieving the optimal situation in which the buffer and the dye have a similar pK_a. Nevertheless the presence of a carboxylic acid in the structure results in complex acid-base equilibriums and consequently complex analysis. Pennsylvania Green compounds [17] are a smart combination of the Tokyo and Oregon Green dyes resulting in an interesting combination of photophysical and acid-base characteristics. However, the simplest one (**1**, Scheme 1) presents an undesirable fluorescence in both neutral and anionic structures, which precludes its use as an "on-off" probe.

In this work, we have synthesized new Pennsylvania-Based dyes **2**-**4**, being one of them (**2**) able to quantitatively detect acetate concentration in water. Compound **2** was studied deeply in order to obtain the rate constants involved in the ESPT reaction promoted by acetate, and to verify its use as an acetate probe in synthetic serum.

EXPERIMENTAL SECTION

Synthesis

All reagents were used as purchased from standard chemical suppliers and used without further purification. Reactions involving organometallic compounds were carried out under Ar atmosphere. TLC was performed on aluminium-backed plates coated with silica gel 60 (230-240 mesh) with F254 indicator. The spots were visualized with UV light (254 nm). All chromatography purifications were performed

with silica gel 60 (35-70 μm). NMR spectra were measured at room temperature. ^{1}H NMR spectra were recorded at 300, 400, 500 or 600 MHz. Chemical shifts are reported in ppm using residual solvent peak as reference ($CHCl_3$: δ = 7.26 ppm, CH_2Cl_2: δ = 5.32 ppm, CH_3OH: δ = 3.31 ppm). ^{13}C NMR spectra were recorded at 75, 101, 126 or 151 MHz using broadband proton decoupling and chemical shifts are reported in ppm using residual solvent peaks as reference ($CHCl_3$: δ = 77.16 ppm, CH_2Cl_2: δ = 54.0 ppm, CH_3OH: δ = 49.00 ppm). Carbon multiplicities were assigned by DEPT and HSQC techniques. High resolution mass spectra (HRMS) were recorded using EI at 70e V on a Micromass AutoSpec (Waters) or by ESI-TOFF mass spectrometry carried out on a Waters Synapt G2 mass spectrometer.

Sample preparation

A stock solution of dyes (9×10^{-5} M) in 10^{-3} M NaOH was prepared using Milli-Q water. For samples preparation in acetate buffer solutions, sodium acetate and acetic acid (both Sigma puriss. p.a.) were used in appropriate amounts to obtain the required pH and dye concentration. Solutions without buffer were prepared using NaOH and $HClO_4$ (0.01 M) both from Sigma-Aldrich, spectroscopic grade. All the solutions were prepared using Milli-Q water as a solvent. All of the chemicals were used as received without further purification. The solutions were kept cool in the dark when not in use to avoid possible deterioration through exposure to light and heat.

Photophysical Study

Absorption spectra were recorded using a Perkin-Elmer Lambda 650 UV/Vis spectrophotometer with a Peltier temperature controller. Steady-state fluorescence emission spectra were collected using a JASCO FP-8300 spectrofluorometer equipped with a 450−W xenon lamp for excitation. All measurements were recorded at room

temperature using 10 × 10 mm cuvettes. The pH of the solutions was measured immediately before and after recording each spectrum.

Fluorescence decay traces of solutions were recorded by the single-photon timing method using a FluoTime 200 fluorometer (PicoQuant, Inc.). [15, 21] The excitation was achieved using a LDH−485 and LDH−440 (PicoQuant, Inc.), and the observation was performed through a monochromator at 510, 515, 520 and 525 nm. The pulse repetition rate was 20 MHz. Fluorescence decay histograms were collected in 1320 channels using 10 × 10 mm cuvettes. The time increment per channel was 37 ps. Histograms of the instrument response functions (using a LUDOX scatterer) and sample decays were recorded until they typically reached 2×10^4 counts in the peak channel. Three fluorescence decays were recorded for all of the samples. The fluorescence decay traces were individually analysed using an iterative deconvolution method with exponential models using FluoFit software (PicoQuant).

FLIM analysis

FLIM images were collected by a Pico Quant MicroTime 200 microscope system with an excitation source of LDH-485 laser. The light beam passed through a dichroic mirror (510dcxr, Chroma) and through the oil immersion objective (1.4 NA, 100×) specific to an inverted microscope system (IX-71, Olympus). After passing the immersion objective, the fluorescence light was filtered by a long-pass filter (500LP, AHF/Chroma) and directed to a 75-µm confocal aperture. The light was transmitted to a FF01-520/35 bandpass filter (Thorlabs) and focused on single-photon avalanche diodes (SPCM-AQR 14, Perkin Elmer). The data were collected by a TimeHarp 200 TCSPC module (PicoQuant) and raw Fluorescence lifetime images were acquired by a scanner with 512 x 512 pixels resolution. To obtain the fitted FLIM images, it was realized a binning of 2 x 2 in SymphoTime software and the matrix data were exported and analysed by a home-coded *Fiji* ([*Fiji Is Just*] *ImageJ*) program [22]. For this aim, and firstly of all, outliers data points were removed using a selective median

filter that replaces a pixel by the median of the pixels in the surrounding (s.d. = 7 pixels) if it deviates from the median by more than a certain value. Finally, in order to achieve a larger number of counts in each pixel, it was done a binning of 4 x 4 and later, a Gaussian smoothing function (s.d. = 1 pixel) filters were applied.

RESULTS AND DISCUSSIONS

1: R^1 = Me, R^2 = H
2: R^1 = Me, R^2 = OMe
3: R^1 = OMe, R^2 = Me
4: R^1 = OMe, R^2 = *t*Bu

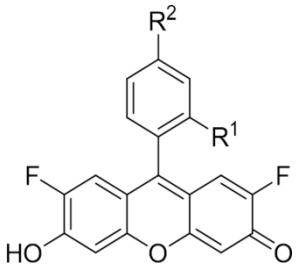

Scheme 1: Molecular structure of the synthesized compounds.

The careful selection of the pK_a of the fluorescent probe is crucial for the acetate anion sensing. For this reason we decided to use 2,7-difluorinated xanthene as fluorescent core owing to the inductive effect of fluorine atoms and the consequent increase in the acidity of xanthenes derivatives. We have recently reported that the pK_a of a functionalized xanthene can be also fine-tuned with a judicious selection of the substitution at C-9.[19] It is also known that the "on-off" characteristics can be modulated by the substituents in the C-9 position. After some synthetic effort we found that Pennsylvania-type xanthene **2** presented the best photophysical and acid-base characteristics for our objective. Based on our previously described methodology[16] we synthesized compounds **1**-**4** in good yields as it is reported in the Supplementary Material. [18, 23]

Absorption measurements for compound **2** in water strongly depend on the pH (Figure 1). Spectra showed a maximum at 492 nm at higher pH values measured (corresponding to the anion form) and two maxima (450/478 nm) at lower pH values

(corresponding to the neutral form). The isosbestic point suggests a chemical equilibrium between two species; i.e. the neutral and anion forms as chemical structures suggest. From those spectra the pK_a and the molar absorption coefficients ε_I (λ_{abs}) could be extracted using non-lineal global fitting of absorbance surface *vs* pH and λ_{abs} [24] (see Supplementary Material). Experimental pK_a corresponds to 4.04 ± 0.02, around three units lower than the non-fluoride compounds[19, 25] and reasonably close to the acetate pK_a value (4.76).

Figures 2 and 3 show plots of individual absorbance at different pH values and the recovered values of molar absorption coefficients of both neutral (ε_N) and anionic form (ε_A) in the absence of acetate buffer.

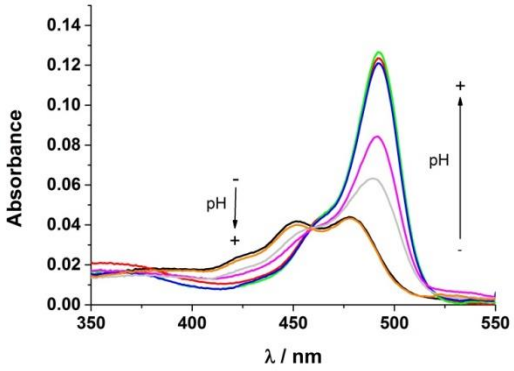

Figure 1: Absorption spectra of compound **2** (3.2×10^{-6} M) at different pH values (from 2.14 to 6.71).

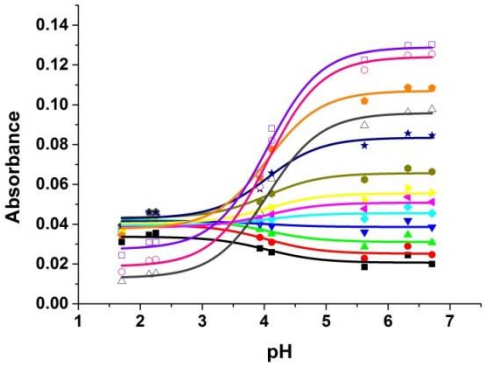

Figure 2: Curves generated by fitting the individual A (λ_{abs}) versus pH data.

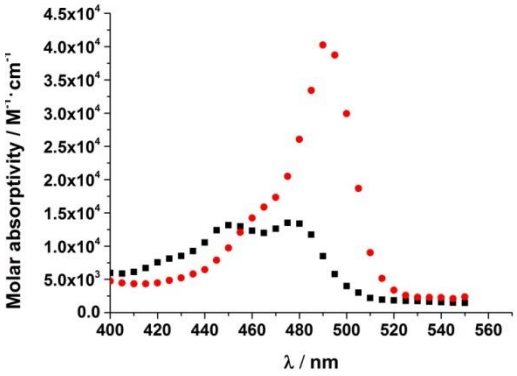

Figure 3: Recovered molar absorption coefficients versus wavelength for the neutral (black) and anionic (red) form of compound **2.**

As can be observed, the shape of the absorption coefficients is similar to the previous dyes as shown in bibliography.[17-19] For the anion, it is shown a maximum at 492 nm and a shoulder at around 460 nm. The neutral absorption coefficient shows two maxima at 450 and 480 nm. However, it is almost three times lower than the anion maximum.

A steady-state fluorescence study resulted in the emission spectra profiles corresponding to the two prototropic species involved in the chemical equilibrium. The anionic species have an emission maximum at 515 nm and the neutral emission maxima are centered at 510 nm (see Figure S4 in Supplementary Material). Moreover, the quantum yields (Φ) of every species were calculated and for compound **2** it was obtained 0.65 for the anionic form and a very low value of 0.02 for the neutral form, which is an ideal photophysical characteristic for our purpose.

We recovered the pK_a in the excited state (pK_a^*) by steady-state fluorescence using high acetate concentration so that buffer mediated ESPT reaction would occur during the excited lifetime. The resulting pK_a^* (4.42 ± 0.07) was similar to the pK_a in the ground state (Figure S5). Figure 4 shows the emission spectra of compound **2** at different pH values. It is remarkable the very low intensity values at lower pH with a decrease of about 160 times in the fluorescence signal, evidencing the "on-off" character of the dye.

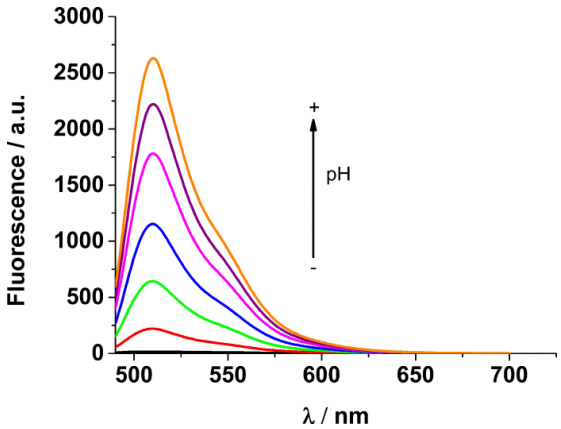

Figure 4: Fluorescence emission spectra of compound **2** (6×10^{-6} M) in acetate (400 mM) solution at different pH values (from 1.37 to 7.79).

Finally, using time-resolved fluorescence, we recovered the decay times. In concordance with steady-state emission, anion species decay time (3.30 ns) is higher than neutral one, becoming almost insignificant (0.02 ns).

Some xanthene derivatives can undergo an ESPT reaction when an appropriate proton donor/acceptor, as acetate, is present. These reactions can modify the steady-state or time-resolved fluorescence signal. Important experimental information of the ESPT reaction mechanism is accessible through time-resolved fluorescence measurements, by which the kinetic behavior of the system in the excited state can be obtained. Figure 5 shows the scheme involved in the ESPT reaction and fluorescence emission for the two species of compound **2** present at the pH range studied, considering a causal, linear, time-invariant, intermolecular system. The theory of buffer-mediated ESPT reactions has been well established (See Supplementary Material).[26]

Firstly, we measured compound **2** in absence of acetate buffer. We did a global analysis of 40 curves corresponding to C^B = 0 mM, at pH range from 4.28 to 6.65, at λ_{ex} = 485 and 440nm and λ_{em} = 510, 520, 530, 540 and 550 nm, providing pH independent reliable decay time estimations: τ_1 = 0.021 ± 0.003 ns and τ_2 = 3.300 ± 0.002 ns (χ_g^2 = 1.176). This behavior confirms that in the absence of acetate ions the buffer-mediated ESPT reaction does not occur. When the pH was much higher than the pK_a value, only the anion species is present. In this condition, fluorescence decay was given by a monoexponential function with the decay time τ_2 = 3.300 ± 0.002 ns. At high pH values the proton concentration is very low, and hence the reprotonation reaction in the excited state is very slow and does not compete with the radiative constant. Therefore, this decay time unequivocally defines a value for $k_{02} = 1/\tau_2$. Decreasing the pH the neutral species were also presented, being the main form at pH values lower than the pK_a. However, the anionic form is preferentially excited at λ_{ex} = 485 nm, due to its large molar absorption coefficient. Moreover the higher

quantum yield of anionic species, as well as the low fluorescence quantum yield of the neutral form ("on-off"), makes the fluorescence of this latter one difficult to detect. Although such shorter decay time appears at lower values of pH (pH below 3.8) results in a very small α_1 contribution in the full decay time. By using λ_{ex} = 440 nm, the neutral form was preferentially excited, and the short decay time (τ_1 = 0.021 ± 0.003 ns) is detectable even at higher pH values (pH higher than 4.50); but keeping in any case a small α_1 contribution. In contrast, the τ_1 decay time may not be specifically assigned to the neutral, k_{01}, radiative constant because this decay time also contains the excited-state dissociation rate constant k_{21}. From the global analyses of decay traces collected in the absence of acetate buffer, we estimated a value for k_{02} = (3.02 ± 0.01) $\times$ 10^8 s^{-1} and for the sum of rate constants (k_{01} + k_{21}) = (5.25 ± 0.71) $\times$ 10^{10} s^{-1}.

In order to fully describe the ESPT reaction mediated by acetate buffer the following fluorescence decay surface was collected: pH range from 3.11 to 8.05, and different C^B (0, 21, 85, 170, 200, 340 and 400 mM) as a function of λ_{em} (510, 520, 530, 540 and 550 nm), with λ_{ex} of 485 and 440 nm.

The complete decay surface was analysed by using the global analysis (GA) approach, which allows the direct determination of the underlying rate constants k_{ij}. [26, 27] Recovered decay times were fit to equation S7-12 in order to obtain the kinetic constants of the proton transfer reaction in the excited state (Figure 6).

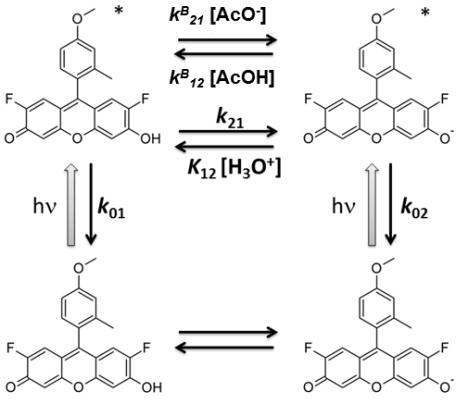

Figure 5: Kinetic model of ground- and excited-state proton-transfer reactions of compound **2** in presence of acetate buffer.

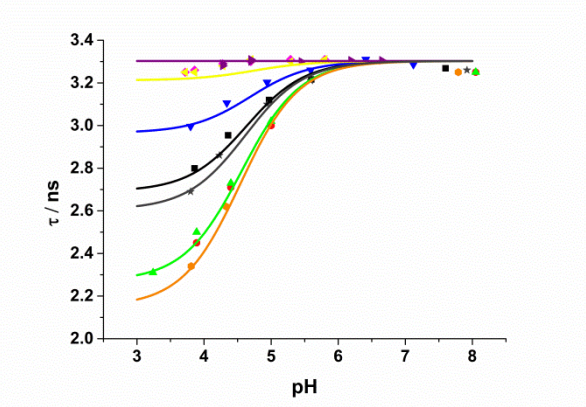

Figure 6: Global fitting (solid lines) of the theoretical equations (eqs S7−S12 in the Supplementary Material) to the decay times at different acetate buffer concentrations (0, 21, 85, 170, 200, 340 and 400 mM) and pH values (3.17-8.05).

Rate Constant	Value
$(k_{01}+k_{21})$ / s^{-1}	5.25 ($\pm$ 0.71) $\times$ 10^{10}
k_{02} / s^{-1}	3.02 ($\pm$ 0.01) $\times$ 10^{8}
k_{12}^{B} / M^{-1} s^{-1}	4.07 ($\pm$ 0.12) $\times$ 10^{8}
k_{21}^{B} / M^{-1} s^{-1}	1.99 ($\pm$ 0.34) $\times$ 10^{11}

Table 1: Recovered ESPT rate constant values from the Global Analysis of the Fluorescence decays of Figure 6.

The good fitting obtained provided estimations, compiled in Table 1, for all the rate constants in Figure 6. The rate constant values clearly show the much faster deactivation of the neutral form, around two orders of magnitude more rapid than the anion deactivation, which causes the fluorescence being dominated by the anion emission. This correspondence of the simulated curves with the decay times obtained and the sensitivity toward the acetate concentration establishes **2** as an appropriate dye for screening the concentration of acetate at pH around 4.

In order to study the specific response of the dye to acetate in biological samples, we also investigated the potential interference by the presence of other anions presented in serum (pyruvate, glucose, phosphate, bicarbonate and fluoride). No changes in the fluorescence of the dye were found in the presence of these anions except from fluoride, where was observed a slight effect, but without significance in biological samples (see Supplementary Material).

To take advantage of these results, we checked the capability of the dye to determine acetate in biological samples trough Fluorescence Lifetime Imaging Microscopy (FLIM) using synthetic serum. As monoexponential behavior in decay traces is a useful property for a fluorescence-lifetime based sensor dye, we selected a pH value in which **2** had monoexponential decay in the presence of acetate in order to obtain higher sensitivity. To mimic the liquid biopsies, we used commercial solution of Dulbecco´s modified Eagle´s medium (DMEM) (Sigma-Aldrich D6546)

containing inorganic salts, aminoacids, vitamins, high glucose, and other components at different acetate concentration ranging from 15 mM to 120 mM at pH 4.00. To recover the FLIM images, a biexponential function model was used to analyse the decay in each pixel. Shorter decay time was fixed at 1.5 ns that include the background signal of the medium autofluorescence, as well as the possible dye-matrix interactions. The longer decay time was freely fitted being tuned by the acetate concentration. Figure 7A shows the FLIM images representing the dependent decay times recovered at different acetate concentration. By using an arbitrary color scale the difference in the decay times can be appreciated by change in the colors. Figure 7B shows the respective histograms recovered from Figure 7A.

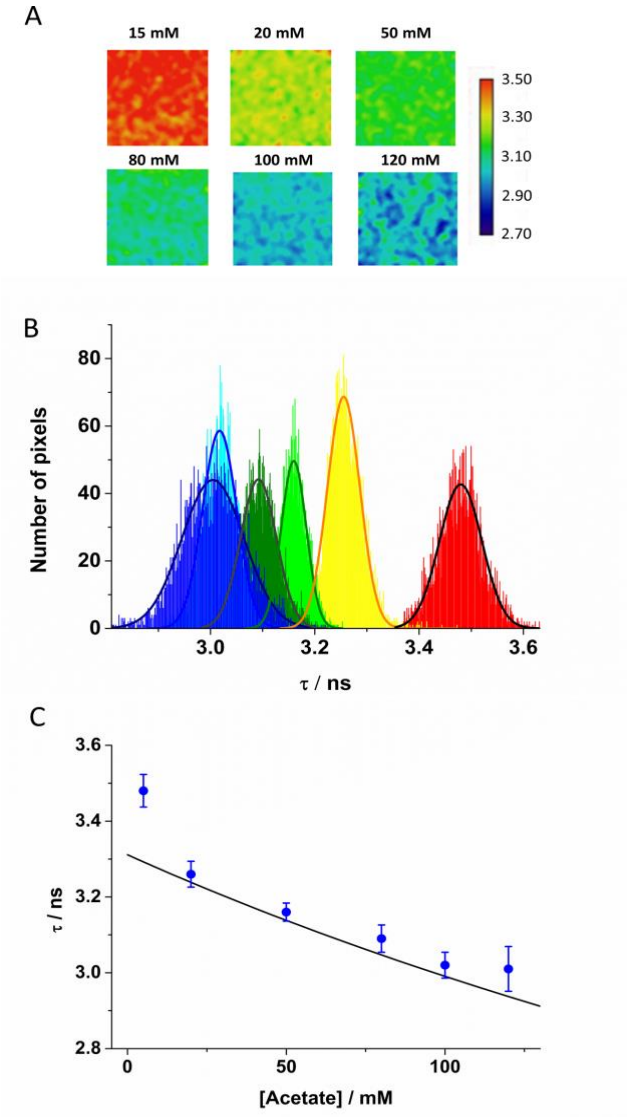

Figure 7: A) FLIM images from compound **2** in DMEM medium with different acetate concentration at pH = 4.00. B) Histograms of lifetimes recovered from Figure 7A. C) Decay time (dot) of the dye in DMEM medium at pH 4.00 obtained from FLIM images and recovered lifetime (line) from the kinetic constants. Scale bars represent the standard deviation.

The average lifetimes of FLIM were also recovered and are shown in Figure 7C, joint with the lifetimes predicted by the kinetic constants at pH 4.00. Even using samples with a complex matrix, the similarity between the lifetime predicted and the experimental is staggering.

CONCLUSIONS

In summary, a new fluorescent compound **2** has been synthesized, allowing acetate determination in biological samples using fluorescence decay time sensors.

We recovered the kinetic constants of the species involved in the chemical equilibrium presented in the pH range of interest. Finally, to inspect its future application as acetate sensor in liquid biopsies, we checked the ability of this new dye to detect acetate concentration changes using synthetic serum by FLIM. The results were very similar to the decay times predicted by the kinetic constants. Futhermore, it is remarkable that, under the conditions of the experiments performed in this work, the dye achieved the millimolar order sensitivity.

References

1. S. Seshadri, A. Beiser, J. Selhub, P. F. Jacques, I. H. Rosenberg, R. B. D'Agostino, P. W. Wilson and P. A. Wolf, *The New England journal of medicine*, 2002, **346**, 476-483.
2. O. Nygard, S. E. Vollset, H. Refsum, L. Brattstrom and P. M. Ueland, *Journal of internal medicine*, 1999, **246**, 425-454.
3. R. P. Steegers-Theunissen, G. H. Boers, F. J. Trijbels, J. D. Finkelstein, H. J. Blom, C. M. Thomas, G. F. Borm, M. G. Wouters and T. K. Eskes, *Metabolism: clinical and experimental*, 1994, **43**, 1475-1480.
4. C. J. Boushey, S. A. Beresford, G. S. Omenn and A. G. Motulsky, *Jama*, 1995, **274**, 1049-1057.
5. G. R. Beck, B. Zerler and E. Moran, *Proceedings of the National Academy of Sciences of the United States of America*, 2000, **97**, 8352-8357.
6. M. Yoshimoto, A. Waki, Y. Yonekura, N. Sadato, T. Murata, N. Omata, N. Takahashi, M. J. Welch and Y. Fujibayashi, *Nuclear medicine and biology*, 2001, **28**, 117-122.
7. R. L. Wahl, J. Harney, G. Hutchins and H. B. Grossman, *The Journal of urology*, 1991, **146**, 1470-1474.
8. G. A. Dienel and N. F. Cruz, *Neurochemistry international*, 2006, **48**, 586-595.
9. T. Mashimo, K. Pichumani, V. Vemireddy, K. J. Hatanpaa, D. K. Singh, S. Sirasanagandla, S. Nannepaga, S. G. Piccirillo, Z. Kovacs, C. Foong, Z. Huang, S. Barnett, B. E. Mickey, R. J. DeBerardinis, B. P. Tu, E. A. Maher and R. M. Bachoo, *Cell*, 2014, **159**, 1603-1614.
10. C. Marques, C. S. Oliveira, S. Alves, S. R. Chaves, O. P. Coutinho, M. Corte-Real and A. Preto, *Cell death & disease*, 2013, **4**, e507.
11. P. Kapusta, *Advanced Photon Counting*, 2015.
12. K. R. Castleman and I. T. Young, in *Microscope Image Processing*, Academic Press, Burlington, 2008, pp. 1-9.
13. J. M. Paredes, M. D. Giron, M. J. Ruedas-Rama, A. Orte, L. Crovetto, E. M. Talavera, R. Salto and J. M. Alvarez-Pez, *Journal of Physical Chemistry B*, 2013, **117**, 8143-8149.
14. J. M. Paredes, L. Crovetto, R. Rios, A. Orte, J. M. Alvarez-Pez and E. M. Talavera, *Phys. Chem. Chem. Phys.*, 2009, **11**, 5400-5407.
15. J. R. Lakowicz, *Principles of Fluorescence Spectroscopy*, 3rd edn., Springer, 2006.
16. M. A. Mansoor, A. B. Guttormsen, T. Fiskerstrand, H. Refsum, P. M. Ueland and A. M. Svardal, *Clinical chemistry*, 1993, **39**, 980-985.
17. K. R. Castleman and I. T. Young, in *Microscope Image Processing*, Academic Press, Burlington, 2008, pp. 11-25.

18. K. R. Castleman, in *Microscope Image Processing*, Academic Press, Burlington, 2008, pp. 27-38.
19. A. Martinez-Peragon, D. Miguel, A. Orte, A. J. Mota, M. J. Ruedas-Rama, J. Justicia, J. M. Alvarez-Pez, J. M. Cuerva and L. Crovetto, *Organic & biomolecular chemistry*, 2014, **12**, 6432-6439.
20. A. Orte, R. Bermejo, E. M. Talavera, L. Crovetto and J. M. Alvarez-Pez, *J. Phys. Chem. A*, 2005, **109**, 2840-2846.
21. K. R. Castleman, in *Microscope Image Processing*, Academic Press, Burlington, 2008, pp. 39-49.
22. J. Schindelin, I. Arganda-Carreras, E. Frise, V. Kaynig, M. Longair, T. Pietzsch, S. Preibisch, C. Rueden, S. Saalfeld, B. Schmid, J. Y. Tinevez, D. J. White, V. Hartenstein, K. Eliceiri, P. Tomancak and A. Cardona, *Nature Methods*, 2012, **9**, 676-682.
23. A. Martinez-Peragon, D. Miguel, R. Jurado, J. Justicia, J. M. Alvarez-Pez, J. M. Cuerva and L. Crovetto, *Chemistry*, 2014, **20**, 447-455.
24. J. Yguerabide, E. Talavera, J. M. Alvarez and B. Quintero, *Photochemistry and Photobiology*, 1994, **60**, 435-441.
25. L. Crovetto, J. M. Paredes, R. Rios, E. M. Talavera and J. M. Alvarez-Pez, *J. Phys. Chem. A*, 2007, **111**, 13311-13320.
26. L. Crovetto, A. Orte, E. M. Talavera, J. M. Alvarez-Pez, M. Cotlet, J. Thielemans, F. C. De Schryver and N. Boens, *J. Phys. Chem. B*, 2004, **108**, 6082-6092.
27. N. Boens, N. Basaric, E. Novikov, L. Crovetto, A. Orte, E. M. Talavera and J. M. Alvarez-Pez, *J. Phys. Chem. A*, 2004, **108**, 8180-8189.

SUPPLEMENTARY MATERIAL

Synthetic part

General details

All reagents were used as purchased from standard chemical suppliers and used without further purification. TLC was performed on aluminium-backed plates coated with silica gel 60 (230-240 mesh) with F254 indicator. The spots were visualized with UV light (254 nm). All chromatography purifications were performed with silica gel 60 (35-70 μm). NMR spectra were measured at room temperature. ^{1}H NMR spectra were recorded at 300, 400, 500 or 600 MHz. Chemical shifts are reported in ppm using residual solvent peak as reference ($CHCl_3$: δ = 7.26 ppm, CH_2Cl_2: δ = 5.32 ppm, CH_3OH: δ = 3.31 ppm). Data are reported as follows: chemical shift, multiplicity (s: singlet, d: doublet, t: triplet, q: quartet, quint: quintuplet, hept: heptuplet, m: multiplet, dd: doublet of doublets, dt: doublet of triplets, td: triplet of doublets, bs: broad singlet), coupling constant (*J* in Hz) and integration; ^{13}C NMR spectra were recorded at 75, 101, 126 or 151 MHz using broadband proton decoupling and chemical shifts are reported in ppm using residual solvent peaks as reference ($CHCl_3$: δ = 77.16 ppm, CH_2Cl_2: δ = 54.0 ppm, CH_3OH: δ = 49.00 ppm). Carbon multiplicities were assigned by DEPT and HSQC techniques. High resolution mass spectra (HRMS) were recorded using EI at 70eV on a Micromass AutoSpec (Waters) or by ESI-TOFF mass spectrometry carried out on a Waters Synapt G2 mass spectrometer. Known compounds **1**[1], **6**[2] were isolated as pure samples and showed NMR spectra matching those of the reported ones.

Synthesis

The corresponding synthesis was accomplished employing a very simple methodology [3, 4] using as a key step a nucleophilic addition of an organolithium

derivative to the corresponding MOM-protected 2,7-difluoroxhanthenone derivative **5** (Scheme 1).

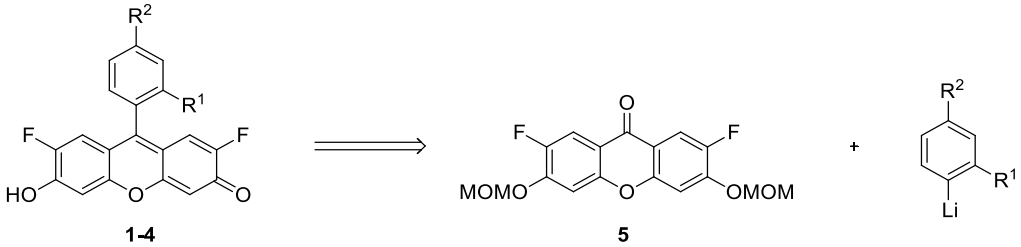

Synthesis of compound 5:

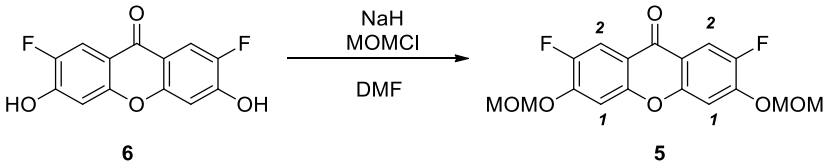

Compound **6**[2] (930 mg, 3.5 mmol) was dissolved in DMF dry (10 mL) and then NaH (703 mg, 17.6 mmol) was added. After stirring for 15 minutes the solution was treated with MOMCl (1.1 mL, 14.0 mmol) and the mixture was stirred at room temperature for 3 h. It was then diluted with EtOAc (20 mL), washed with saturated HCl (aq) (2 x 15 mL), dried over anhydrous Na_2SO_4 and the solvent removed under reduced pressure. The residue was purified by flash chromatography (EtOAc/Hexane mixtures) to give the corresponding protected ketone **5** in a 89 % yield, showing the following spectrocopic data: **^{1}H NMR (500 MHz, $CDCl_3$)** δ 7.94 (d, *J* = 10.6 Hz, 2H, H_2), 7.26 (d, *J* = 6.6 Hz, 2H, H_1), 5.35 (s, 4H, *O-*CH_2*-O*), 3.55 (s, 6H, *O-*CH_3). **^{13}C NMR (126 MHz, $CDCl_3$)** δ 174.7 (t, *J* = 2.1 Hz, C), 153.5 (d, *J* = 1.4 Hz, C), 151.2 (d, *J* = 13.3 Hz, C), 150.1 (d, *J* = 247.2 Hz, C), 115.5 (d, *J* = 6.2 Hz, C), 112.1 (d, *J* = 20.7 Hz, CH), 104.9 (s, CH), 95.5 (s, CH_2), 56.9 (s, CH_3). **HRMS (ESI):** *m/z* $[M-H]^+$ calcd for $C_{17}H_{15}F_2O_6$: 353.0837; found: 353.0837.

General procedure for the synthesis of compounds 1-4:

A solution of the corresponding bromoaryl derivative (0.2 mmol, 1 eq.) in THF (2 mL) at 78ºC, was treated with *n*-BuLi (0.22 mmol, 1.1 eq). After keeping the reaction at that temperature for 20 minutes ketone **5** (0.1 mmol, 0.5 eq) was added to the solution. Then, the mixture was stirred at - 78ºC for 15 minutes and after allowed to reach room temperature. The reaction was monitored by TLC and after consumption of ketone **5** and then HCl (10%) was added promoting and a colour change from pale yellow to orange. Finally solvent was removed under reduced pressure and residue was submitted to flash chromatography in CH_2Cl_2: MeOH mixtures, affording compounds **1**-**4**, whose spectroscopic data are reported below:

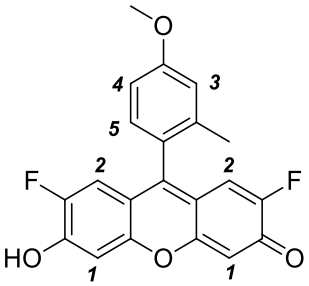

Compound 2: Orange solid obtained in 62 % yield. **^{1}H NMR (500 MHz, MeOD)** δ 7.16 (d, *J* = 8.5 Hz, 1H, H_5), 7.08 (d, *J* = 2.5 Hz, 1H, H_3), 7.03 (dd, *J* = 8.5, 2.5 Hz, 1H, H_4), 6.89 (d, *J* = 7.1 Hz, 2H, H_1), 6.81 (d, *J* = 11.1 Hz, 2H, H_2), 3.92 (s, 3H, -OCH_3), 2.04 (s, 3H, -CH_3). **^{13}C NMR (126 MHz, MeOD)** δ 162.6 (s, C), 156.4 (s, C), 155.6 (s, C), 154.5 (d, *J* = 249.5 Hz, C), 148.1 (s, C), 139.0 (s, C), 131.4 (s, CH), 125.3 (s, C), 117.2 (s, CH), 116.1 (d, *J* = 8.0 Hz, C), 113.1 (s, CH), 113.0 (d, *J* = 22.1 Hz, CH), 106.2 (d, *J* = 4.0 Hz, CH), 55.9 (s, CH_3), 19.9 (s, CH_3). **HRMS (EI, 70 eV):** *m/z* $[M]^+$ calcd for $C_{21}H_{14}F_2O_4$: 368.0860; found: 368.0860.

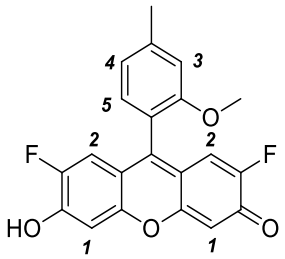

Compound 3: Orange solid obtained in 68 % yield. **^{1}H NMR (500 MHz, MeOD)** δ 7.14 (d, *J* = 8.4 Hz, 1H, H_5), 7.06 (d, *J* = 2.5 Hz, 1H, H_3), 7.01 (dd, *J* = 8.4, 2.6 Hz, 1H, H_4), 6.67 (d, *J* = 7.5 Hz, 2H, H_1), 6.66 (d, *J* = 11.5 Hz, 2H, H_2), 3.92 (s, 3H, -OCH_3), 2.05 (s, 3H, -CH_3).**^{13}C NMR (126 MHz, MeOD)** δ 170.94 (d, *J* = 17.0 Hz), 160.81 (s), 156.14 (s), 155.4 (s), 154.96 (d, *J* = 249.5 Hz), 137.33 (s), 129.81 (s), 124.78 (s), 115.58 (s), 111.36 (s), 110.48 (d, *J* = 22.4 Hz), 110.44 (d, *J* = 8.3 Hz), 104.71 (d, *J* = 5.4 Hz), 54.45 (s), 18.43 (s). **HRMS (ESI):** *m/z* $[M\text{-}Na]^+$ calcd for $C_{21}H_{14}F_2NaO_4$: 391.0752; found: 391.0743.

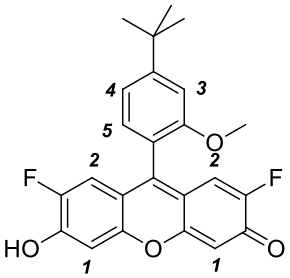

Compound 4: Orange solid obtained in 54 % yield. **^{1}H NMR (600 MHz, MeOD)** δ 7.28 (d, *J* = 1.6 Hz, 1H, H_3), 7.27 (dd, *J* = 7.8 Hz, *J* = 1.6 Hz, 1H, H_4), 7.15 (d, *J* = 7.8 Hz, 1H, H_5), 6.71 (d, *J* = 11.6 Hz, 2H, H_2), 6.64 (d, *J* = 7.5 Hz, 2H, H_1), 3.77 (s, 3H, -OCH_3), 1.46 (s, 9H, *t*Bu). **^{13}C NMR (151 MHz, MeOD)** δ 172.3 (d, *J* = 17.8 Hz, C), 157.8 (s, C), 157.5 (s, C), 156.8 (s, C), 156.2 (d, *J* = 248.9 Hz, C), 155.0 (t, *J* = 5.2 Hz, C), 131.1 (s, CH), 120.3 (s, C), 118.9 (s, CH), 112.2 (d, *J* = 22.5 Hz, CH), 111.9 (d, *J* = 8.6 Hz, C), 110.0 (s,

CH), 105.9 (d, *J* = 5.2 Hz, CH), 56.1 (s, CH_3), 36.2 (s, C), 31.7 (s, CH_3). **HRMS (EI, 70 eV):** *m/z* $[M]^+$ calcd for $C_{24}H_{20}F_2O_4$: 410.1330; found: 410.1333.

^{1}H-NMR:

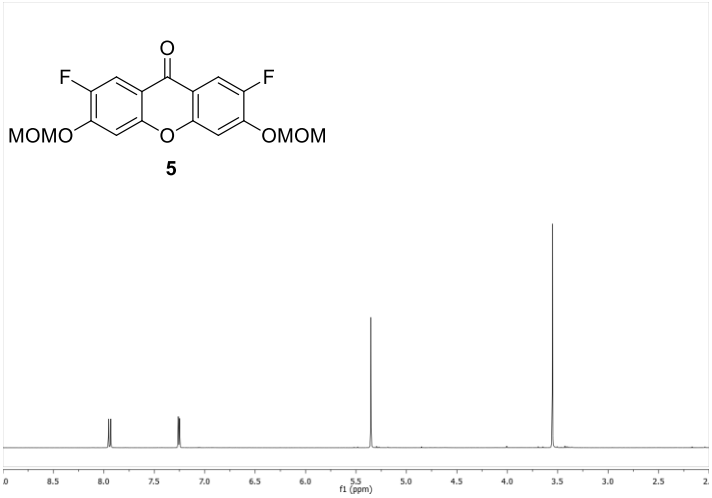

^{13}C-NMR:

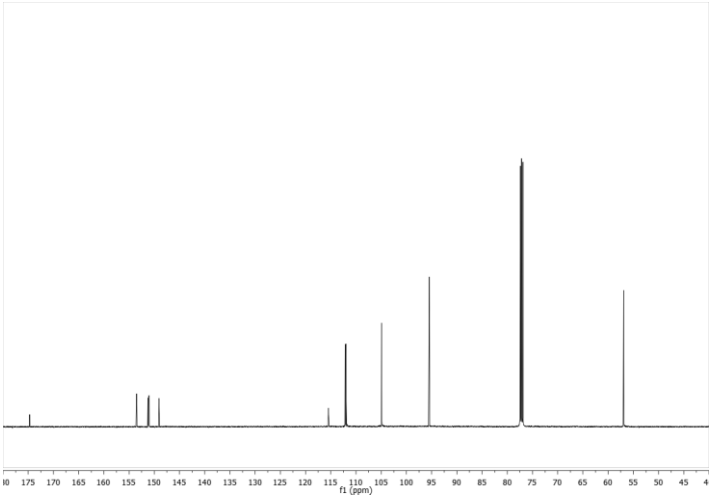

^{1}H-NMR:

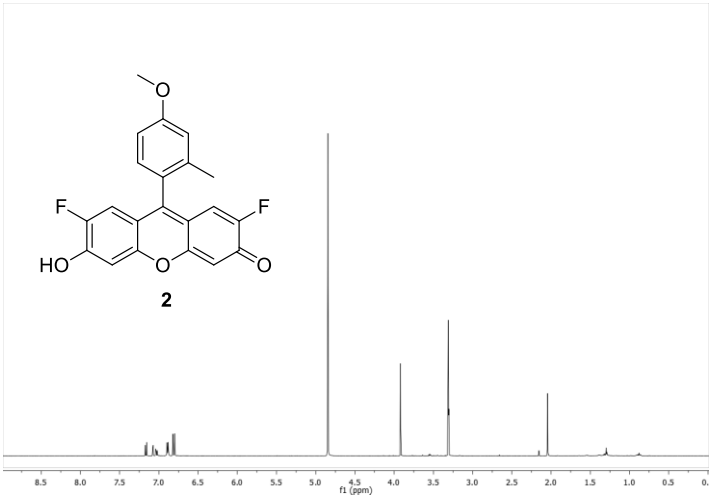

^{13}C-NMR:

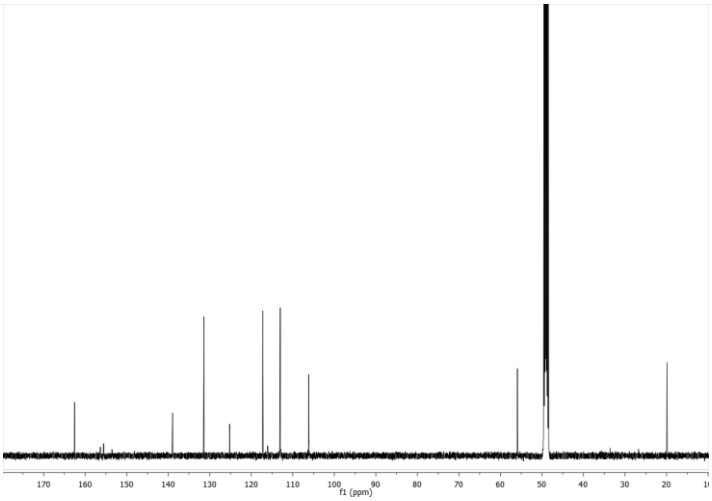

^{1}H-NMR:

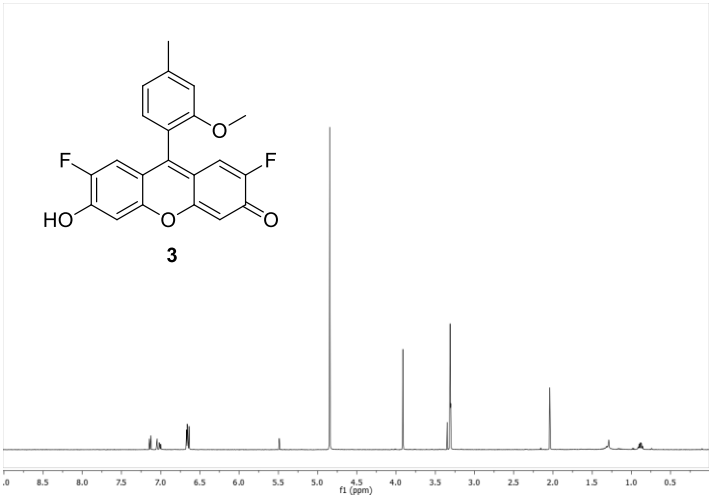

^{13}C-NMR:

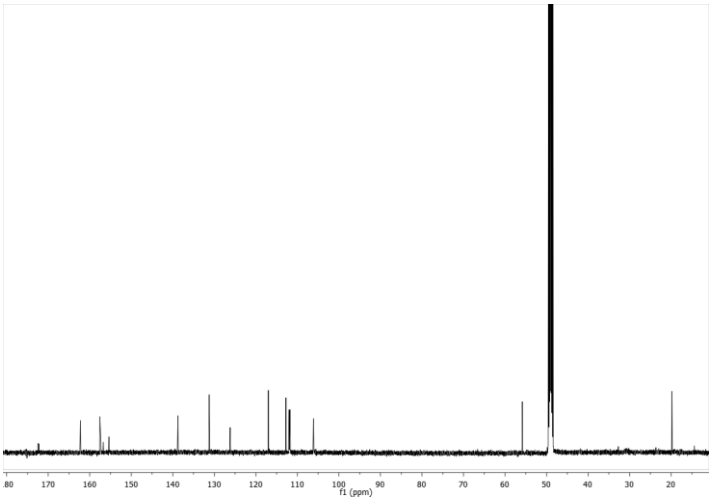

^{1}H-NMR:

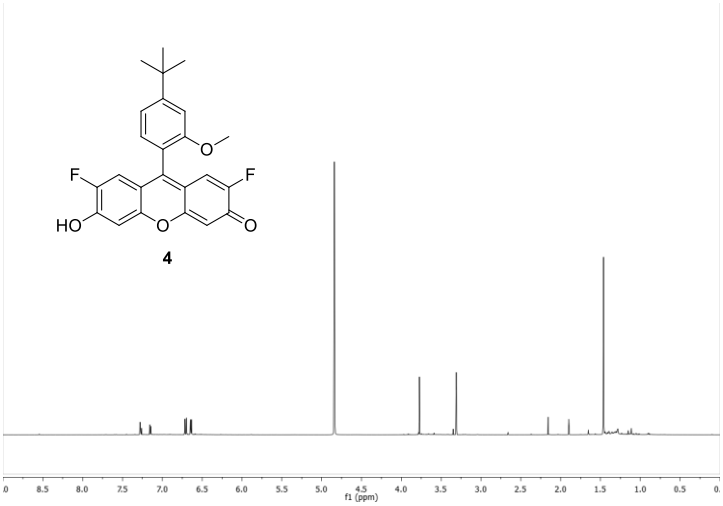

^{13}C-NMR:

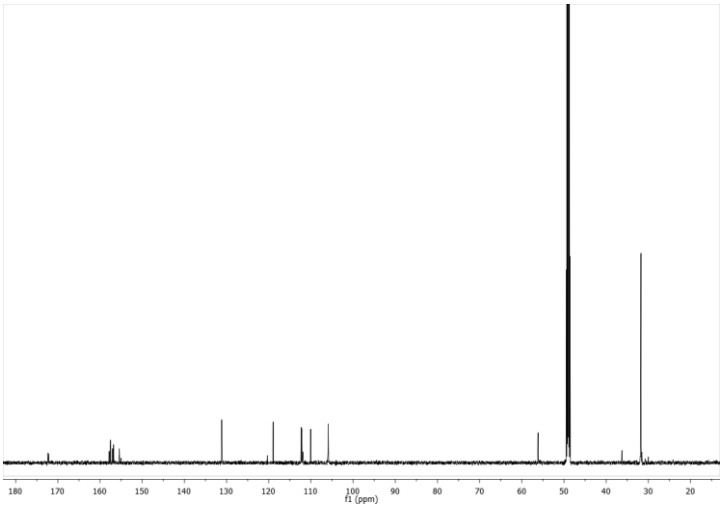

Absorption study

If a neutral/anion system follows Beer's law, at any wavelength (λ_{abs}) and pH, the absorbance (*A*) is given by the expression

$$A(\mathrm{p}H, \lambda_{abs}) = C\left(\sum_i \alpha_i(\mathrm{p}H, \mathrm{p}K_{N-A})\varepsilon_i(\lambda_{abs})\right)d \,, \qquad \text{(S1)}$$

where *C* is the total concentration of the dye, *d* is the optical path length, $\varepsilon_i(\lambda_{abs})$ is the wavelength-dependent molar absorption coefficient of the *i*th prototropic form of the dye, and α_i(p*H*, p$K_{N\text{-}A}$) is the fraction of the dye in the *i*th prototropic form, which depends on both p*H* and p$K_{N\text{-}A}$.

$$a_N = \frac{[H^+]}{[H^+] + K_{N\text{-}A}} \qquad \text{(S2)}$$

$$a_A = \frac{K_{N\text{-}A}}{[H^+] + K_{N\text{-}A}} \qquad \text{(S3)}$$

Steady-State study

The total fluorescence signal $F(\lambda_{ex}, \lambda_{em}, [H^+])$ at proton concentration $[H^+]$ due to excitation at λ_{ex} and observed at emission wavelength λ_{em} can be expressed as

$$F\left(\lambda_{ex}, \lambda_{em}, [\mathrm{H}^+]\right) = \frac{F_{min}[\mathrm{H}^+] + F_{max}K_a}{K_a + [\mathrm{H}^+]} \,, \qquad \text{(S4)}$$

where F_{min} indicates the fluorescence signal of the neutral form of the dye and F_{max} denotes the fluorescence signal of the anion form of the compounds. Fitting eq. S4 to the fluorescence data $F(\lambda_{ex}, \lambda_{em}, [H^+])$ as a function of $[H^+]$ yields values for K_a, F_{min}, and F_{max}.

Quantum yield values from steady-state fluorescence measurements were calculated for the anion forms using fluorescein in 0.1 M NaOH as a reference (Φ_{fluo} = 0.95). The quantum yield of the neutral form was obtained by fitting the steady-state

fluorescence spectra to the equilibrium equation S5 once the values of Φ_A were known.

$$F(\lambda_{ex}, \lambda_{em}, [H^+]) = C^{dye} K_a [\Phi_N \varepsilon_N \alpha_N + \Phi_A \varepsilon_A \alpha_A]$$

(S5)

Excited State Proton transfer reaction studies

The theory and methods of solving buffer-mediated ESPT reactions are well-established.[5-8]

If the photophysical system as shown in Scheme 2 is excited by an infinitely short light pulse that does not significantly alter the concentrations of the ground-state species, then the fluorescence δ-response function, f (λ_{em},λ_{ex},t), at emission wavelength λ_{em} due to excitation at λ_{ex} is given by

$$f(\lambda_{ex}, \lambda_{em}, t) = p_1 e^{\gamma_1 t} + p_2 e^{\gamma_2 t} \qquad t \geq 0 \qquad \text{(S6)}$$

in which eq 6 has been written in the common biexponential format, where

$$\gamma_{1,2} = \frac{-(a+c) \mu \sqrt{(c-a)^2 + 4bd}}{2}; \qquad \text{(S7)}$$

$a=k_{01}+ k_{21}+ k^B_{21}[R]$; (S8)

$b=k_{12}[H^+]+ k^B_{12}[RH]$; (S9)

$c=k_{02} + k_{12}[H^+]+ k^B_{12}[RH]$; and (S10)

$d=k_{21}+ k^B_{21}[R]$. (S11)

[*R*] and [*RH*] are related to the total buffer concentration, C^B=[R]+[*RH*], by the expressions [*RH*] = C^B [H^+]/([H^+]+ K_a^B) and [*R*] = C^B K_a^B/([H^+]+ K_a^B), where K_a^B is the dissociation constant for the reversible reaction $RH \leftrightarrow R + H^+$.

The γ factors are related to the lifetimes τ_1 and τ_2 by the expression

$$\tau_{1,2} = -\frac{1}{\gamma_{1,2}}. \qquad \text{(S12)}$$

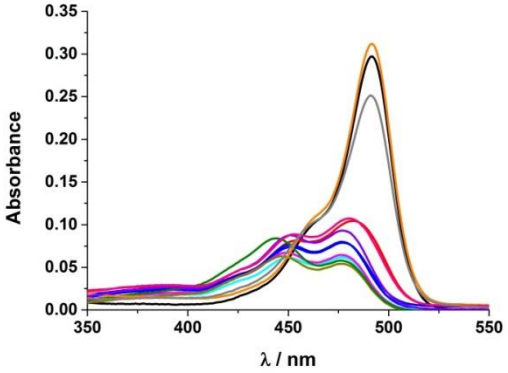

Figure S1: Absorption spectra of compound **1** (6×10^{-6} M) at different pH concentration (from 1.02 to 6.06).

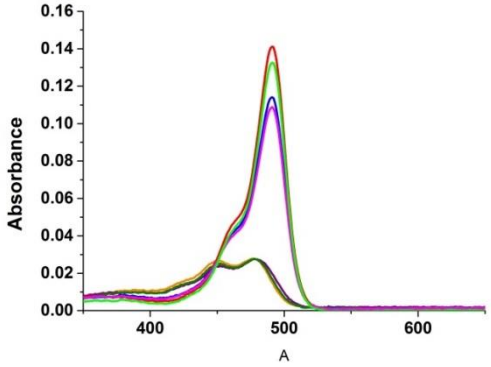

Figure S2: Absorption spectra of compound 3 (3.2×10^{-6} M) at different pH concentration (from 2.65 to 7.73)**.**

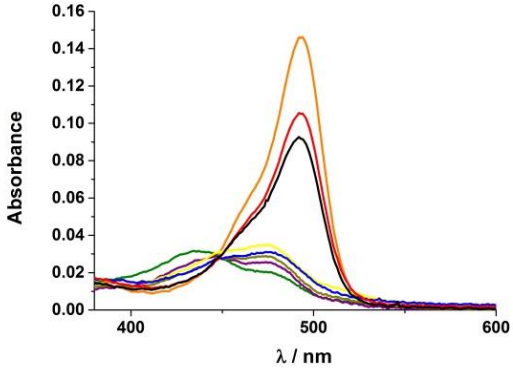

Figure S3: Absorption spectra of compound 4 (3.2×10^{-6} M) at different pH concentration (from 0.83 to 6.04).

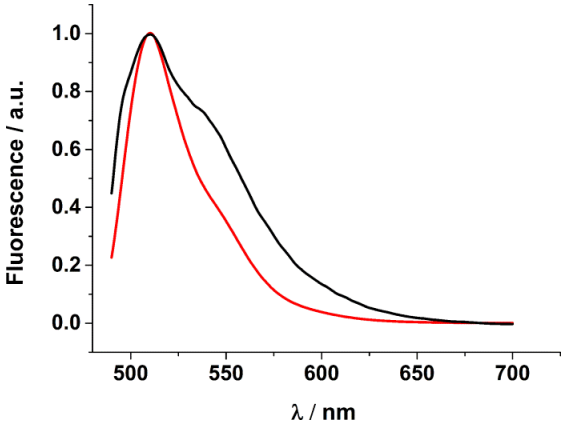

Figure S4: Normalized fluorescence emission of anion and neutral species of compound **2.**

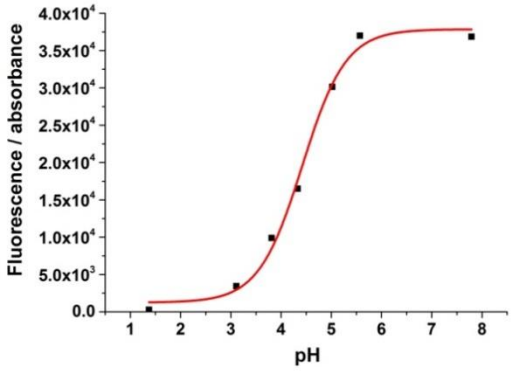

Figure S5: Curves generated by fitting (equation S) the normalized fluorescence by absorbance versus pH. Data recovered from figure 4.

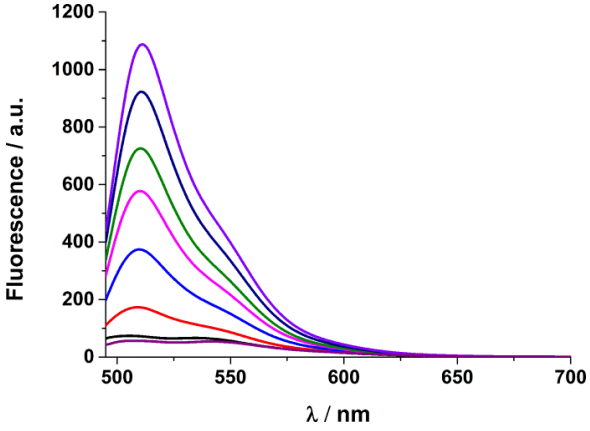

Figure S6: Fluorescence emission spectra of compound 1 (6×10^{-6} M) in acetate (255 mM) solution at different pH values (from 1.84 to 9.33).

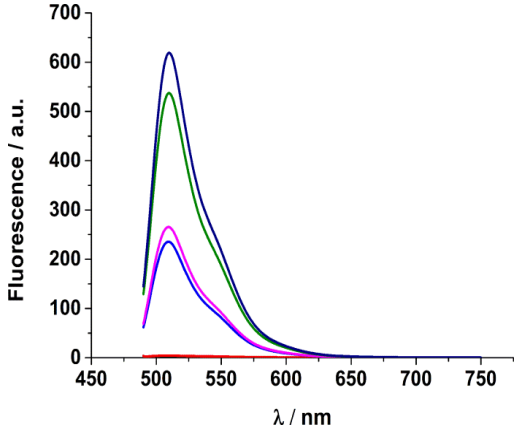

Figure S7: Fluorescence emission spectra of compound 3 (6×10^{-6} M) in acetate (255 mM) solution at different pH values (from 1.84 to 8.06).

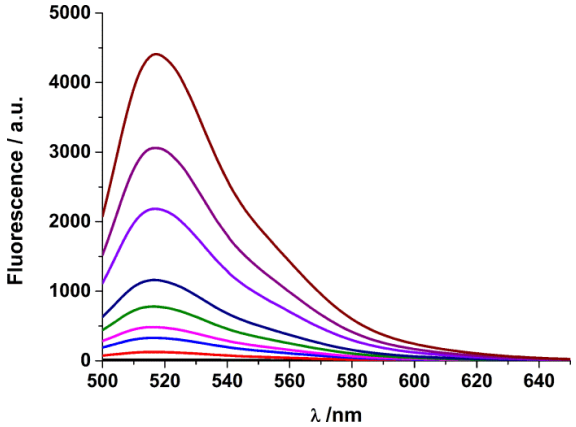

Figure S8: Fluorescence emission spectra of compound 4 (6×10^{-6} M) in acetate (340 mM) solution at different pH values (from 1.95 to 7.23).

Compound	λ_{max} abs anion	λ_{max} abs neutral	Isosbestic point	pK_a(abs)	Φ_A	Φ_N	τ_{anion} (ns)	$\tau_{neutral}$ (ns)
1	492	445/480	457	4.66±0.06	0.79	0.12	4.80	4.00
2	492	450/478	458	4.04±0.02	0.65	0.02	3.30	0.02
3	492	450/478	450	4.78±0.02	0.56	0.01	3.22	0.02
4	492	440/474	447	4.32±0.13	0.64	0.04	3.75	0.01

Table S1: Photophysical parameters of all compounds.

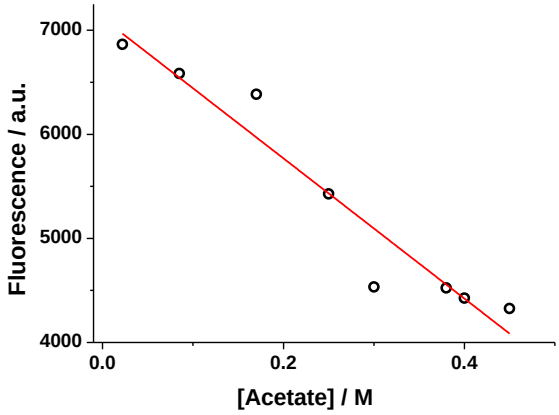

Figure S9: Dependence of the fluorescence emission to acetate concentration. In the range of acetate studied was found an acceptable linearity between fluorescence emission and acetate concentration at pH = 4.00. Linear fit obtained a R^2 = 0.92.

Competitive studies with other anions

We checked common anions present in cell culture medium (pyruvate, glucose, phosphate and bicarbonate) at pH 4 and normal concentration in medium by time resolved fluorescence. Lifetime of the dye is not changed (table S2).

Anion	Lifetime / ns	error
bicarbonate 0.0400 M	3.22	0.0018
bicarbonate 0.0240 M	3.24	0.0019
pyruvate 0.0013 M	3.24	0.0025
glucose 25 mM	3.23	0.0021
phosphate 4.5 mM	3.14	0.0021
phosphate 20mM	3.15	0.0017

Table S2: Lifetimes of compound 2 (6×10-6 M) at pH=4 in the presence of different anions.

Also, F^- and CN^- (table S3) were measurements. Only F^- anions show some reaction with the dye, but lower than acetate (Figure S9). Normal concentration in serum for F^- [9] (0.7 µM - 8 µM) is around 100 times lower than acetate concentration [10] (0.074 - 0.621 mM.) For these reasons, fluorescence or lifetime decrease in serum could be assigned exclusively to acetate.

CN^- / mM	Lifetime / ns	error
0	3.28	0.0052
100	3.29	0.0034
200	3.29	0.0038
300	3.28	0.0030
400	3.29	0.0028
500	3.29	0.0030
600	3.29	0.0035
700	3.29	0.0029

Table S3: Lifetimes of compound 2 (6×10^{-6} M) at pH=4 in the presence of different CN- concentrations.

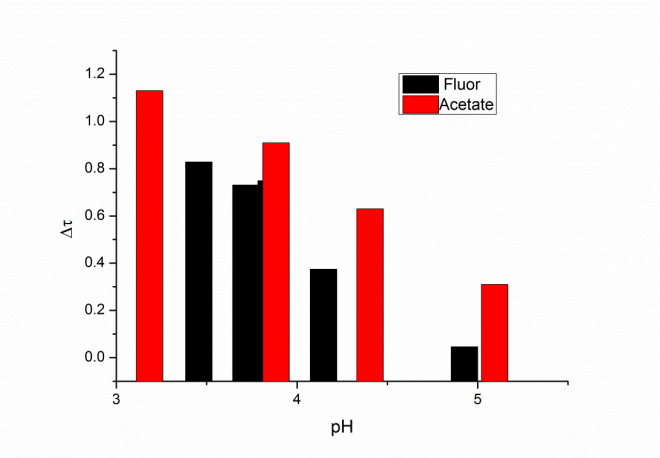

Figure S10: Lifetime changed between dye (6×10^{-6} M) without acetate or fluor anions and in presence of one of them (500 mM) at different pH.

References

1. L. Mottram, S. Boonyarattanakalin, R. E. Kovel and B. R. Peterson, *Organic Letters*, 2006, **8**, 581-584.
2. Z. R. Woydziak, L. Fu and B. R. Peterson, *The Journal of Organic Chemistry*, 2012, **77**, 473-481.
3. A. Martinez-Peragon, D. Miguel, R. Jurado, J. Justicia, J. M. Alvarez-Pez, J. M. Cuerva and L. Crovetto, *Chemistry-a European Journal*, 2014, **20**, 447-455.
4. Y. Urano, M. Kamiya, K. Kanda, T. Ueno, K. Hirose and T. Nagano, *J. Am. Chem. Soc.*, 2005, **127**, 4888-4894.
5. J. M. Alvarez-Pez, L. Ballesteros, E. Talavera and J. Yguerabide, *J. Phys. Chem. A*, 2001, **105**, 6320-6332.
6. A. Martinez-Peragon, D. Miguel, A. Orte, A. J. Mota, M. J. Ruedas-Rama, J. Justicia, J. M. Alvarez-Pez, J. M. Cuerva and L. Crovetto, *Org. Biomol. Chem.*, 2014, **12**, 6432-6439.
7. L. Crovetto, J. M. Paredes, R. Rios, E. M. Talavera and J. M. Alvarez-Pez, *J. Phys. Chem. A*, 2007, **111**, 13311-13320.
8. L. Crovetto, A. Orte, E. M. Talavera, J. M. Alvarez-Pez, M. Cotlet, J. Thielemans, F. C. De Schryver and N. Boens, *Journal of Physical Chemistry B*, 2004, **108**, 6082-6092.
9. D.R. Taves, Normal Human Serum Fluoride Concentrations, Nature, 211(1966) 192-3.
10. Z.T. Schug, J. Vande Voorde, E. Gottlieb, The metabolic fate of acetate in cancer, Nature Reviews Cancer, 16(2016) 708-17.

CONCLUSIONS

Chapter 1: New Dual Fluorescent Probe for Simultaneous Biothiol and Phosphate Bioimaging

- It has been designed and synthesized a new sulfinyl xanthene derivative (DNBS-GG) that can act as a simultaneous dual sensor for biological thiols and phosphate anions detection.
- The mechanism of action implies thiolysis of the sulfinyl group of the weakly fluorescent DNBS-GG by biothiols, releasing a fluorescent GG moiety that simultaneously responds to phosphate anions through fluorescence decay time changes.
- The efficiency of this new dye as a dual sensor was tested in vitro at two significant pH values: pH = 9, where the probe is faster and more sensitive to biothiols, and pH = 7.35, required for biological applications. In both cases, we have detected the presence of cysteine, homocysteine or glutathione and determine phosphate concentration.
- This probe is suitable for thiol detection in cases of cellular stress due to its low response to ROS. Moreover, this new dye was tested intracellularly by FLIM in HeLa cells, showing cell membrane permeability. In this case, the increase in fluorescence intensity reconfirms its ability to detect biothiols, and changes in fluorescence lifetime enable its behaviour as a phosphate concentration sensor.

Chapter 2: A New Fluorescent Dye for Oxidative Detection through Thiol Detection in vivo in Cell Culture

- It has been designed and synthesized a new optimized compound as a biothiol sensor (GGDNPS) for fluorescence imaging microscopy. The

mechanism of action implies the thiolysis of the sulfinyl group by biothiols which promotes an increase in fluorescence intensity easily detectable.

- Our experiments confirmed that this new dye is an excellent tool to detect intracellular biothiols level changes as a response to cellular oxidative stress. We performed some measurements using Hepatocellular Carcinoma cells (HepG2) and photoreceptor-derived cell line (661 W) and the results confirmed the ability of this new dye to detect intracellular biothiol variations as a consequence of light-induced cellular stress. Photoreceptor−like cells showed biothiol reservoir pools to protect themselves from ROS that emptied after a period of ~40 min of light exposure time. After this initial period we measured the intracellular synthesis of biothiols as a response to light−induced oxidative stress until cell degeneration occurred.
- The simplicity of this approach could be easily extended to develop high-throughput tests for new antioxidant drugs to prevent and/or treat photoreceptor oxidative related diseases.

Chapter 3: Efficient Acetate Sensor in Biological Media based on a Selective Excited State Proton Transfer (ESPT) Reaction

- It has been synthesized a new fluorescent probe that allows acetate detection in biological samples using fluorescence decay times.
- We recovered the kinetic constants of the species involved in the chemical equilibrium presented in the pH range of interest. Finally, in order to show its future application as an acetate sensor in liquid biopsies, we checked the ability of this new dye to detect acetate concentration changes using synthetic serum by FLIM. The results were very similar to the decay times predicted by the kinetic constants. Furthermore, it is remarkable that, under

the conditions of the experiments performed in this work, the dye achieved millimolar order sensitivity.